Abstract

This thesis is about power-line communication over the low-voltage grid, which has interested several researchers and utilities during the last decade, trying to achieve higher bit-rates and more reliable communication over the power lines. The main advantage with power-line communication is the use of an existing infrastructure. Wires exist to every household connected to the power-line network.

This thesis starts with a general introduction to power-line communication. Then an existing application, communicating on a low-voltage grid, is investigated in order to obtain some knowledge of how the power line acts as a communication channel. We also expose this system with a load, consisting of a set of industrial machines, to study the change in communication channel quality. After these large-scale measurements we measure some channel characteristics in the same grid. Measurements of the noise level and the attenuation, up to 16 MHz, are reported.

The power-line communication channel can, in general, be modeled as having a time-varying frequency-dependent signal-to-noise ratio over the communication bandwidth. The effect of non-white Gaussian noise on different receiver structures is studied, one ideal and one sub-optimal, and the importance of diversity (in frequency) is illustrated when the set of transmitter waveforms is fixed. We investigate robust, low-complexity, modulation methods which are able to handle unknown phase and attenuation, which simplifies the implementation of the receiver.

Finally we describe a communication strategy that eventually could be used for information transfer over the power-line communication channel. In doing this we combine coding, frequency diversity and the use of sub-channels (similar to Orthogonal Frequency Division Multiplex). This is a flexible structure which can be upgraded and adapted to future needs.

Preface

This is the result of my work as a graduate student at the Department of Information Technology at Lund University. Parts of this thesis have been presented at conferences:

- L. Selander, T. I. Mortensen, G. Lindell, "Load Profile and Communication Channel Characteristics of the Low Voltage Grid", Proc. DistribuTECH DA/DSM Europe 98, London, U.K., 1998.

- L. Selander, T. I. Mortensen, "Technical and Commercial Evaluation of the IDAM System in Ronneby, Sweden", Proc. NORDAC-98, Bålsta, Sweden, 1998.

- G. Lindell, L. Selander, "On Coding-, Diversity- and Receiver Strategies for the Power-line Communication Channel", Proc. 3rd International Symposium on Power-line Communications and its Applications, Lancaster, UK, 1999.

These papers correspond to the work presented in Chapter 2, 3 and 5, and was mainly done during my first year as a Ph.D. student. The results from the second year are not presented at any conference, and are entirely written for this thesis. These are shown in Chapter 4 and 6. The thesis starts with an introduction to power-line communication and ends with conclusions.

Parts of this material have also been presented in the following seminar:

- Communication Systems for the Low-voltage Grid, Seminar on Power Line Communications, NESA A/S, Copenhagen, Denmark, 1998.

Acknowledgments

There are many people who have supported and encouraged me during these years. This have meant a lot to me and I am very grateful to all of you. I would like to take this

opportunity to especially acknowledge the following people for their various contributions to this thesis.

First I would like to thank all of the students I have had during the years 94-99. Teaching has been the best part of this work and a major reason to why I became a Ph.D. student. I am very grateful to Mats Cedervall, who let me be a teaching assistant for him in Digital Design, which gave me a good start. I am also thankful to Mats Brorsson who let me teach a whole range of courses at the department of Computer Engineering.

Göran Lindell, my supervisor, has supported my work during my Ph.D. studies from the very first beginning. His ability to see the practical use of theoretical results has helped me on the way. He has also been proofreading this thesis, and his comments and suggestions, during these years, have been very educational and inspiring.

I am going to miss the Ph.D. students at the department, with who I have had much fun. I would especially like to thank Ola Wintzell, who have joined me in different sport activities and with whom I have had daily non-research discussions.

Everyone at the technical staff at the department of Information Technology has been a great help during these two years, something I thank them for. Especially Ilia Bolanowski, who have contributed to this project in many ways: supplied me with components, technical support, discussions about research and life in general, and being a good friend. Lennart Magnusson has assisted me in many ways, servicing my, not always functioning, equipment and contributing with his knowledge concerning technical issues. I am certainly going to miss being a teaching assistant with you both.

I would also like to thank some of the people at the former department of Computer Engineering: Jan Eric Larsson, Mats Brorsson, Fredrik Dahlstrand and Bengt Öhman, who I have had a lot in common with. Fredrik and Bengt have always been open for discussions and fun. I would also like to take this opportunity to recommend Jan Eric's course in thesis reading. Without that course this thesis would have looked much different.

Laila Lembke has been doing a great job supporting the project. Kamil Sh. Zigangirov and the rest of the staff at the department of Information Technology also deserve my gratitude for their support.

Ronneby Energi AB has supported this project in many ways. Anders Andersson, Christer Förberg and Rolf Håkansson have helped me with many practical details concerning the experiments in Ronneby. Especially Rolf has, with patience, put up with strange requirements and questions from a non-electrician. The people in the Påtorp area also have to be acknowledged. They have, without complaints, woken up to the sound of a welding unit, and have put up with wires routed on their paths.

During my first year I spent a lot of time working with Tony Mortensen at NESA A/S in Denmark. He helped me with the experiments in the Påtorp area and many ideas from this research have been generated through our discussions. Steen Munk, NESA A/S, also participated in these experiments.

Richard Krejstrup, Mats Bäckström and Marko Krejic were of great help during my measurements in Påtorp, they helped me with my experiments and have contributed with many ideas to this thesis.

I have had the opportunity of having regularly meetings with my sponsors. These meetings have put the research in a new perspective and have generated many ideas. Without these meetings this project would have been very different. This work has been supported by the Swedish National Energy Administration (Energimyndigheten) and by Elforsk (supported by Sveriges Elleverantörer, Stiftelsen Ronneby Soft Center, Telia Research, EnerSearch AB, NESA A/S, Fortum Power and Heat). I would also like to acknowledge Hans Ottosson, head of EnerSearch AB, who initiated this project and has been supporting this work at all times.

I would like to thank everyone at Hardi Electronics AB, who, after my decision to quit my work at the department, offered me the best job anybody could get.

I would like to give a special thanks to some of my friends: Ola Sundberg and Tim Nelson, for all get-togethers, playing the guitar, and all of the friends who have joined me in winter bathing, especially, Mattias Hansson and Gunnar Dahlgren. I also thank the remainder of my friends for distracting me from this work.

My parents have supported me from pre-school to graduate studies and have in many ways inspired me in my work and guided me through life to the individual I am. The same goes for my brother.

Finally, I am very grateful to my wife Viveca, who in many ways have contributed to this work: proofreading, assisting me during the measurements in Påtorp, discussing research, and taking care of me when I have not had the time myself. I love you.

CHAPTER 1 *Introduction*

The communication flow of today is very high. Many applications are operating at high speed and a fixed connection is often preferred. If the power utilities could supply communication over the power-line to the costumers it could make a tremendous breakthrough in communications. Every household would be connected at any time and services being provided at real-time. Using the power-line as a communication medium could also be a cost-effective way compared to other systems because it uses an existing infrastructure, wires exists to every household connected to the power-line network.

The deregulated market has forced the power utilities to explore new markets to find new business opportunities, which have increased the research in power-line communications the last decade. The research has initially been focused on providing services related to power distribution such as load control, meter reading, tariff control, remote control and smart homes. These value-added services would open up new markets for the power utilities and hence increase the profit. The moderate demands of these applications make it easier to obtain reliable communication. Firstly, the information bit rate is low, secondly, they do not require real-time performance.

During the last years the use of Internet has increased. If it would be possible to supply this kind of network communication over the power-line, the utilities could also become communication providers, a rapidly growing market. On the contrary to power related applications, network communications require very high bit rates and in some cases real-time responses are needed (such as video and TV). This complicates the design of a communication system but has been the focus of many researchers during the last years. Systems under trial exist today that claim a bit rate of 1 Mb/s, but most commercially available systems use low bit rates, about 10-100 kb/s, and provides low-demanding services such as meter reading.

The power-line was initially designed to distribute power in an efficient way, hence it is not adapted for communication and advanced communication methods are needed.

Today's research is mainly focused on increasing the bit rate to support high-speed network applications.

This thesis is about communication on the power-line (on the low-voltage grid). Section 1.1 gives a general description of power-line communications. Section 1.2 explains some preliminaries needed in digital communications and Section 1.3 describes the power-line channel, its characteristics, problems and limitations, and also serves as a survey of current research. Finally Section 1.4 gives an outline of the rest of this thesis. Other introductory descriptions on power-line communications are given in [14], [20], and [36]. Reference [36] also studies new business opportunities for the power utilities and reports research on coming technology.

1.1 Power-Line Communications

The power-line network is a large infrastructure covering most parts of the inhabited areas. In Sweden the power is typically generated by, e.g., a power plant and then transported on high-voltage (e.g., 400kV) cables to a medium-voltage sub station, which transforms the voltage into, e.g., 10kV and distributes the power to a large number of *low-voltage grids.*

Figure 1-1 shows an example of a typical low-voltage grid.

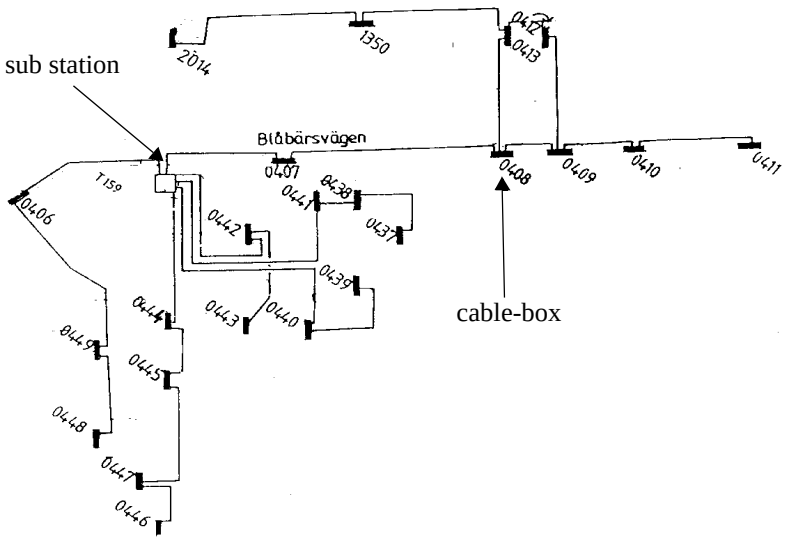

FIGURE 1-1 An example of a low-voltage grid.

Each low-voltage grid has one *sub station*, which transforms the voltage into 400 V and delivers it to the connected households, via low-voltage lines. Typically several *low-voltage lines* are connected to the sub station. Each low-voltage line consists of four wires, three phases and neutral. Coupled to the lines are *cable-boxes*, which are used to attach households to the grid.

This thesis is about communication on the low-voltage grid, communication between the sub station and the households. Related issues are how to communicate inside a household and how to communicate on the medium-voltage grid.

Many systems today use a topology with a central node (the sub station) communicating with clients (the households). All communication is between the sub station and the households and there is no communication between households. Because there is a physical connection between every two households it would also be possible to support this kind of communication. As an alternative, this communication could be routed through the sub station.

The configuration with a central node and a set of clients may be compared with systems for mobile telephony, e.g., GSM [33]. In GSM a base station (central node) is connected to all mobile phones (clients) within a restricted area. Thus the network topology is not unusual, but used in practice.

Power-line communication is based on electrical signals, carrying information, propagating over the power-line. A communication *channel* is defined as the physical path between two communication nodes on which the communication signal is propagated [1], [41]. In a low-voltage grid there is a lot of different channels, in fact the links between the sub station and each household are all different channels with different characteristics and *qualities*. If the communication system supports communication between households all these links are also different channels.

The quality is estimated from how good the communication is on a channel. The quality is mostly a parameter of the *noise level* at the receiver and the *attenuation* of the electrical signal at different frequencies. The higher the noise level the harder it is to detect the received signal. If the signal gets attenuated on its way to the receiver it could also make the decision harder because the signal gets more hidden by the noise.

On the power-line the noise is generated from all loads connected to the grid. Also broadcast radio interferes with the communication. The attenuation is a parameter of the physical length of the channel and impedance mismatches in the grid. The power-line is often considered a harsh environment because of the time-variant characteristics of the noise and the attenuation, but this is also the case in most communication systems and only limits the performance that can be achieved. Advanced communication systems exists today, designed to overcome the problems with such channels as, e.g., GSM. The characteristics of the power-line channel are further described in Section 1.3.

This thesis is focused on the research on the power-line as a communication channel. The objective is to come up with advanced digital communication methods to support higher bit rates and more reliable communication on the low-voltage grid. To understand

the problem field some preliminaries are needed from digital communications. This is the subject of the next section.

1.2 Digital Communications

In this section we study some preliminaries from digital communications. A model of a digital communication system is given in the next section and the last two sections give a short introduction to *bandwidth* and *diversity.*

1.2.1 System Model

Figure 1-2 shows a simplified model of a digital communication system. Recommended textbooks on this subject are [1], [41] and [54]. The objective of the communication system is to communicate digital information (a sequence of binary information digits) over a noisy channel at as high bit rates as possible. The data to be transmitted could origin from any source of information. In case the information is an analog signal, such as speech, then an A/D converter must precede the transmitter.

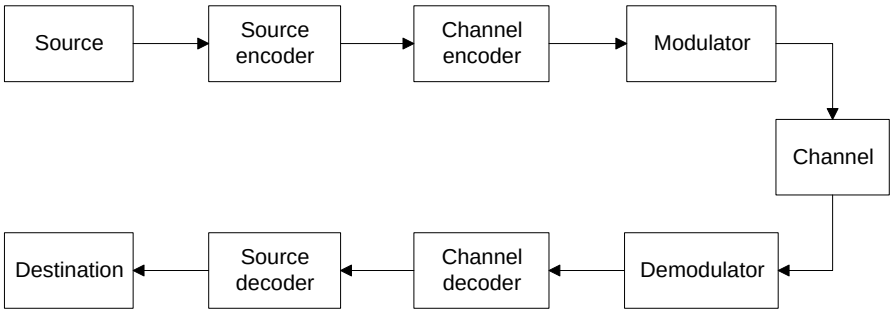

FIGURE 1-2 A model of a digital communication system.

The source encoder outputs data that are to be transmitted over the channel at a certain *information bit rate*, R_b. As a measure of performance we define the *bit error probability*, P_b, as the probability that a bit is incorrectly received at the destination. As we will see later, the channel may interfere with the communication, thus increasing the bit error probability.

Source Coding

Most data contains redundancy, which makes it possible to compress the data. This is done by the *source encoder* and minimizes the amount of bits transmitted over the channel. At the receiver the source decoder unpacks the data to either an exact replica of the source (lossless data compression) or a distorted version (lossy data compression). If the received sequence does not have to be an exact copy of the transmitted stream then the degree of compression can be increased.

Channel Coding

In order to reduce the bit error probability the *channel encoder* adds redundancy (extra control bits) to the bit sequence in a controlled way. When an error appears in the bit stream the extra information may be used by the channel decoder, to detect, and possibly correct, the error. The redundancy added is depending on the amount of correction needed but is also tuned to the characteristics of the channel.

Two coding techniques often used are *block codes* [41] and *convolutional codes* [27], [41].

Modulator

The *modulator* produces an information-carrying signal, propagating over the channel. At this stage the data is converted from a stream of bits into an analog signal that the channel can handle. The modulator has a set of analog waveforms at its disposal and maps a certain waveform to a binary digit or a sequence of digits. At the receiver, the demodulator tries to detect which waveform was transmitted, and convert the analog information back to a sequence of bits.

Several modulation techniques exists, e.g., spread-spectrum [41], OFDM (Orthogonal Frequency Division Multiplex) [18], GMSK (Gaussian Minimum Shift Keying) [33], FSK (Frequency Shift Keying) [41], PSK (Phase Shift Keying) [41] and QAM (Quadrature Amplitude Modulation) [41].

Channel

The channel might be any physical medium, such as coaxial cable, air, water or telephone wires. It is important to know the characteristics of the channel, such as the attenuation and the noise level, because these parameters directly affect the performance of the communication system.

1.2.2 Bandwidth

The frequency content of the information-carrying signal is of great importance. The frequency interval used by the communication system is called bandwidth, W [41]. For a specific communication method, the bandwidth needed is proportional to the bit rate. Thus a higher bit rate needs a larger bandwidth for a fixed method. If the bandwidth is doubled then the bit rate is also doubled.

In today's environment bandwidth is a limited and precious resource and the bandwidth is often constrained to a certain small interval. This puts a restriction on the communication system to communicate within the assigned bandwidth.

To compare different communication systems the *bandwidth efficiency*, ρ, is defined as

$$\rho = \frac{R_b}{W} \tag{1-1}$$

and is a measure of how good the communication system is [41]. Today, an advanced telephone modem can achieve a bit rate of 56.6 kb/s using a bandwidth of 4 kHz and the bandwidth efficiency is 14.15 b/s/Hz. A meter reading system for the power-line channel that has a bit rate of 10 kb/s and communicates within the CENELEC A band has a bandwidth efficiency of 0.11 b/s/Hz, thus the performance of the telephone modem is much higher.

1.2.3 Diversity

To reduce the error probability of harsh channels, *diversity techniques* [41] may be used. Examples are *time diversity* and *frequency diversity.*

In time diversity the same information is transmitted more than once at several different time instants. If the channel is bad at some time instant the information might pass through at some other time when the channel is good (or better). This is especially useful on time-varying channels.

Frequency diversity transmits the same information at different locations in the frequency domain. It can be compared to having two antennas transmitting at different frequencies, if one of them fail the other might work.

1.3 The Power-Line as a Communication Channel

In this section we study the power-line as a communication channel and discuss the current research. In Section 1.1 we defined a channel as a physical path between a transmitter and a receiver. Note that a low-voltage grid consists of many channels each with its own characteristics and quality.

Figure 1-3 below shows a digital communication system using the power-line as a communication channel. The transmitter is shown to the left and the receiver to the right. Important parameters of the communication system are the output impedance, Z_t, of the transmitter and the input impedance, Z_l, of the receiver.

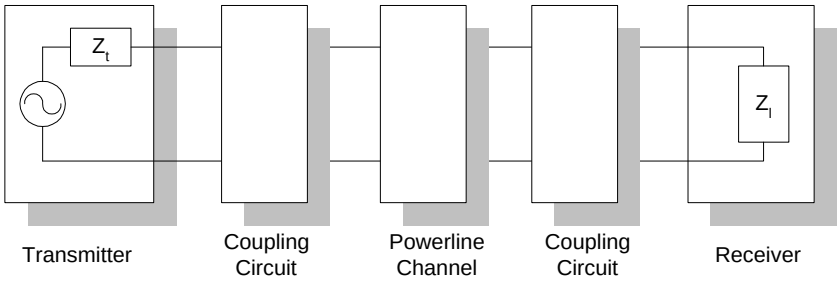

FIGURE 1-3 A digital communication system for the power-line channel.

A coupling circuit is used to connect the communication system to the power-line. The purpose of the coupling circuits is two-fold. Firstly, it prevents the damaging 50 Hz signal, used for power distribution, to enter the equipment. Secondly, it certifies that the major part of the received/transmitted signal is within the frequency band used for communication. This increases the dynamic range of the receiver and makes sure the transmitter introduces no interfering signals on the channel.

In the following sections we study different behaviors and properties of the power-line channel. In Section 1.3.6 we use a model of the power-line communication channel, incorporating these characteristics.

1.3.1 Bandwidth Limitations

As described above the bandwidth is proportional to the bit rate, thus a large bandwidth is needed in order to communicate with high bit rates.

In Europe the allowed bandwidth is regulated by the CENELEC standard, see [8]. The standard only allows frequencies between 3 kHz and 148.5 kHz. This puts a hard restriction on power-line communications and might not be enough to support high bit rate applications, such as real-time video, depending on the performance needed.

Figure 1-4 shows the bandwidth, as specified by the CENELEC standard. The frequency range is subdivided into five sub-bands. The first two bands (3-9 and 9-95 kHz) are limited to energy providers and the other three are limited to the customers of the energy providers. In addition to specifying the allowed bandwidth the standard also limits the power output at the transmitter.

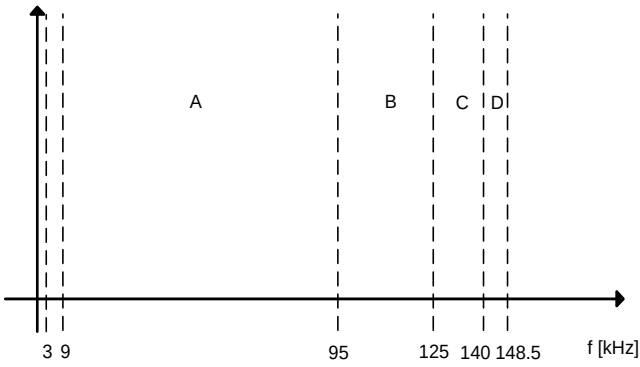

FIGURE 1-4 The frequency bands in the CENELEC standard.

In order to increase the bit rate, larger bandwidth may be needed. Recent research has suggested the use of frequencies in the interval between 1 and 20 MHz [4], [5], [20]. If this range could be used it would make an enormous increase in bandwidth and would perhaps allow high bit rate applications on the power-line. An important problem is that parts of this frequency band is assigned to other communication system and must not be disturbed. Other communication systems using these frequencies might also disturb the communication on the power-line. Examples of communication systems in this interval are broadcast radio, amateur radio and airplane navigating, see [20], [40].

1.3.2 Radiation of the Transmitted Signal

When transmitting a signal on the power-line the signal is radiated in the air. One can think of the power-line as a huge antenna, receiving signals and transmitting signals. It is important that the signal radiated from the power-line does not interfere with other communication systems.

When using the frequency interval 1-20 MHz for communication the radiation is extremely important because many other radio applications are assigned in this frequency interval. It is not appropriate for a system to interfere with, e.g., airplane navigation or broadcast systems. Recent research has studied this problem and tries to set up a maximum power level of transmission [28], [46], [55]. It is important that this work is finished in the near future since it limits the use of this bandwidth and the development of communication systems for the power-line channel.

When the cables are below ground the radiation is small. Instead it is the radiation from the households that makes the major contribution. Wires inside households are not shielded and thus radiate heavily. A solution might be to use filters to block the communication signal from entering the household [4], [35].

1.3.3 Impedance Mismatches

Normally, at conventional communication, impedance matching is attempted, such as the use of 50 ohm cables and 50 ohm transceivers. The power-line network is not matched. The input (and output) impedance varies in time, with different loads and location. It can be as low as milli Ohms and as high as several thousands of Ohms and is especially low at the sub station [2], [24], [31], [34], [38], [53].

Except the access impedance several other impedance mismatches might occur in the power-line channel. E.g., cable-boxes do not match the cables and hence the signal gets attenuated.

Recent research has suggested the use of filters stabilizing the network [35]. The cost of these filters might be high and they must be installed in every household and perhaps also in every cable-box.

1.3.4 Signal-to-Noise-Ratio

A key parameter when estimating the performance of a communication system, is the *signal-to-noise power ratio*, *SNR* [41]:

$$SNR = \frac{\text{Received power}}{\text{Noise power}} \tag{1-2}$$

This parameter is related to the performance of a communication system. The higher SNR the better communication.

The noise power on the power-line is a sum of many different disturbances. Loads connected to the grid, such as TV, computers and vacuum cleaners generate noise propagating over the power-line. Other communication systems might also disturb the communication, thus introducing noise at the receiver. Noise measurements are found in [2], [6], [15], [20], [24], [32], [38].

When the signal is propagating from the transmitter to the receiver the signal gets attenuated. If the attenuation is very high the received power gets very low and might not be detected. The attenuation on the power-line has shown to be very high (up to 100 dB) and puts a restriction on the distance from the transmitter to the receiver [2], [15], [20], [24]. An option might be to use repeaters in the cable-boxes, thus increasing the communication length.

The use of filters could improve the signal-to-noise ratio [35]. If a filter is placed at each household blocking the noise generated indoors from entering the grid, the noise level in the grid will decrease, but the cost is a higher complexity.

It is important to point out that although the power-line is considered a harsh environment when it comes to attenuation and disturbances, these parameters exists in any communication system used today.

1.3.5 The Time-variant Behavior of the Grid

A problem with the power-line channel is the time-variance of the impairments, see e.g., [2]. The noise level and the attenuation depend partly on the set of connected loads, which varies in time. A channel which is time-variant, complicates the design of a communication system. At some time instants the communication might work well but at other times a strong noise source could be inherent on the channel, thus blocking the communication.

To solve this a possible solution is to let the communication system adapt to the channel [41]. At any time the characteristics of the channel are estimated, e.g., through measurements, and the effect is evaluated to make a better decision. The cost of this is higher complexity.

1.3.6 A Channel Model of the Power-Line Communication Channel

In the previous section we have seen some impairments that reduce the performance of a power-line communication system:

- Impedance mismatches at the transmitter
- Channel attenuation
- Disturbances (noise)
- Impedance mismatches at the receiver
- Time-variations of the impairments

Figure 1-5 shows a model of the power-line channel with the parameters above. All impairments except the noise are shown as time-variant linear filters [41], [42] characterized by its frequency response. The disturbance is shown as an additive interfering random process.

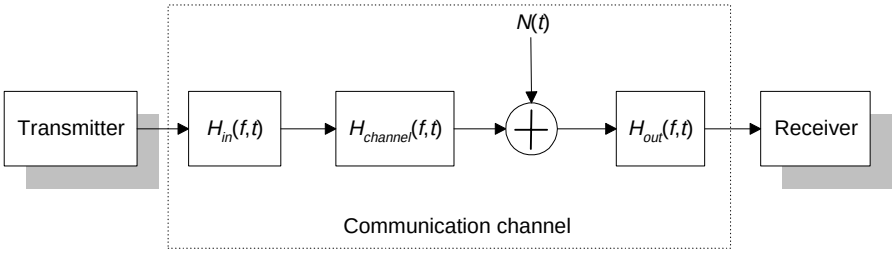

FIGURE 1-5 Impairments present on the power-line channel.

All the impairments above can be incorporated into a single filter model, shown in Figure 1-6, consisting of a time-variant filter and additive noise.

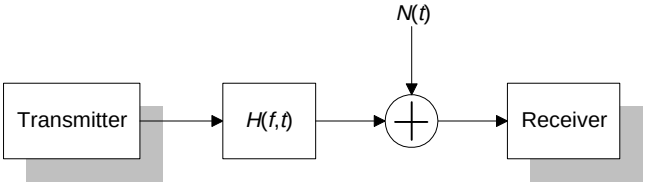

FIGURE 1-6 A simplified model of the power-line channel.

Despite of its simple form this model captures a whole range of properties essential to communication system design and to the corresponding performance [41].

The transfer function and the noise can either be estimated through measurements or derived by theoretical analysis. Measurements on the power-line channel are found in [2], [6], [15], [20], [24], [31], [32], [34] and theoretical models in [3], [10], [13], [16], [20], [39], [56]. Still a lot of measurements and modeling are needed to get a thorough understanding of the grid due to the variance of the characteristics.

1.3.7 Summary

In this section we summarize the references in the previous sections and also add some new references.

Current research is focused on the characteristics of the power-line as a communication channel and the development of effective communication methods.

The characteristics, such as attenuation, noise level and access impedance have been studied in different papers. The references [2], [24], [31] study frequencies up to 150 kHz and [6], [15], [20], [31], [34], [38] present measurements for higher frequencies. Especially recommended are [2], [15], [24] and [38], where the last one is focused on indoor communication. The outdoor grid and the indoor grid are two different environments and the behavior is not the same. Measurements have been done by several projects, but it is still hard to give a precise model of the power-line out of these measurements because of the variance in time, at location and with loads.

Instead of measuring the channel characteristics, one alternative is to theoretically derive specific channel characteristics. Different theoretical methods to do this analysis have been studied, see e.g., [3], [10], [13], [16], [20], [39], [56].

A recommended serie of papers is [24], [25], [26] and study frequencies up to 100 kHz. First the channel parameters are measured and statistically described, then bounds on the channel capacity are calculated. Reference [20] is a tutorial on power-line communications on the low-voltage grid. It contains market analysis, overviews, communication protocols, measurements, and descriptions and simulations of different types of cables and topologies.

The radiation problem is described in [28], [46], [55], which report measurements of the radiation and also try to set up a limit of the transmitter power.

Standardization of power-line communication in a regulatory perspective is found in [22] and a general discussion of different standards for power-line communication is given in [35].

Other papers dealing with most aspects of power-line communication can be found in Proceedings from the International Symposium on Power-line Communications conferences, see [43], [44] and [45].

Different modulation methods have been proposed to be used on the low-voltage grid. Methods often considered as candidates are OFDM (Orthogonal Frequency Division Multiplex), spread-spectrum and GMSK (Gaussian Minimum Shift Keying). These methods are described in [18], [41] and [33].

1.4 Thesis Outline

The remaining six chapters are concerned with different aspects of power-line communications.

Chapter 2 Communication Channel Properties of the Low-voltage Grid

In this chapter we study some basic properties of the power-line channel. By observing an existing system using the low-voltage grid as a communication medium it is possible to draw conclusions of how large-scale variations affect the communication, such as the variation in time and energy usage in the grid. Also the performance of individual channels are measured and related to the distance between the transmitter and the receiver and the location in the grid.

Chapter 3 On the Effect of Loads on Power-Line Communications

Loads change the condition of a grid. It is therefore interesting to study how this change of state affects the communication. By using a moveable load source consisting of a set of industrial machines we have been able to relate the effect of this load to the degradation of performance of a running communication system. It is also studied how the distance to the load is related to quality of the channels.

Chapter 4 Measurements of the Characteristics of the Low-voltage Grid

To further explore the characteristics of the power-line, measurements have been done in a specific low-voltage grid. We show measurements of the noise level and the attenuation of the power-line channel. Frequencies in the bandwidth regulated by the CENELEC standard [8] is studied, but also frequencies up to 16 MHz. The results are also related to the performance analysis in Chapter 2.

Chapter 5 Receiver Strategies for the Power-Line Communication Channel

From the measurements in Chapter 4 it is clear that the noise level can not be modeled as an additive white gaussian noise process (AWGN) [41], thus it is non-white. (An AWGN process is characterized by the power being evenly distributed over the whole frequency band). In this chapter we study the effect of this non-white noise on specific receiver structures. Two receiver structures are compared with respect to robustness and narrow-band disturbances.

Chapter 6 A Modulation Method for the Power-Line Communication Channel

The experiments in Chapter 2 and 3 and the measurements in Chapter 4 imply that a robust modulation method might be used, robust against phase changes and attenuation. In this chapter we introduce a modulation method designed to support robustness. The method is a combination of FSK and PSK [41]. The error probability and the bandwidth efficiency of the method are calculated and compared to other robust methods.

In this chapter we also summarize the key result from previous chapters and try to use this to design a communication system for the power-line. The outcome is a communication strategy designed to support robustness and ease of implementation. Modulation methods, coding and diversity are used.

Chapter 7 Conclusions

Here we conclude the thesis and report the key results.

CHAPTER 2

Communication Channel Properties of the Low-voltage Grid

2.1 Introduction

In order to design a communication system for a specific channel it is preferable to have some basic knowledge of the characteristics of the channel. If a communication system can be matched to a channel, it increases the performance [41].

The intention with the project described in this chapter is to study the properties/behavior of the communication channel by observing an existing system used on the low-voltage grid in a typical application. Here we focus on large-scale variations of the communication channel, e.g., how its quality depends on different time-windows, distances and loads.

It is well-known from communication theory that any practical communication system will have communication problems if the signal-to-noise ratio at the receiver drops below a certain level [41]. This can of course happen also in the power-line communication channel as a result of channel impairments, e.g., signal attenuation, signal degradation and noise sources along the signal path. In the following the quality of a channel is a measure of how good the communication system work.

In order to obtain quantitative results, parameters related to the quality of the communication channel are estimated. The most frequently used parameter, in this chapter, is an estimate of the probability that re-transmissions of so-called transactions are made. This parameter is used as an indicator of the quality of the communication channel, since a re-transmission is made when the receiver is unable to make a reliable decision, which in turn normally is due to channel impairments. Hence, a low value on the probability of re-transmissions indicates a "good" communication channel.

It should be observed that the estimated probability above does not measure the reliability in the final decisions produced by the communication system. In general, a high reli-

ability in the final decisions can be obtained with communication systems using re-transmissions. However, the focus of this work is on the quality of the communication channel, and that is the reason why we estimate parameters that reflect how often channel impairments result in re-transmissions.

The communication system we have used is located in Ronneby, Sweden, in an area called Påtorp. The system was chosen because it is in use within the project and it has been tested on several locations in different environments. Furthermore it is fully implemented and commercially available. In the rest of this thesis we denote this system PLC-P (a Power-line Communication System in Påtorp).

The purpose has not been to evaluate the PLC-P system, but rather to extract information from PLC-P that can be used to estimate the quality of the power-line as a communication channel.

The disposition of this chapter is as follows:

- A description of the PLC-P system, Section 2.2.
- The overall performance of the communication channels in the low-voltage grid, Section 2.3.
- The performance of the communication channels at various locations in the low-voltage grid, Section 2.4.
- The relation between the load profile and the quality of the communication channels, Section 2.5.
- Discussion and conclusions, Section 2.6.

Chapter 3 is related to the work in this chapter and studies the effect of loads on the communication, also using the PLC-P system as a reference.

2.2 The PLC-P System

The backbone of PLC-P is its possibility to support meter reading but it is also designed to support other services such as alarm systems. The structure of PLC-P is designed to be an open-system architecture and easily extendable to both producer and consumer specific applications. PLC-P is also described in [49].

PLC-P consists of three major parts. The Multi Function Node (MFN), the Concentrator & Communication Node (CCN) and the Operation and Management System (OMS). Figure 2-1 shows how the parts are connected in a typical system.

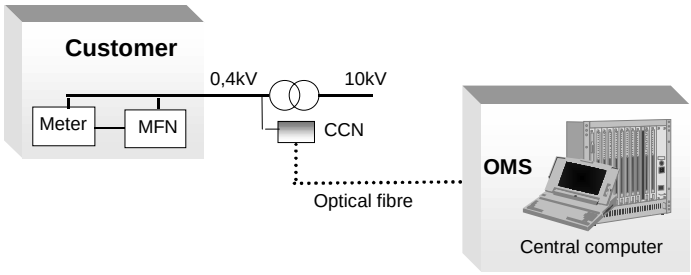

FIGURE 2-1 The different parts of the PLC-P system and how they are connected.

The MFN is a unit that is installed in each household either as an integrated or separate part of the meter. It reads the meter value each hour and stores it in a memory. The memory can store up to 40 days of meter values.

The CCN manages all MFNs in an area, e.g., a low-voltage grid, and it is responsible for collecting their meter values. Typically, the CCN is installed in a sub station and it consists of an ordinary PC.

An OMS manage a set of CCNs. The meter values collected by the CCN are stored in the OMS where they can be accessed and analyzed.

2.2.1 The Implementation in Påtorp

Figure 2-2 shows a map of the low-voltage grid in Påtorp where the experiments have been carried out. The area consists of about 70 households and is supported by the sub station T159. The households are connected to the low-voltage grid via cable-boxes also shown in Figure 2-2. The markers placed on some of the low-voltage lines mean that the connection is off. More information concerning this grid can be found in [49].

In Påtorp a MFN is installed in each household. The MFN is connected to the low-voltage grid and to the meter, which in most cases is placed outside the house. The CCN is installed in the sub station T159 and it is connected to the OMS via an optical fibre. The OMS is placed inside a house a couple of kilometers from Påtorp.

The results in this chapter are based on the 59 households that regularly deliver meter values to the PLC-P system.

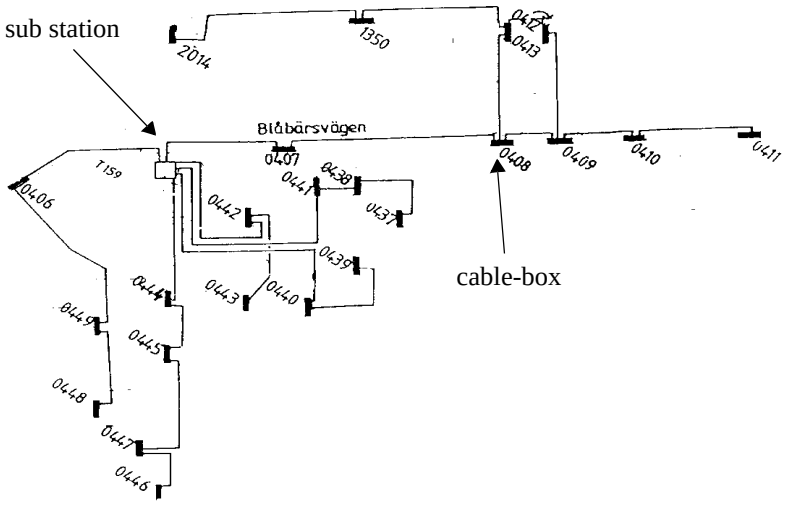

FIGURE 2-2 The low-voltage grid in Påtorp. The numbers are related to the cable-boxes (shown with black rectangles) and the sub station is denoted T159.

2.2.2 The Communication in PLC-P

The communication between the CCN and the MFNs is in all cases over the power-line. Every hour the CCN polls each MFN in order to get the meter values. To control the MFNs, and to read the meter values, a series of transactions are needed. A transaction is defined as the combined sequence of a request by the CCN followed by a reply, with some data, from a MFN. For every transaction, the communication system, on which PLC-P is built (see Section 2.2.3), is invoked. If a transaction fails then PLC-P is notified and the CCN tries again until the transaction is succeeded. All communication is between the CCN and the MFNs. There is no communication between the households in the area.

The result of each transaction, whether it has failed or not, is noted in a logfile for further processing. This logfile can be used to retrieve information about the communication performance. The information that has been used in this paper is the following:

e_i, the number of failed transactions to household i

N_i, the total number of transactions to household i

New values are obtained each hour. If the communication is error-free, N_i is typically two per hour and e_i is zero per hour.

All estimated results related to communication channel properties in this chapter have been calculated with the parameters above.

The collected meter values are stored in a file in the OMS. These values have been used to study the effect of the loads on the channel quality, see Section 2.5.

2.2.3 The Communication Technique

PLC-P communicates in the frequency band 9-95 kHz. This is the frequency bandwidth set up by the CENELEC standard [8] exclusively for utilities, the so-called A Band. The bit rate is low, a few kb/s, and the communication technique used is spread-spectrum [41] based.

2.3 Estimated Overall Performance of the Communication Channels

In Påtorp the CCN communicates with 59 MFNs, which are geographically spread. Hence, this means that 59 communication channels are present in the area, and the quality of these channels can be very different. In this section, the overall (average) performance of these communication channels is estimated and discussed.

With the information given in the logfiles, an estimate, P_i, of the probability for re-transmission of a transaction between the CCN and household number *i* (MFN number *i*), can be obtained as:

$$P_i = \frac{e_i}{N_i} \tag{2-1}$$

This parameter is an estimate of the probability of rejection of an individual transaction at the CCN due to channel impairments, but we prefer to refer to P_i as an estimated *channel impairment indicator* to household *i*.

To be able to follow how the quality of the communication channels changes over time (large-scale variations), new estimates are calculated for each hour (normally). Though the available statistical data is limited, the obtained quantitative results can be used as an indication of how the quality of the communication channels depends on different time-windows, distances and loads.

2.3.1 The Average Performance of the Channels

The average, P, of the channel impairment indicators, P_i, is a measure of the overall average quality of the K (=59) communication channels in the area during an hour and is obtained as:

$$P = \frac{1}{K}\sum_{i=1}^{K} P_i \qquad (2\text{-}2)$$

Figure 2-3 shows P for Monday to Sunday a week in February and a week in May. A week in March is also shown in Figure 2-9 together with the so-called load profile.

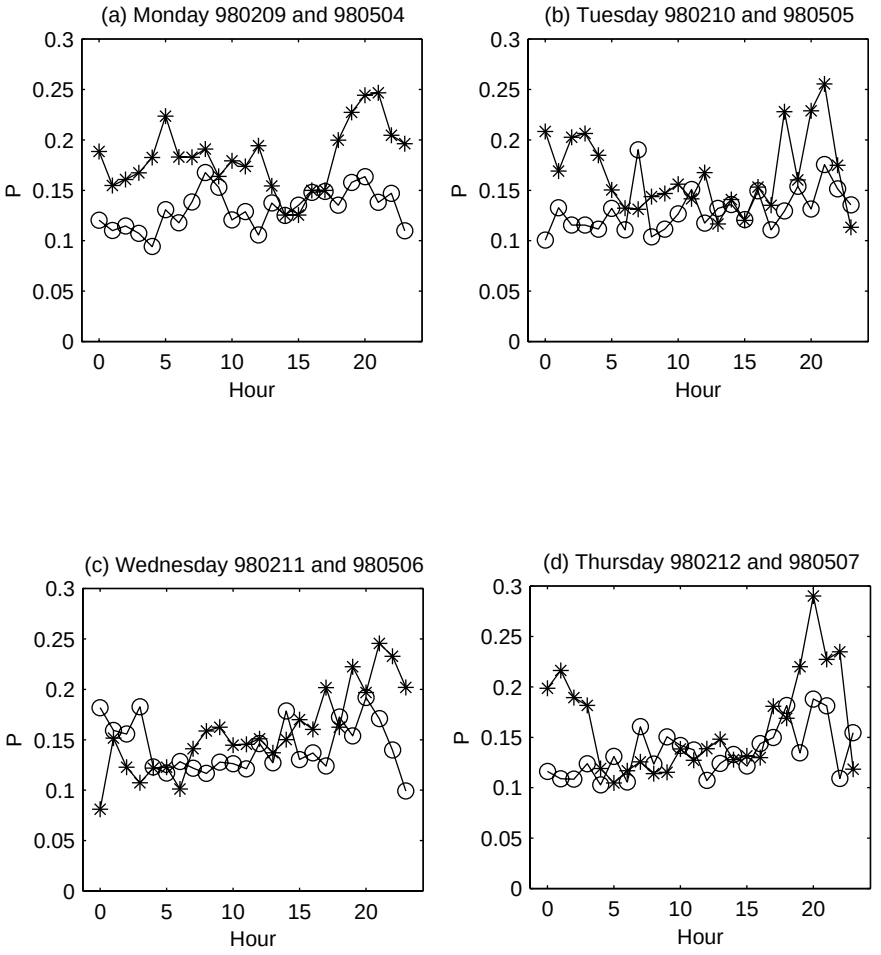

FIGURE 2-3 Continued on next page

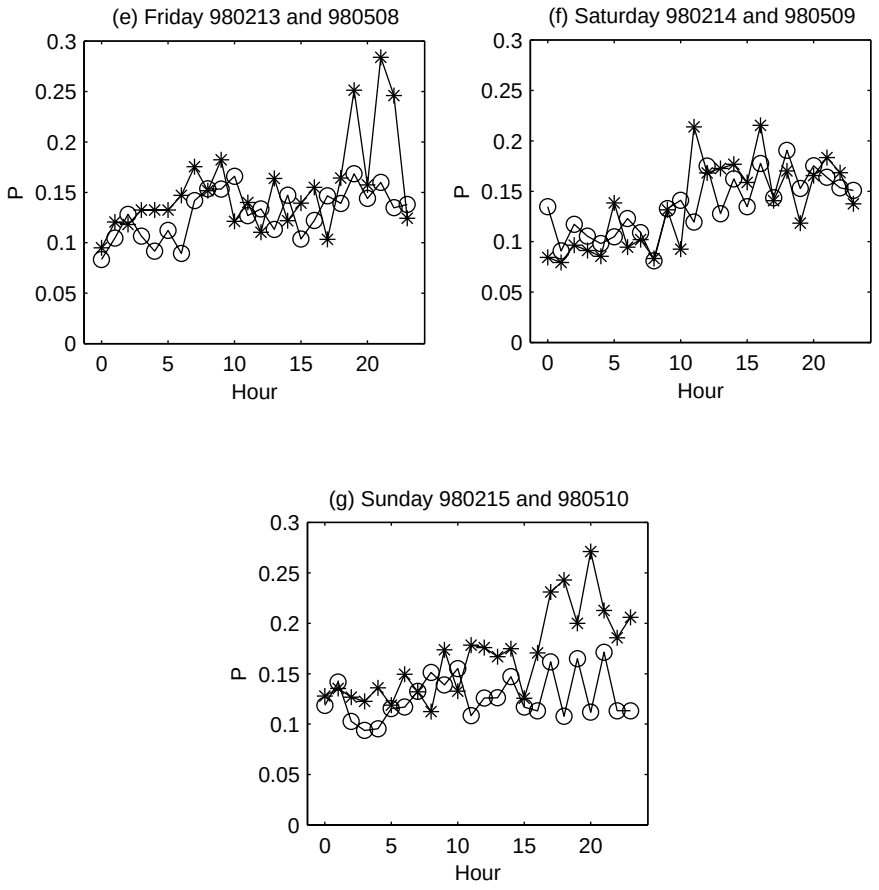

FIGURE 2-3 Average of all estimated channel impairment indicators, *P,* for each hour (0-23) during a week in February (the points marked with asterisks) and a week in May (the points marked with circles).

Figure 2-3 and Figure 2-9 show that the average value is around 0.10-0.15. This means that if the same amount of transactions are sent to each house, then about 10-15% of the transactions fail on the average. It is also seen in the figures that a peak often occurs during the morning and in the evening. The impairments seem to be especially high around 8 pm. Figure 2-3 and Figure 2-9 indicate that the impairments vary with time. It is also seen that the three weeks show some similarities between corresponding days.

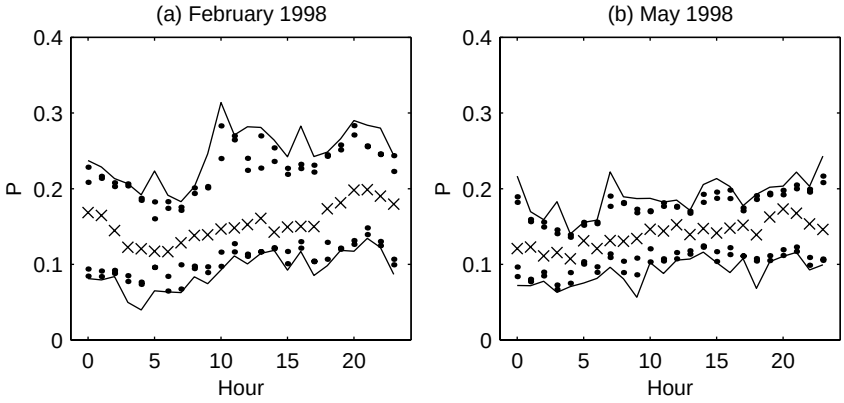

FIGURE 2-4 The collected data of the parameter *P* in February (a) and May (b). Shown is, for each hour (0-23) during respective month, the median (crosses) and the minimum and the maximum values. The three largest and three smallest values are plotted with dots in the graphs.

Figure 2-4 shows all the estimated values of *P* during February and May. The figure shows that the minimum values occur during the night and in the morning and the maximum values during the day and in the evening. It is also seen that the quality of the communication channels is better in May than in February. This indicates a seasonal behavior of the channel quality. The median values are about the same but the maximum values in February are higher.

2.3.2 The Number of Households Experiencing at Least One Re-transmission

The number of transactions initiated to each household in PLC-P is in general not the same because the amount of re-transmissions depends on the quality of the corresponding communication channel. A different measure of how well the communication works is to count the number of households having a non-zero value, e_i. Note that these results are only valid as long as only the meter reading system is in use. If the number of transactions increase (e.g., new applications), the number of houses experiencing re-transmissions will of course increase.

Figure 2-5 shows the number of households experiencing at least one re-transmission each hour (hence $e_i \neq 0$). It is seen that this is the case for about 10-15 MFNs each hour. This is about 20% of the total number of MFNs. Note that a peak occur at 1 pm because the PLC-P system during this period initiates at least five transactions to each household instead of the usual two transactions. As in Figure 2-4, it is seen that the quality of the communication channels is better in May than in February.

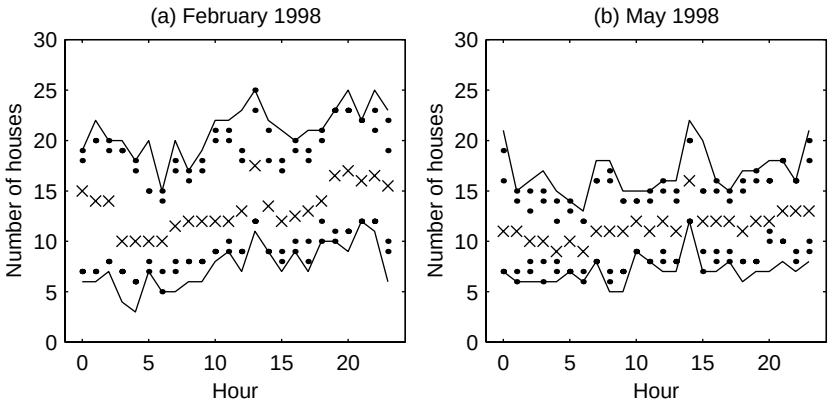

FIGURE 2-5 The number of households experiencing re-transmissions in February (a) and May (b). Shown is, for each hour (0-23) during respective month, the median (crosses) and the minimum and the maximum values. The three largest and three smallest values are plotted with dots in the graphs.

2.3.3 The Overall Re-transmission Probability

Because PLC-P does re-transmissions to households corresponding to low-quality channels one might believe that the information is collected by just doing a few re-transmissions. The fact is that a lot of re-transmissions are in general needed to collect all the data. Each hour the CCN initiates two transactions to each MFN (except at 1 pm when five transactions are initiated). If all channels were high-quality channels only 118 transactions per hour would be needed (except at 1 pm when 295 transactions would be needed). The overall estimated re-transmission probability, P_{CCN}, is estimated as:

$$P_{CCN} = \frac{\sum_{i=1}^{K} e_i}{\sum_{i=1} N_i} \qquad (2\text{-}3)$$

From the logfiles it is found that roughly 70% of the total number of transactions are rejected ($P_{CCN} \approx 0.7$). The reason for this is that the main part of the communication is directed to households corresponding to low-quality communication channels. By studying the logfiles it is also seen that some households sometimes are addressed about 70 times per hour while some houses are almost never the target of a re-transmission. Hence, this indicates a significant spread in quality among the 59 communication channels. Figure 2.4 will go further into this subject.

2.4 Channel Performance Associated with Specific Cable-Boxes in the Grid

It is seen in Figure 2-2 that the studied low-voltage grid consists of six low-voltage cables connected to the sub station. Furthermore, a number of cable-boxes are connected to each cable (3, 4, 2, 2, 3 and 9 respectively). To each cable-box, a number of households are connected (typically 4 households per cable-box). The low-voltage lines going through the cable-boxes 444 and 407 connects 16 respective about 20 houses. The other lines have at most 12 households connected.

In this section we are interested in the quality of the communication channels associated with a specific cable-box. To get quantitative results for a specific cable-box, we calculate P_{cb}, similar to (2-2), as the average value of the estimated channel impairment indicators to the corresponding households. As an example; assume that four households are connected to a specific cable-box and that the corresponding channel impairment indicators are P_a, P_b, P_c, and P_d respectively. The parameter P_{cb} for that specific cable-box is then calculated as $P_{cb}=(P_a+P_b+P_c+P_d)/4$.

Figure 2-6 shows one graph for each low-voltage line. Each graph shows the average channel impairment indicator for each of the cable-boxes connected to the corresponding low-voltage line. The cable-boxes are sorted after increasing distance to the sub station. Estimates are shown for a week in February and the parameter P_{cb} above is averaged during a day, denoted $P_{cb,av}$.

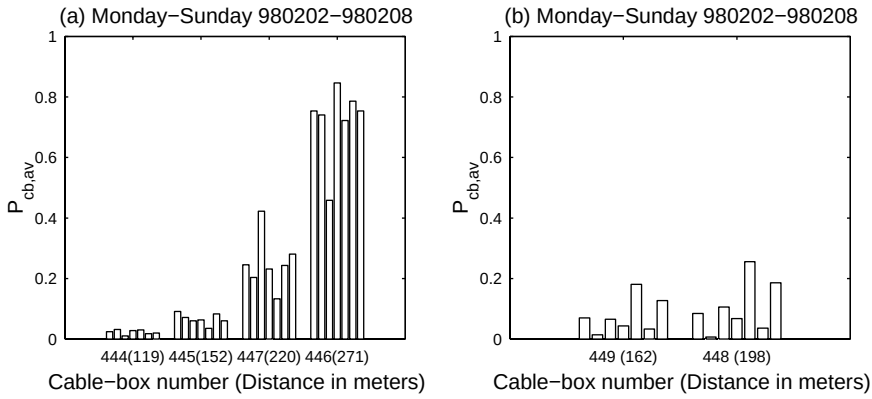

FIGURE 2-6 Continued on next page.

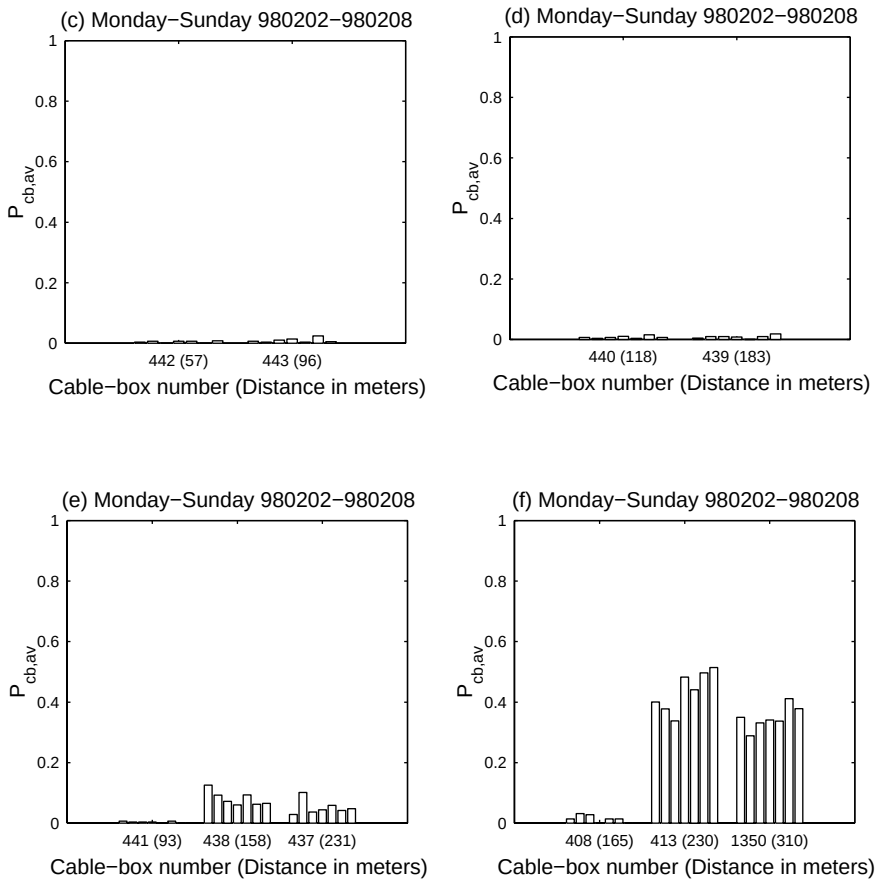

FIGURE 2-6 The average of the channel impairment indicators associated with each cable-box in the grid (24-hour average). Each graph shows the cable-boxes associated with each of the six low-voltage lines connected to the sub station. The bar to the left corresponds to Monday and the bar to the right corresponds to Sunday.

The graphs show that most cable-boxes are associated with relatively good channels, while some have significantly worse performance. An important question is why this behavior occurs. Known facts is that the low-voltage lines corresponding to graph (a) and (f) serves more houses than the other four and the distance of these low-voltage lines is also longer than the others.

Figure 2-7 shows the same as Figure 2-6, but now the cable-boxes are sorted after the distance to the sub station. It shows that, in general, a high level of channel impairments can be expected at large communication distances. This is reasonable, since a larger distance normally imply a larger signal attenuation and/or degradation. However, the figure also shows that some cable-boxes, e.g., 437 function well despite the long distance. The problem is therefore not only the distance but rather the combined effect of distance, signal attenuation, signal degradation and interference level at the receiver.

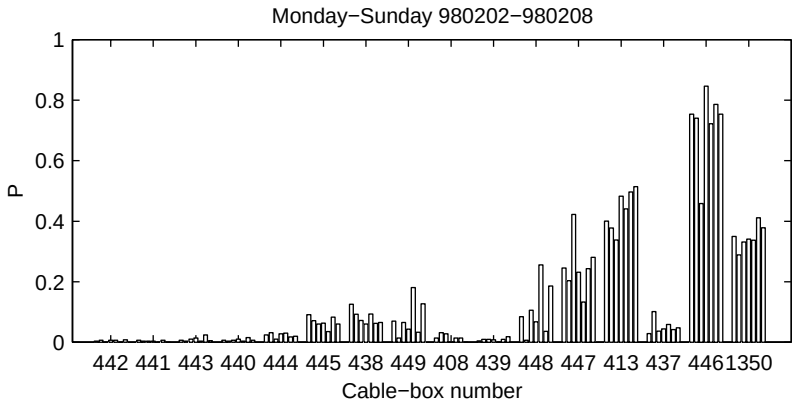

FIGURE 2-7 The average of the channel impairment indicators associated with each cable-box in the grid (24-hour average) for a week in February. The cable-boxes are sorted after increasing distance to the sub station.

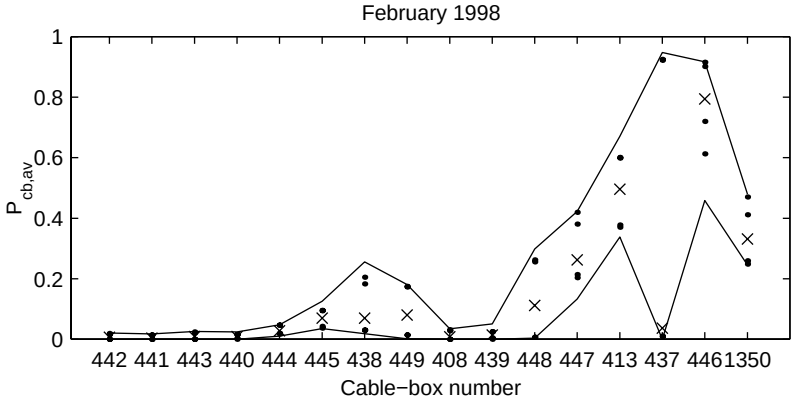

FIGURE 2-8 The average of the channel impairment indicators associated with each cable-box in the grid (24-hour average) for all estimated values in February. Shown is for each cable-box during February, the median for each cable-box (shown with crosses), the minimum and maximum values (shown with lines) and the three largest and the three smallest values (plotted with dots). The cable-boxes are sorted after increasing distance to the sub station.

In Figure 2-7 it is seen that the performance associated with a certain cable-box is about the same each day, i.e., it varies around an average level. Figure 2-8 shows all collected data in February. The figure indicates that the quality of the channels, in average, is within a rather small interval. This figure also indicates that impairments exist that make the channel quality vary around an average level. Cable-box 437 is an exception, the collected data shows that it is only a couple of samples that has a value significantly above 0.10 and these values are sequenced in time. Some impairment existed during a period of a couple of days that disturbed these receivers.

2.5 Load Profile

We may define a load as a device connected to the low-voltage grid. A load interferes with the power-line communication in different ways. The interference caused by the load can disturb the receiver, and the input impedance of the load can alter the signal attenuation/degradation of the channel.

The collected meter data gives the so-called load profile, which is equivalent to the energy used in the Påtorp area at different times. By comparing the load profile with the average of the estimated channel impairment indicators it is possible to study the influence of loads on the quality of the communication channels.

2.5.1 Load Profile and Communication Channel Impairments

Since the meter values are only read on an hourly basis it is not possible to make reliable conclusions for a single household. The reason is that communication to a specific household is only in progress during a short time, just enough to collect the meter data, and these data says little about the load during the (short) time interval when the household was accessed. Figure 2-9 shows the average of the estimated channel impairment indicators, *P,* together with the load profile of the area for a week in March.

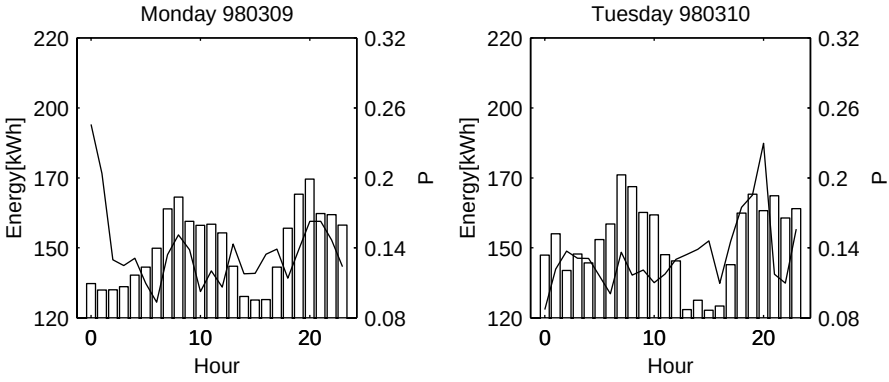

FIGURE 2-9 Continued on next page.

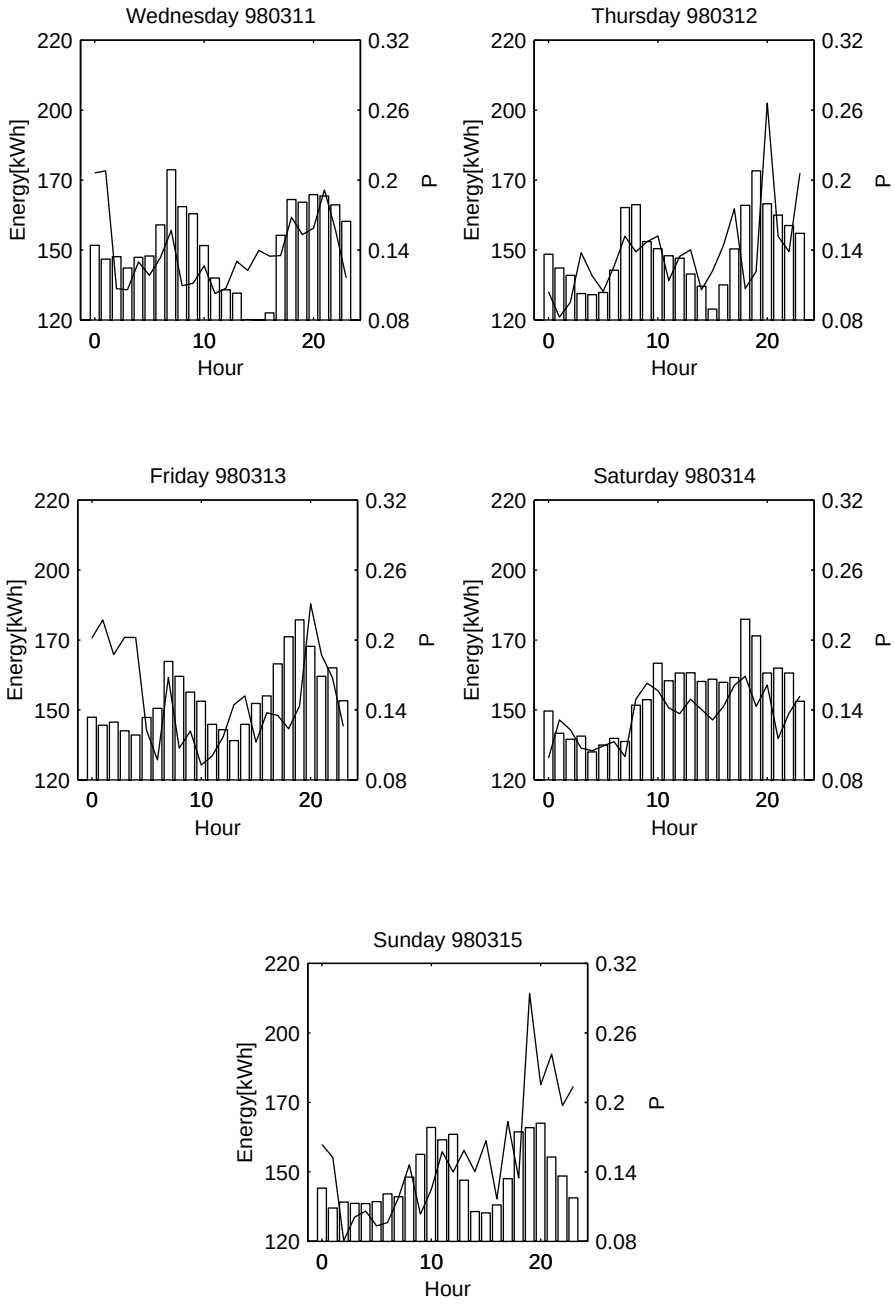

FIGURE 2-9 The average of all channel impairment indicators, *P*, and the load profile during a week. The load profile is shown with bars and the parameter *P* as a line.

The figure shows that peaks in the load profile occur in the morning and in the evening. During the weekend the morning peak is delayed. The behavior shown is typical in a low-voltage grid consisting of only households.

It is also seen that in many cases when the energy usage is high the quality of the communication channels is low (the channel impairment indicators are high). This is as expected because when the energy usage is high, more devices are connected to the grid and hence more possible sources of impairments exist.

The relation between the two parameters is not linear because the dependence between the energy usage of a device and its impairment on the channel is not linear. Therefore the quality of the channels can be low even though the energy usage is low.

2.6 Conclusions

In this chapter, focus is on the quality of the communication channels in a specific low-voltage grid. By processing collected data, obtained from a running meter reading system (PLC-P) operating in the low-voltage grid, estimates of channel impairment parameters are obtained. Hence, the PLC-P system is not evaluated here, rather it is used to extract information that can be used for (large-scale) channel quality estimation. This study is based on collected data representing communication with 59 households (hence, 59 communication channels are considered), and the low-voltage grid is located in Ronneby, Sweden.

The overall average quality of the communication channels fluctuates more or less randomly for each hour within a day, and also for each day within a week. However, the average quality seems to vary around a level that corresponds to a re-transmission probability roughly equal to 0.15. By comparing the results for February and for May, it is seen that less variations are obtained for May, which indicates a seasonal behavior of the channel quality.

Large variations in the quality between the individual communication channels have also been found. Especially, for the considered low-voltage grid, low-quality communication channels have been found along two, of the six, lines leaving the transformer. A low-quality communication channel is normally the result of the combined effect of channel impairments such as signal attenuation, signal degradation and interference level at the receiver. However, based on the collected data, we are not able to decide which is the dominating impairment. From the results it is also seen that there is a clear tendency that the quality of a specific communication channel varies randomly around an "average quality level", which in turn depends on the path of the channel in the grid.

It is well-known that re-transmission methods can be used where real-time operation is not a critical issue and where the information bit rate is low (e.g., meter reading systems). A consequence of low-quality communication channels is that the main part of the communication is over these channels, since many re-transmissions are in general necessary to obtain reliability. The PLC-P system is designed for collecting meter values and it

uses a re-transmission method for this purpose. Hence, it takes some time until all the 59 meter values are collected. However, this time-delay is not critical in the current application.

The loads connected to the low-voltage grid can have a serious impact on the communication performance. In general a load can introduce several effects; it can, e.g., change the attenuation and/or the degradation of the information-carrying signals. Furthermore, a load can also introduce interfering signals. A general problem is that the set of active loads in a given time interval is random. Despite these difficulties it is interesting to study the level of channel impairments in relation to the amount of energy delivered to the grid (the so-called load profile). From the observed data it is hard to draw any definitive conclusions. However, a period of high energy consumption (typically mornings and evenings) in the grid have a tendency to decrease the channel quality. It is also observed that the quality of the channels can be low at nights, though the energy consumption is low. An explanation might be that the loads in this case generate severe interfering signals. To further explore the effect of loads in power-line communications a load designed for test purposes was moved to Påtorp. The impact of this specific load is described in the following chapter.

The investigations reported in this chapter can be characterized as an attempt to get an overview of some communication channel properties of the low-voltage grid. Though additional specific (small-scale) measurements have to be made, it is already clear that advanced communication methods must be used in forthcoming applications requiring high information bit rates. Key parameters are the available bandwidth and the corresponding signal-to noise ratio at the receiver. Several well-known communication methods are possible candidates for future use in power-line applications. Examples are OFDM-type methods [18], GMSK-type methods [33], and methods based on spread-spectrum techniques [41]. For a given application, parameters that will influence the choice of communication method are; the characteristics of the communication channel within the communication bandwidth, the required information bit rate, real-time demands and the required level of robustness.

CHAPTER 3

On the Effect of Loads on Power-Line Communications

3.1 Introduction

In the previous chapter we have studied some properties of specific channels in a specific low-voltage grid. As Section 2.5 indicates, the various loads connected to the power-line can decrease the quality of the communication channels. However, based on the collected data it can not be said how strong this influence is. To investigate this further a moveable load has been transported to the grid in Påtorp (for a description of this grid see Section 2.2.1). This load is designed by NESA A/S (a utility distributor in Denmark) and it consists of a set of industrial machines mounted within a container.

More specifically, the moveable load consists of a 65 kVA voltage source inverter, which drives a 40 kW induction motor, which drives a 48 kVA synchronous generator, supplying power to some 45 kW heaters. Inside the container there is also a 35 kVA welding unit. The energy usage of the load when all devices are active is roughly 68 kWh per hour. This can be compared with the total energy usage per hour shown in Figure 2-9.

The moveable load was connected to various places in the low-voltage grid in order to investigate how it affected the quality of the communication channels. It was placed in the sub station to see how it affected all channels, and in cable-boxes to see the influence on specific communication channels. Because the PLC-P system (see Section 2.2) uses one hour to access all households it was necessary to let the load be on during at least an entire hour without interruption. The results of these experiments are shown in Section 3.2.

An objective with these experiments has also been to measure the harmonic disturbances introduced in the grid by the load. The frequencies considered in this chapter are harmonics (of the 50 Hz mains signaling voltage) up to 2.5 kHz. This is described in Section 3.3.

3.2 The Influence of the Load on the Communication

3.2.1 The Influence of the Load when Connected to the Sub Station

The moveable load was first connected to the sub station, see Figure 2-2. By doing this it was made sure that the load influenced every message sent (received) from (at) the CCN.

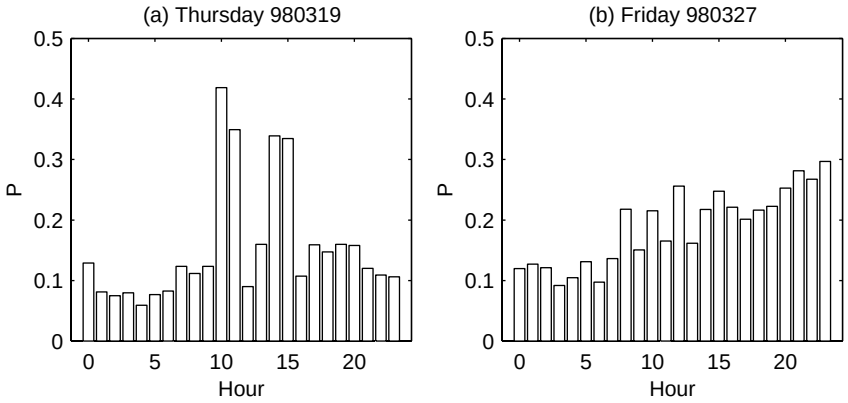

FIGURE 3-1 Average of all estimated channel impairment indicators, *P*. (a) shows *P* on March the 19th when the load was connected to the sub station. (b) shows *P* on March the 27th when the load was connected to cable-box 447.

Figure 3-1a shows the results from one of the experiments made, the value of *P* (see (2-2)) for Thursday March the 19th. This day the moveable load was active between 10-12 am and 2-4 pm. It is seen in Figure 3-1a that the channel impairments increased considerably when the load was active. *P* increased from 15% to 35-40%. It was also found that the number of houses requiring at least one re-transmission increased from about 10 to roughly 30 households when the load was active.

The results in Section 2.3 indicate that no high peaks, like those in Figure 3-1a, appear in the normal case when the moveable load is absent.

3.2.2 The Influence of the Load when Connected to a Cable-Box

To further investigate the influence of the load on the channel quality, the moveable load was moved to different locations in the grid.

An experiment was made on March the 27th. During this experiment the load was connected to cable-box 447, see Figure 2-2. This cable-box is located 220 m from the sub station. The corresponding low-voltage line, on which it is connected, serves 16 houses connected to four cable-boxes. First, the load was active for one hour at a time, between 8-9 am, 10-11 am and 12 am - 1 pm. Thereafter the load was active between 2-12 pm. All

the machines were used during the whole experiment except the welding unit, which only was on between 10-11 am, 12 am - 1 pm and 2-3 pm.

Figure 3-1b shows the value of P (see (2-2)) for March the 27th. This figure shows that at this location the moveable load did not degrade the channel quality as much as when it was located at the sub station. The average of the channel impairment indicators increased from 15% to 20-25%. One reason is the long distance between the load and the sub station. Hence, not so many communication channels are affected by the load. Only 25% of the households are connected to this low-voltage line so assuming the load does not cause too much interference in the other low-voltage lines the value of P should be lower.

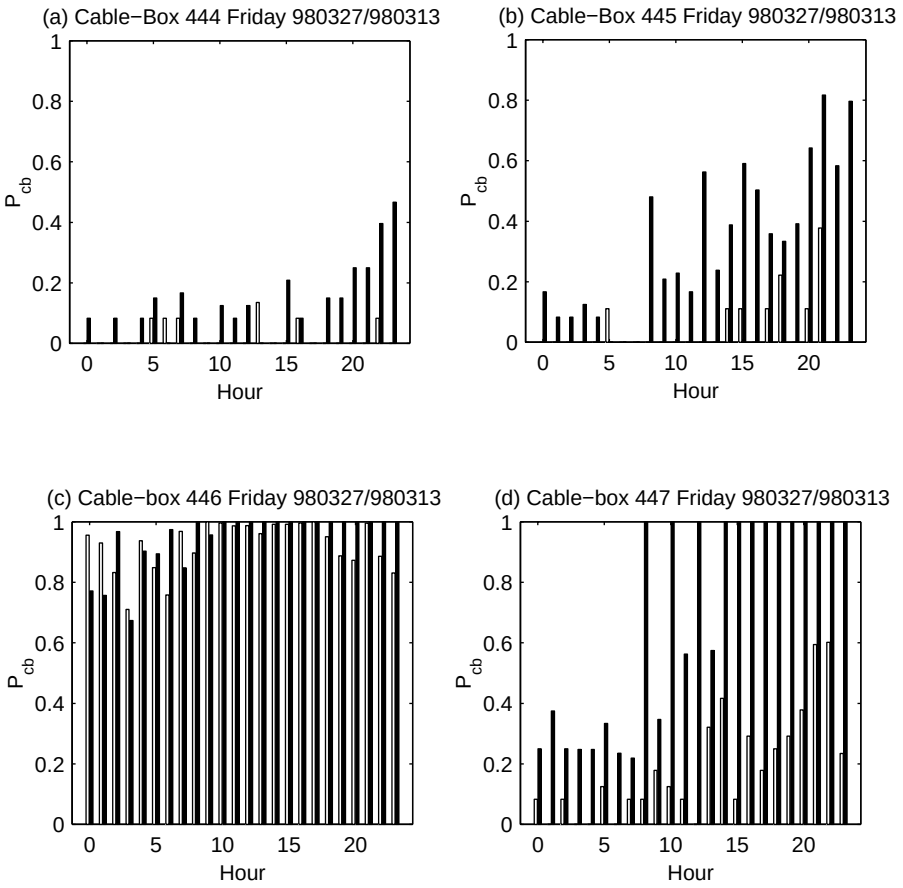

FIGURE 3-2 The average of the channel impairment indicators associated with each of the cable-boxes connected to the same low-voltage line as cable-box 447. The black bars correspond to March the 27th and the white bars to March the 13th.

Figure 3-2 shows the average of the channel impairment indicators associated with each of the cable-boxes (P_{cb}) connected to the same low-voltage line as cable-box 447. Samples are shown for March the 27th and the Friday two weeks before, when the load was

not connected. The figure indicates that when the load was active a severe degradation of channel quality occurred to households connected to the cable-box where the load was connected.

Cable-box 446 is placed on a longer distance to the sub station than cable-box 447 and represents a low-quality channel. As Figure 3-2 shows, this cable-box was a low-quality channel even when the load was not connected. The channels associated with the cable-boxes located closer to the sub station were also effected by the load. Peaks are shown for cable-box 445 at times when the load was active. A study of cable-boxes 442 and 443, which belong to another low-voltage line, shows that they are very little affected.

Even when the load was not active one heater was on warming the container. This can explain why P_{cb} seems to be higher even when the load is not active.

3.3 Measurements of the Harmonic Voltages and Currents Introduced by the Load

In order to show the harmonic disturbance introduced in the grid by the load, harmonic voltages and currents have been measured at various locations in the grid. The measurements have been carried out with an Oscillostore P513 [50] from Siemens and a Scop-Meter F99 [19] from Fluke. P513 is capable of measuring, e.g., voltage, current, power and harmonics (up to 2.5 kHz), has 12-bit resolution and a sample frequency of 12.8 kHz. F99 is a handheld 50 MHz oscilloscope with a vertical resolution of 8 bits and can measure *THD* (Total Harmonic Distorsion) [9].

The load is considered a three-phase unit but measurements show that the current drawn from the welding unit is asymmetrical. The highest average harmonic currents are drawn from phase two and this phase is used as a reference in this section. Test measurements have also shown that the highest harmonic voltages and currents of the load is located in the odd harmonics between 3 and 19. Therefore only the odd harmonics from 3 to 19 have been measured (the reason is also because of the limited storage capacity in the measurement device).

The measurements presented in the rest of this section are from the same experiment as described in Section 3.2.2. During this experiment the load was connected to cable-box 447, see Figure 2-2. First, the load was active for one hour at a time, between 8-9 am, 10-11 am and 12 am - 1 pm. Thereafter the load was active between 2-12 pm. In this section, only the time interval between 8 am and 15 pm is considered. All the machines were used during the whole experiment (considered in this section) except the welding unit, which was not on in the first time interval.

Note that the PLC-P system (at the time of trials) was 15 minutes before real time, therefore the measurements have been started 15 minutes earlier to comply with the time in PLC-P.

3.3.1 The Harmonic Disturbance Introduced in the Grid

Figure 3-3 shows the measured fundamental current and the odd harmonics (for orders up to seven) drawn by the load in the considered time interval. The current change when the welding unit was in use is approximately 20 A. This arose because the welding electrode had to be replaced each time it was used up.

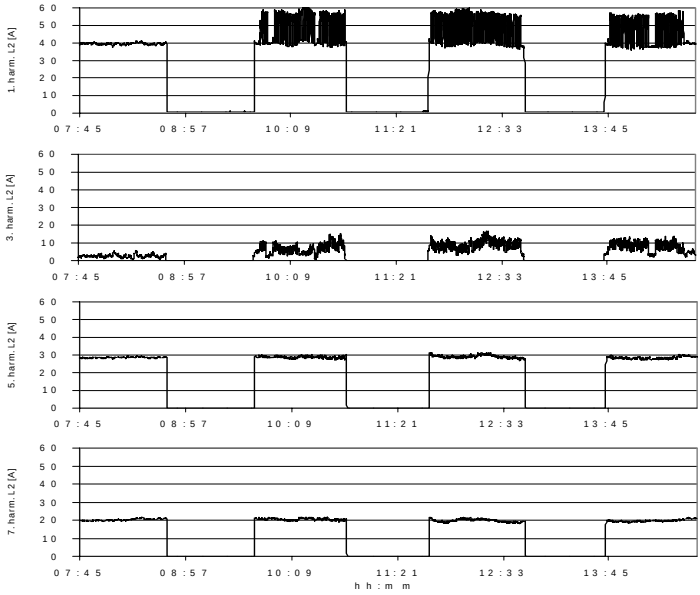

FIGURE 3-3 The measured fundamental current and the odd harmonic currents (for orders up to seven) drawn by the load. The x-axis shows time and the y-axis the current in Ampere.

The maximum amplitude for the fundamental current and the odd harmonic currents (for orders up to 19) in the time interval 8 am - 15 pm are shown in Figure 3-4.

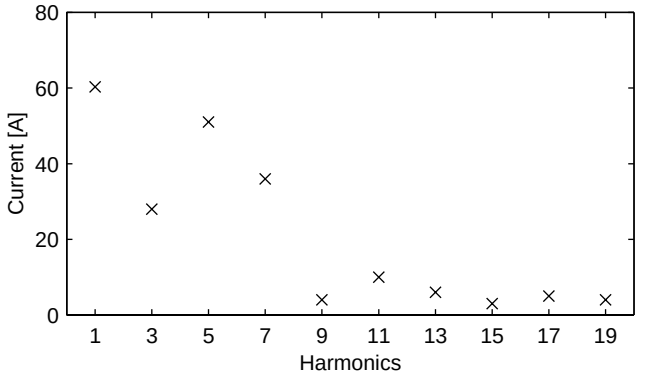

FIGURE 3-4 The maximum amplitude of the fundamental current and the harmonic currents (for orders up to 19).

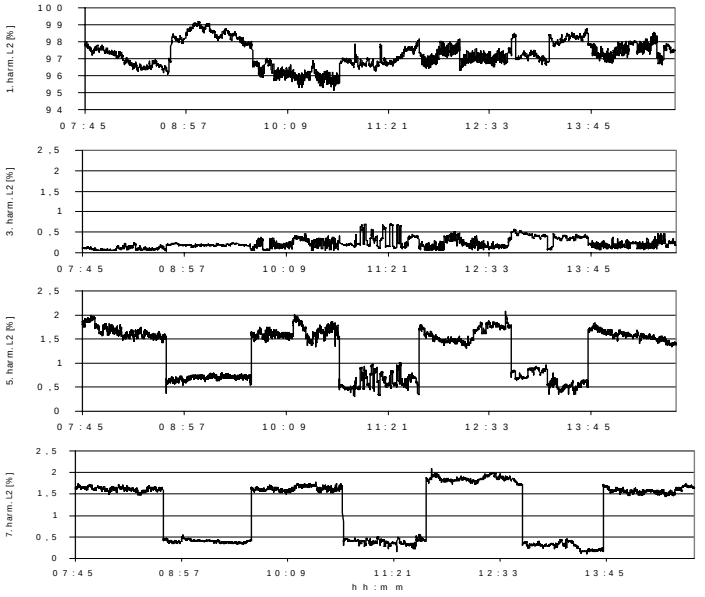

FIGURE 3-5 The measured fundamental voltage and the odd harmonics (for orders up to seven), shown as a percentage of the fundamental voltage. The x-axis shows time.

The corresponding voltages, as a percentage of the fundamental voltage, are shown in Figure 3-5. It is interesting to compare the harmonic voltage drawn by the load with the normal condition of a grid. A maximum allowed level of the harmonic voltage in a low-voltage grid is found in [9] and may be used as a reference. In [9] it is also given that the maximum Total Harmonic Distortion (*THD*) of the supply voltage (including all harmonics up to the order of 40) shall be less than or equal to 8%. The *THD* is calculated using the following expression:

$$THD = \sqrt{\sum_{h=2}^{40} (\mu_h)^2} \tag{3-1}$$

where μ_h is the relative amplitude of the hth harmonic related to the fundamental voltage.

The maximum amplitude of the harmonic voltages in the time interval 8 am - 15 pm and the harmonic voltage limit set up in [9] are shown in Figure 3-6.

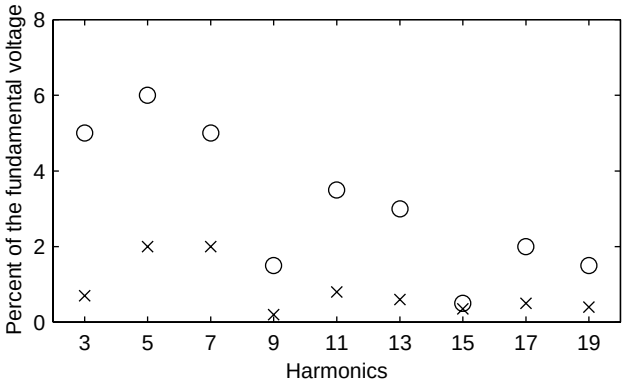

FIGURE 3-6 The maximum amplitude for each of the harmonic voltages shown as cross-marks and the harmonic voltage limit given in [9] shown as circles (odd up to the order of 19).

Figure 3-6 indicates that the harmonic voltages are beneath the required level given in [9]. Measurements of the total harmonic distortion showed that $THD \approx 6.9\%$, thus lower than the limit in [9].

3.3.2 The Propagation of the Harmonic Disturbances

Measurements have been done at other locations in the grid in order to show the propagation of the harmonic disturbances.

Figure 3-7 shows the fundamental current and the odd harmonic currents (for orders up to seven) measured in cable-box 406 (see Figure 2-2), which is located on another low-voltage line. The measurement was not started until 8.45 am instead of 7.45 am as in the previous section. The corresponding harmonic voltages are shown in Figure 3-8.

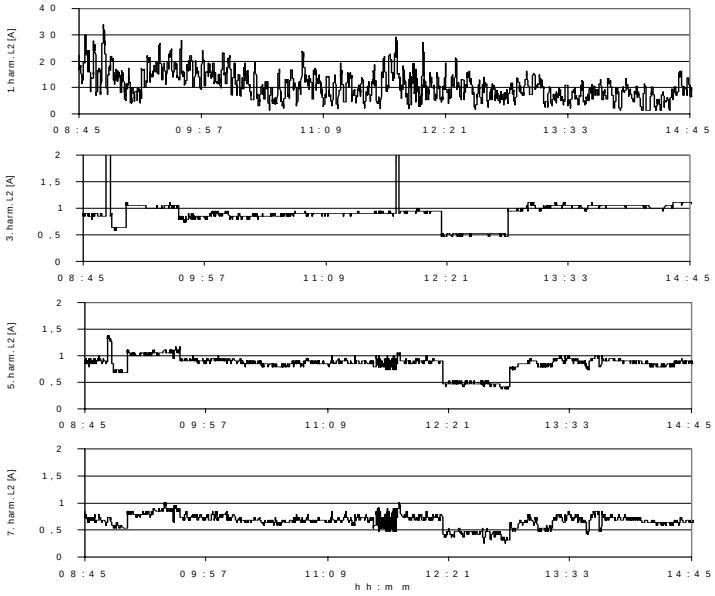

FIGURE 3-7 The measured fundamental current and the odd harmonic currents (for orders up to seven) in cable-box 406. The x-axis shows time and the y-axis the current in Ampere.

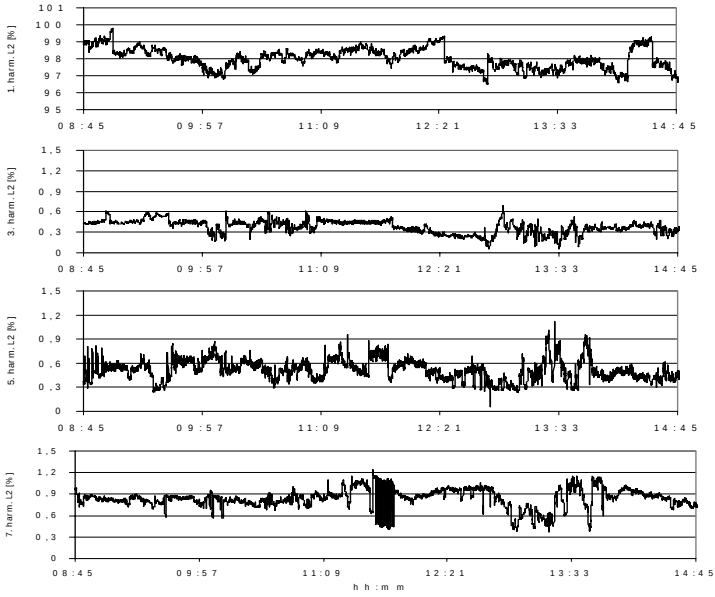

FIGURE 3-8 The measured fundamental voltage and harmonic voltages (for orders up to seven) in cable-box 406, shown as a percentage of the fundamental voltage. The x-axis shows time

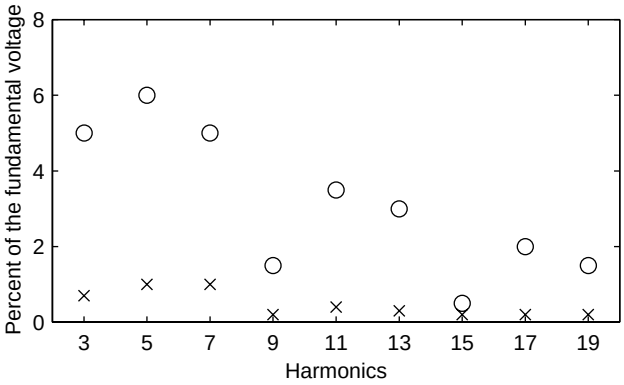

FIGURE 3-9 The maximum amplitude, in cable-box 406, for each of the harmonic voltages shown with cross-marks and the harmonic voltage limit given in [9] shown with circles (odd up to the order of 19).

The maximum amplitude for each of the harmonic voltages (for orders up to 19) and the harmonic voltage limit specified in [9] are shown in Figure 3-9, indicating that the harmonic voltages are beneath the required level given in [9]. Furthermore, the *THD* is found to be 5.6%, which is less than the 8% given in [9]. It is clear that the harmonic disturbances in cable-box 406 are smaller, than close to the load. Studies of the channel quality (as described in Chapter 2) at the other low-voltage lines showed that they were almost not affected by the load.

3.4 Conclusions

By processing collected data, obtained from a running meter reading system (PLC-P) operating in the low-voltage grid, the effect of a load on power-line communication is observed.

To investigate the influence of a specific load on the quality of the communication channels, a moveable load consisting of a set of industrial machines was connected to several locations in the grid. When the load was connected at the central communication node which is located at the sub station, all communication channels were directly influenced by the load, and the average channel impairment parameter increased significantly from roughly 0.15 to 0.40. When the load was connected at a cable-box, 220 m from the sub station, the corresponding parameter increased to roughly 0.25. This is reasonable since the negative effects of the load will be most noticeable on the communication channels which are close to the load. Hence, channels corresponding to other low-voltage lines are much less affected. However, households (i.e., channels) very close to the load experienced a dramatic decrease in channel quality.

Measurements have also been done on the harmonic disturbances introduced in the grid by the load. From the results it is not possible to draw any conclusions if it is the har-

monic disturbances that interrupts the communication or if it is the result of impairments in higher frequency bands. Measurements indicate that the injected harmonic voltage is lower than the limit in [9]. This means that the load source can not be referred to as an abnormal condition of a grid.

CHAPTER 4

Measurements of the Characteristics of the Low-voltage Grid

The performance of a communication system is directly related to the noise level at the receiver and the attenuation of the channel. If the noise level or the attenuation is too high then any communication system will have problems. In order to design a communication system, it is useful to have as much knowledge as possible of these parameters. If, e.g., the attenuation is known then a proper combination of coding, diversity and choice of modulation method can increase the performance of the communication system [41].

In this chapter we study the characteristics of some channels in a specific low-voltage grid. Measurements have been done at several locations in the grid, corresponding to these channels, to estimate the noise level and the attenuation of the power-line channel. The measurements have been carried out in the same area as the studies in Chapter 2 and Chapter 3. For a description of this grid see Section 2.2.1.

The disposition of this chapter is as follows

- Section 4.1 describes the measurement setup.
- Section 4.2 explains how the measurements have been performed.
- Measurements at frequencies up to 16 MHz are shown in Section 4.3.
- Measurements in the 20-450 kHz frequency band are shown in Section 4.4.
- Section 4.5 concludes this chapter.

4.1 Measurement Setup

The measurements have been carried out with an oscilloscope and a function generator. To protect the sensitive equipment from the damaging 220 V / 50 Hz signal used for power distribution, passive coupling circuits have been used. A schematic of the setup is shown in Figure 4-1 (compare with Figure 1-3).

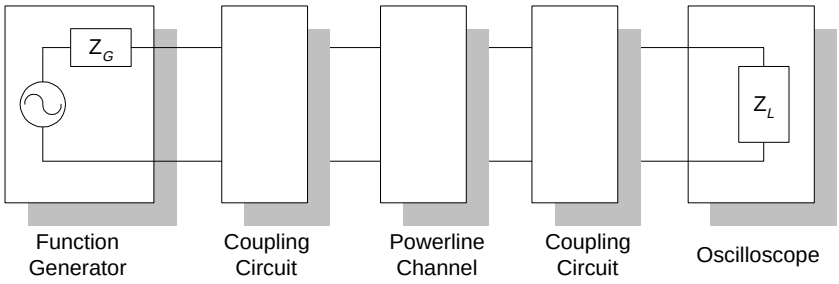

FIGURE 4-1 A schematic of the measurement setup.

Z_G is the output impedance of the function generator and Z_L the input impedance of the oscilloscope. These impedances have been set to 50 Ohm, which is supported by most measurement devices and also used in many communication applications.

In the next two sections we describe the measurement devices and the coupling circuits.

4.1.1 Measurement Devices

The oscilloscope that has been used is a Lecroy 9310CL Oscilloscope [29] with the following specifications

- 100 MS/s sample rate
- 1 MB memory per channel
- 2 channels
- 120 MB PCMCIA hard disk

The function generator is a Wavetek Model 193 with a bandwidth of 20 MHz and an option to generate a chirp signal over the entire frequency band.

The power to the devices has been taken from the same cable-boxes used for transmitting and receiving, but not at the same phase that has been used for communication.

4.1.2 Coupling Circuits

As coupling circuits, passive filters have been used. Figure 4-2 shows a schematic of the filter.

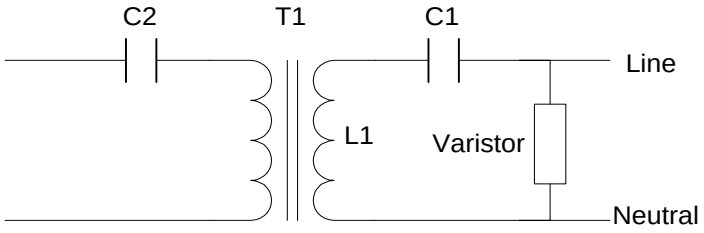

FIGURE 4-2 The coupling filter used to connect the measurement devices to the power-line.

The filter is a transformer isolated, differential mode, coupling circuit, and isolates the connected device from the power-line. The capacitor C1 and the self-inductance, L1, of the transformer, T1, form a series resonance circuit, a high pass filter to effectively remove the 50 Hz signal and its harmonics, but also other spectral components with low frequencies. The varistor serves as a surge protection unit, minimizing the effect of transients. Capacitor C2 prevents the transformer from shorting out the DC offset of the transmitter and has not been mounted when the filter has been used as a receiver. A description of how to design filters for the power-line is given in [17].

Two variations of this filter have been used, Filter A and Filter B, see Table 4-1. The cut-off frequency, specified in Table 4-1, is the frequency for which the transfer function magnitude is -3dB.

	Filter A	**Filter B**
C1	0.68 µF	0.1 µF
C2	10 µF	10 µF
L1	3.9 mH	1 mH
Cutoff frequency	3 kHz	25 kHz

TABLE 4-1 Component specification for Filter A and Filter B.

The squared magnitude of the frequency response of Filter A and Filter B is shown in Figure 4-3.

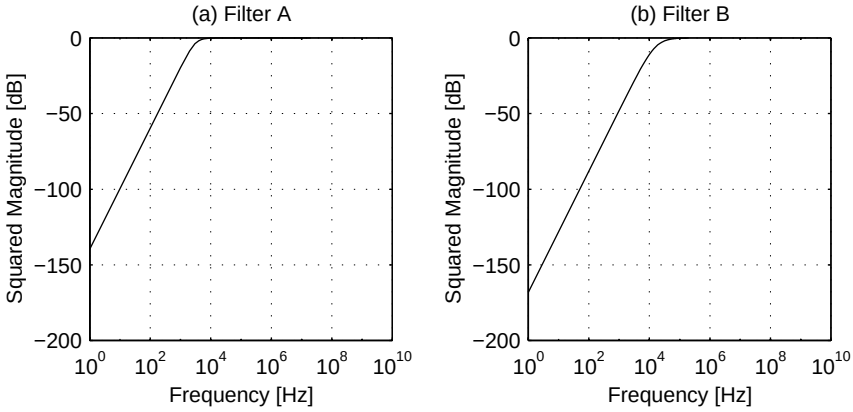

FIGURE 4-3 The squared magnitude of the frequency response of the filters called Filter A (a) and Filter B (b).

As the figure shows, both filters attenuate low frequencies, thus the 50 Hz signal and its harmonics are effectively removed (to a certain degree). Filter A has a flat frequency response above 10 kHz and is very well suited for the CENELEC A band (9-95 kHz) [8].

Filter B, to a greater extent, attenuates low frequencies to further increase the dynamic range of the receiver and is especially suited for frequencies above 100 kHz, e.g., the CENELEC B and C bands. Because the filter has a non-flat frequency response below 100 kHz the input impedance of the filter is affected in this region (the absolute value of the impedance increases). Test measurements have shown that the reduction in power of the noise and the signal on the power-line is small above 25 kHz. Below that frequency, the noise and the signal is scaled by a factor, which is the combination of the attenuation of the filter and the impedance mismatch between the filter and the power-line.

In all cases Filter B has been used to receive the signal and to measure the noise level. Filter A has been used to transmit signals with frequencies up to 450 kHz, while Filter B has been used to transmit higher frequencies.

The effect of aliasing has shown to be low when sampling at high rates (100 MS/s), since the noise level is low at high frequencies. Measurements in the frequency band up to 450 kHz have been done with a lower sample rate and in order to prevent aliasing, a high-pass filter attenuating frequencies above half the sample rate had to be used.

4.2 Measurement Techniques

4.2.1 Noise Measurements

As a measure of the noise level we have chosen to estimate the power spectrum, $R(f)$. The power spectrum describes how the power of a signal is distributed in the frequency domain [41], [42].

To estimate the power spectrum of a signal, N samples have been taken in the time-domain, at a sample rate of F_s samples (S) /second (s) during N/F_s seconds. By calculating the discrete fourier transform [42] on the samples it is possible to obtain an estimate of the power spectrum. Section 4.2.3 explains this procedure.

In all cases the number of samples have been set to 1 MB (the limit of the oscilloscope) and the sample rate and the window length have been set depending on the frequency band of interest.

4.2.2 Attenuation Measurements

The attenuation has been measured using a function generator, transmitting a chirp signal with constant amplitude (into a fixed impedance) at the sub station. A chirp signal is a signal that starts at a given frequency and continuously increase (or decrease) the frequency until it reaches the end frequency. The function generator has been set to generate this signal periodically with a sweep time of two minutes.

When the chirp signal arrives at the receiver it has been affected by the channel and has been attenuated. Because the attenuation vary in frequency, different parts of the chirp signal are attenuated differently and the received signal is a measure of the frequency response of the channel.

To estimate the attenuation, blocks of length N samples has been taken repeatedly of the received signal (at a much higher rate than the sweep rate of the function generator) at a sample rate of F_s samples/second. The power spectrum of each block has then been estimated with the technique described in Section 4.2.3. By taking the maximum of all blocks (for each frequency), we get an estimate of the attenuation for each frequency (assuming the power in the received signal is greater than the power of the noise). Because the blocks are much shorter (in time) than the length of the sweep time we get a fine-grain resolution of the frequency response. This process is the same method as transmitting a pure sinusoidal tone, calculating the power spectrum of this tone, changing the frequency to another tone, and so on until the frequency response for an arbitrary number of blocks has been measured. A similar method is used in [20].

The amplitude of the transmitted signal has been set to 2.5 V (into 50 Ohm) and the range of the chirp has been tuned to the frequency band of interest.

4.2.3 Theory of Power Spectrum Estimation

The power spectrum has been obtained by means of the discrete fourier transform. This section studies the theory behind this calculation, and follows [42] and [52]. In this section *f* is the normalized frequency, i.e., the original frequency divided by the sample rate. Assume that we have a sequence of *N* samples, $x(n)$, from a stationary random process, $x_a(t)$, with true power spectrum $R_{xx}(f)$. The discrete fourier transform, *X(f)*, of this sequence is calculated as

$$X(f) = \sum_{n=0}^{N-1} x(n)e^{-j2\pi nf} \tag{4-1}$$

The power spectrum of the stochastic process is estimated as

$$\tilde{R}_{xx}(f) = \frac{1}{N}\left|\sum_{n=0}^{N-1} x(n)e^{-j2\pi nf}\right|^2 \tag{4-2}$$

and is called a periodogram [42].

The variance of this estimation when *N* goes to infinity and the data sequence is a Gaussian random process is [42]

$$\lim_{N\to\infty} var[\tilde{R}_{xx}(f)] = R_{xx}^2(f) \tag{4-3}$$

Thus, the estimation is not a consistent estimate (the variance does not converge to zero) of the true power spectrum. To reduce the variance, various methods are used. A well-known technique is Welchs method [42], [52]. In Welchs method several periodograms are averaged to reduce the variance. The cost of this scheme is a reduction in frequency resolution.

Assume that we have a sequence of *N* samples, $x(n)$, from a stationary stochastic process. The *N* samples may be subdivided into *L* segments of *M* samples. Thus, the segments are represented as

$$x_i(n) = x(n + iD) \qquad i = 0, 1, ..., L-1, \quad n = 0, 1, ..., M-1 \tag{4-4}$$

The segments are allowed to overlap and therefore *D* is not necessarily equal to *M*.

Before computing the periodogram each segment is windowed with a function $w(n)$ (e.g., a Hamming window) to get the modified periodogram of each sequence *i*.

$$\tilde{R}_{xx}^{i}(f) = \frac{1}{MU}\left|\sum_{n=0}^{N-1} x(n)w(n)e^{-j2\pi nf}\right|^2, \; i = 0, 1, ..., L-1 \tag{4-5}$$

where U is

$$U = \frac{1}{M}\sum_{n=0}^{M-1} w^2(n) \tag{4-6}$$

The power spectrum estimate, $R_{xx}^{W}(f)$, in Welchs method is the average of the L modified periodograms:

$$R_{xx}^{W}(f) = \frac{1}{L}\sum_{n=0}^{L-1} \tilde{R}_{xx}^{i}(f) \tag{4-7}$$

The expectation and the variance (no overlap) of this estimation is [42]:

$$var[R_{xx}^{W}(f)] = \frac{1}{L}R_{xx}^{2}(f) \tag{4-8}$$

$$E[R_{xx}^{W}(f)] = \int_{-1/2}^{1/2} R_{xx}(\theta)W(f-\theta)d\theta \tag{4-9}$$

where

$$W(f) = \frac{1}{MU}\left|\sum_{n=0}^{M-1} w(n)e^{-j2\pi fn}\right|^2 \tag{4-10}$$

As $N \to \infty$ and $M \to \infty$ the mean converges to the true power spectrum, $R_{xx}(f)$, and the variance converges to zero, which makes the estimate consistent.

The expectation of the estimation, (4-9), for a finite sequence contains a bias. This is seen if *W(f)* and *U* are substituted into the expectation.

$$E[R_{xx}^{W}(f)] = \frac{1}{\sum_{n=0}^{M-1} w^2(n)}\int_{-1/2}^{1/2} R_{xx}(\theta)\left|\sum_{n=0}^{M-1} w(n)e^{-j2\pi(f-\theta)n}\right|^2 d\theta = R_{xx}(f)*W(f) \tag{4-11}$$

The result shows that the true power spectrum is convoluted with the fourier transform of the window function and the scaling factor is

$$\frac{\left|\sum_{n=0}^{M-1} w(n)\right|^2}{\sum_{n=0}^{M-1} w^2(n)} \tag{4-12}$$

if the window is narrow compared to the distance, in frequency, to surrounding spectral peaks [52].

In this thesis we have used Welchs method to estimate the power spectrum and the scaling factor has been compensated for on all data.

4.3 Outdoor Measurements in the 1-16 MHz Frequency Band

In this section we study the characteristics of the power-line channel in the 1-16 MHz frequency band. The interest in this frequency interval has increased because of the assumed lower and more stable noise level in this frequency band. Another reason is the demand for higher bit rates, which suggests a wide bandwidth.

Chapter 2 showed that the quality of the channels in this grid varies depending on the location in the grid (among other factors). In this section we study one low-voltage line with some low-quality channels and one with only high-quality channels. Note that the quality of the channels was estimated from the PLC-P system, which uses the CENELEC A band. The measurements in this section are located at much higher frequencies and the results in chapter 2 do not necessarily imply the same relative quality at these frequencies.

We have chosen to study cable-boxes 444, 447 (these are connected to the same low-voltage line) and 443, see Figure 2-2. 444 and 443 can (out of the results in Chapter 2) be considered as high-quality channels and 447 represents a low-quality channel.

4.3.1 The Noise Level

Figure 4-4 to 4-6 show examples of measurements of the power spectrum of the noise in the considered cable-boxes. Measurements are shown at two different phases, phase one and phase three. The number of samples is 1 MS, the window length 8192 S and the sample rate 100 MS/s.

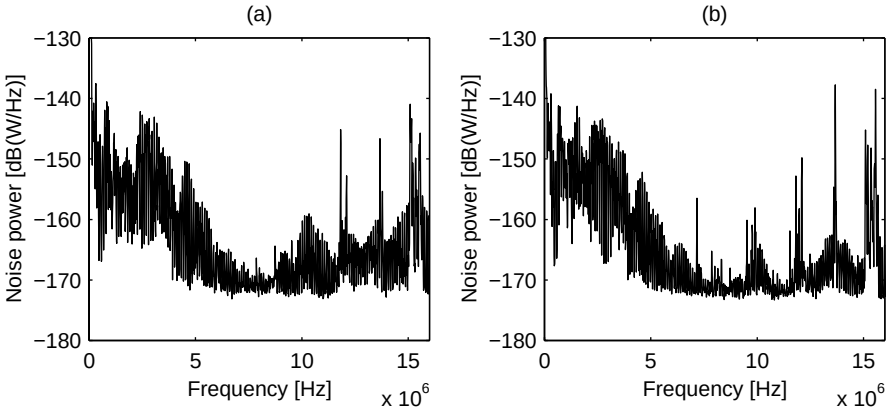

FIGURE 4-4 The power spectrum of the noise in cable-box 443 at phase 1 (a) and 3 (b).

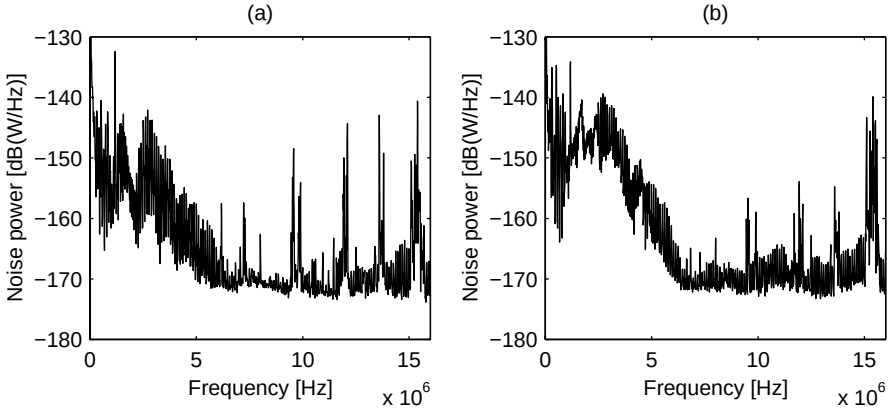

FIGURE 4-5 The power spectrum of the noise in cable-box 444 at phase 1 (a) and 3 (b).

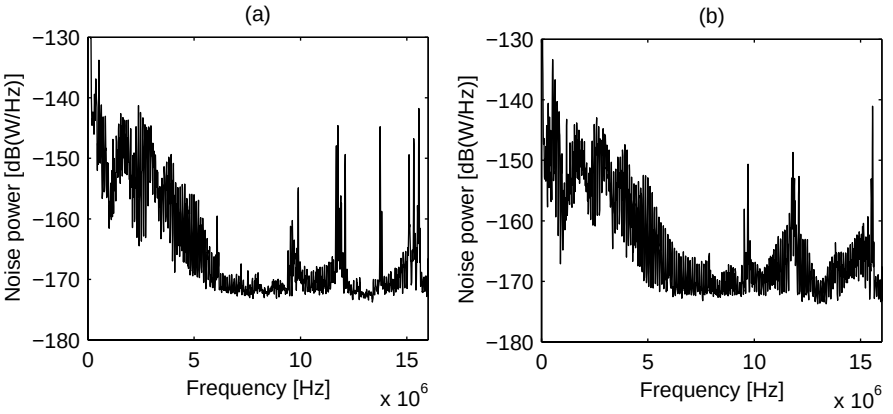

FIGURE 4-6 The power spectrum of the noise in cable-box 447 at phase 1 (a) and 3 (b).

The figures show that the noise level is rather similar in different cable-boxes although the actual levels differs. At 1 MHz the background noise is roughly -150 dB(W/Hz), it decays with frequency and at 7 MHz it is close to (and at some frequencies is) being out of dynamic range of the oscilloscope.

At higher frequencies, such as around 12 and 15 MHz, narrow-band frequencies may be found, probably corresponding to the frequencies used in broadcast radio. The location and strength of these disturbances varies depending on the actual cable-box.

Measurements in [15] and [20] show about the same behavior and levels as the measurements presented in this section, non-white noise that decays with frequency and narrow-band disturbances.

4.3.2 The Attenuation

To measure the attenuation of the power-line channel, the function generator has been connected to the sub station, transmitting a chirp signal in the range of 1 to 16 MHz with a magnitude of 2.5 V (into 50 ohm). The signal was then decoupled at each cable-box and the power spectrum of the received signal and the noise have been estimated with the technique described in Section 4.2.

Figure 4-7 - 4-9 show the power spectrum of the received signal and the noise in the selected cable-boxes. The bottom trace in each figure shows the average noise level measured at the receiver (as measured in the previous section), the trace in the middle is the maximum noise (calculated with the samples in the previous section) and the upper trace is the received signal. The transmitted signal has a power of -62 dB(W/Hz), the window length is 2002 S, the number of samples 1 MS, and the sample rate 100 MS/s. The figures show that the signal strength decays (the attenuation increases) with frequency and above 10 MHz it is in some cases hard to distinguish the received signal from the background noise.

The *SNR* in cable-boxes 443 and 444 are rather good, below 10 MHz it is above 20 dB. These two cable-boxes are located about 100 m from the sub station. Cable-box 447 is located on the same low-voltage line as cable-box 444, at a distance of 220 m from the sub station. This cable-box has a *SNR* up to roughly 25 dB lower than cable-box 444. This is reasonable since a longer physical channel imply a higher attenuation. Figure 4-7 - 4-9 also show that the actual *SNR* varies with frequency.

It is also clear that a lot of power is wasted in the sub station. When the signal reaches the first cable-box at least 25 dB (for high frequencies much more) has been lost. This might be, e.g., due to impedance mismatches between the transmitter and the power-line and other impedance mismatches within the sub station.

Measurements in [15] and [20] show a similar transfer function as we have measured, a frequency-selective channel, decaying with frequency.

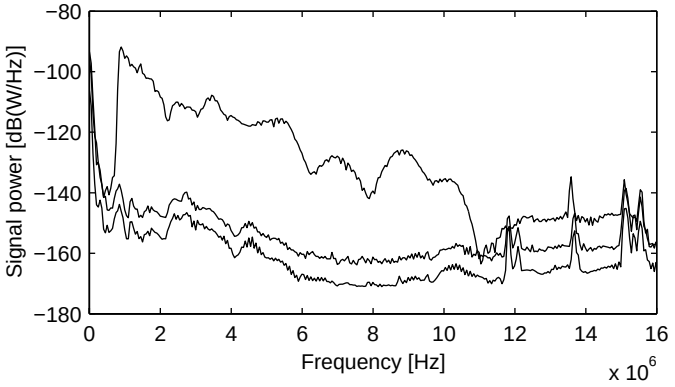

FIGURE 4-7 The received signal and the power spectrum of the noise in cable-box 443. The upper trace shows the received signal, the middle trace the maximum noise and the bottom trace the average noise level.

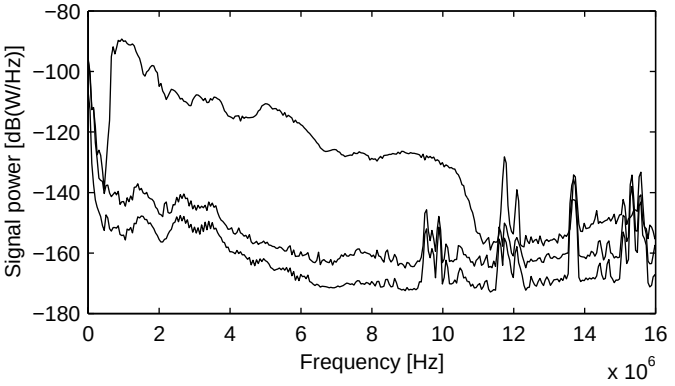

FIGURE 4-8 The received signal and the power spectrum of the noise in cable-box 444. The upper trace shows the received signal, the middle trace the maximum noise and the bottom trace the average noise level.

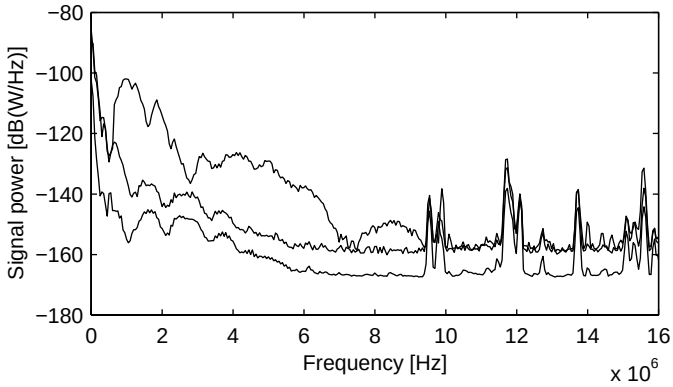

FIGURE 4-9 The received signal and the power spectrum of the noise in cable-box 447. The upper trace shows the received signal, the middle trace the maximum noise and the bottom trace the average noise level.

4.4 Outdoor Measurements in the 20-450 kHz Frequency Band

The frequency band up to 450 kHz is of particular interest because it enclose the allowed bandwidth in Europe [8] and also includes the bandwidth normally used in the United States and Japan. In this section we study the noise level and the attenuation of these frequencies for the same cable-boxes as in the previous section, cable-box 443, 444 and 447.

The results in Chapter 2 show that 443 and 444 can be considered as having relatively high-quality channels, on the contrary 447 is considered a low-quality channel. The PLC-P system, which is the system observed in that chapter, uses frequencies in the CENELEC A band (9-95 kHz), which is within the frequency band considered here. An objective with these measurements has also been to try to point out which parameters reduce the quality of some channels in the PLC-P system. Note that we do not evaluate PLC-P, but the quality of the channels that is used in the system.

4.4.1 The Noise Level

Figure 4-10 - 4-12 show the noise level in each cable-box considered. Measurements are shown for a weekday and a weekend. The number of samples is 1 MS, the window length 32768 S and the sample rate 10 MS/s. The measurements show that the noise level decays with frequency and is especially high in the frequency band up to 95 kHz, the CENELEC A band. At 25 kHz the noise level is about -110 dB(W/Hz). It is also seen that several narrow-band signals exist on the channel, with varying location and strength, depending on the actual cable-box. The measurements show that the noise level tends to be higher during the weekend, which might imply a time-varying effect of the channel.

Measurements up to 100 kHz are done in [24] and shows about the same noise level as presented here.

Cable-box 447 is considered a low-quality channel and Figure 4-10 - 4-12 show that the noise in the CENELEC A band seems to be higher for this cable-box than the other two, which could explain some of the problems with this channel experienced by the PLC-P system.

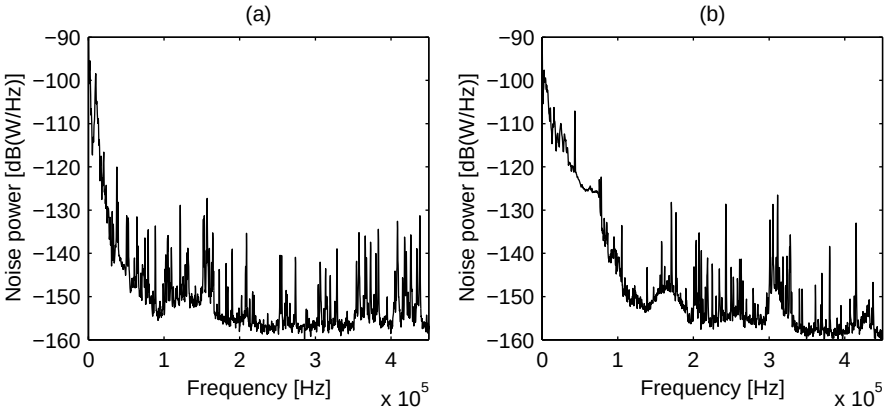

FIGURE 4-10 Examples of the power spectrum of the noise in cable-box 443 for a weekday (a) and a weekend (b).

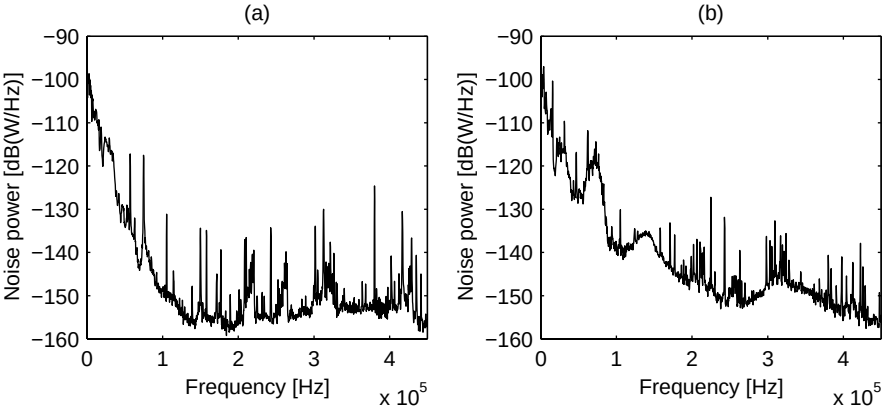

FIGURE 4-11 Examples of the power spectrum of the noise in cable-box 444 for a weekday (a) and a weekend (b).

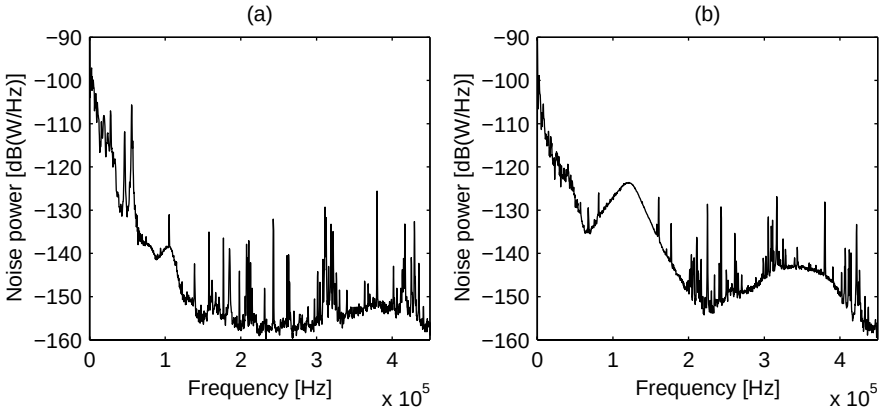

FIGURE 4-12 Examples of the power spectrum of the noise in cable-box 447 for a weekday (a) and a weekend (b).

4.4.2 The Attenuation

The attenuation of the power-line in this frequency band has been measured with the technique described in Section 4.2.2. A chirp signal from 20 kHz (this frequency has been chosen because of a limitation in the function generator) to 450 kHz with a magnitude of 2.5 V (into 50 Ohm) has been transmitted at the sub station and the signal has been received in each cable-box considered. The power of the transmitted signal is -45 dB(W/Hz). The window length used, is 10002 S, the number of samples 1 MS and the sample rate is 10 MS/s.

Figure 4-13 - 4-15 show the power spectrum of the noise and the received signal for the cases considered. The figures do not show the large variation in attenuation as in higher frequency bands, instead the transfer function is rather flat and without many notches. However, the transfer function in the frequency band up to 100 kHz varies with frequency and the *SNR* in this region is also lower. This could depend on the lower impedance in this region, which limits the input signal. Also here a lot of power is lost at the transmitter. Cable-box 443, which is located closest to the sub station, has lost about 30-60 dB of the power. This is more than the loss between cable-boxes 444 and 447 (the distance between these two is the same as between 443 and the sub station) and is probably due to impedance mismatches within the sub station.

The measurements also show that the low-quality channel in cable-box 447 has a higher attenuation than the other cable-boxes, which is reasonable due to the longer communication distance.

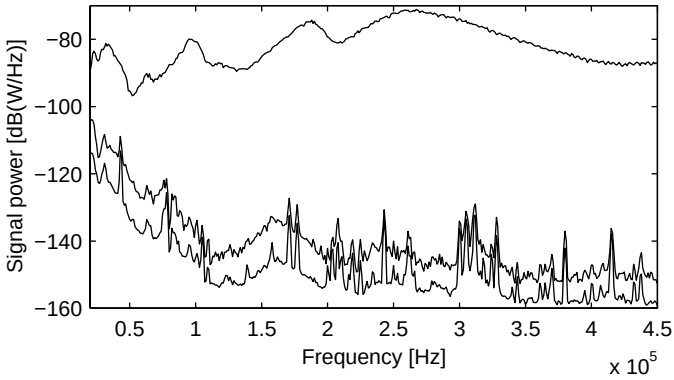

FIGURE 4-13 The power spectrum of the received signal and the noise in cable-box 443. The upper trace shows the received signal, the middle trace the maximum noise and the bottom trace the average noise level.

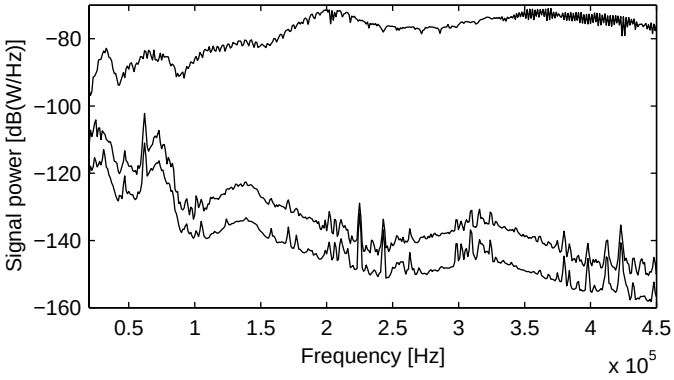

FIGURE 4-14 The power spectrum of the received signal and the noise in cable-box 444. The upper trace shows the received signal, the middle trace the maximum noise and the bottom trace the average noise level.

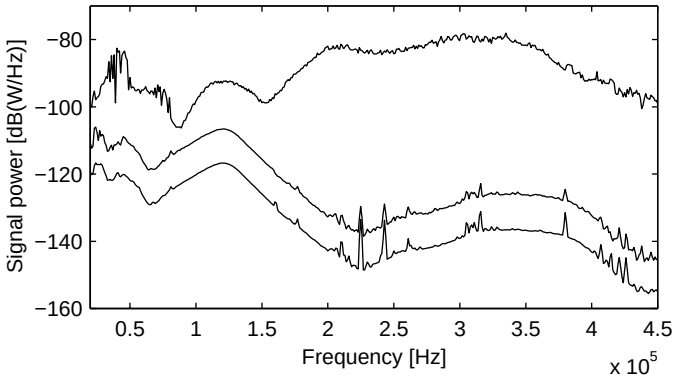

FIGURE 4-15 The power spectrum of the received signal and the noise in cable-box 447. The upper trace shows the received signal, the middle trace the maximum noise and the bottom trace the average noise level.

4.5 Conclusions

In this chapter we have seen several examples of the noise level and the attenuation of the power-line in a specific low-voltage grid. Although the number of measurements are limited it is clear that these parameters have to be taken into account when designing a communication system for the power-line channel.

Measurements of the noise level in the 20-450 kHz and 1-16 MHz frequency bands are presented. The measurements show that the noise is roughly -110 dB(W/Hz) at 25 kHz, is non-white, and decays with increasing frequency. Also several narrow-band disturbances have been found. This complicates the receiver and the effect of this noise on different receiver structures is studied in the next chapter.

The attenuation has been found to increase with frequency. Above 10 MHz it is hard to distinguish the received signal from the background noise, which limits the communication distance. The magnitude of the frequency response of the channel is not flat, except from decaying with increasing frequency, degradation in certain frequency bands occur, thus the channel is frequency-selective.

It has also been shown that a lot of power is wasted at the transmitter, probably due to impedance mismatches. This means that impedance matching should be attempted. To lower the output impedance of the transmitter could improve the performance because the input impedance at the sub station is often low.

Results from Chapter 2 has also been compared with the measured channel characteristics and it is found that a considered low-quality cable-box, at the time of measurements, was exposed to a higher noise level and higher attenuation than the others.

The measurements have also been compared to other measurements, which show similar behavior and levels. It is important to do measurements at several locations and in different countries, to increase the understanding of the power-line as a communication channel.

CHAPTER 5

Receiver Strategies for the Power-Line Communication Channel

5.1 Introduction

The previous chapter shows that the noise of the power-line channel can not be described as AWGN (Additive White Gaussian Noise) [41], which is the case in many communication models. In this chapter, we study the effect of this non-white noise on specific receiver structures.

Though the characteristics of communication channels located at different positions in the frequency domain can be quite different, many of the basic problems are the same. The coding and the modulation scheme has to be chosen in such a way that the received signal energy, with high probability, is large enough such that the decision algorithm of the receiver efficiently can combat the disturbances.

The technical solution to this problem becomes harder as the ratio between information bit rate and communication bandwidth is increased.

We apply Euclidean distance arguments to coded signal sequences in an attempt to quantify some effects of additive non-white gaussian noise on minimum Euclidean distance receivers. A simple case with AWGN and narrow-band disturbances is considered. Two receiver structures are studied, and compared with respect to robustness against narrow-band disturbances. The reason we have chosen to study the Euclidean distance is its relation to the error probability.

Convolutional coding, a fixed set of transmitter waveforms, and a frequency selective communication channel are some underlying assumptions.

5.2 Assumptions and the Communication System Model

Figure 5-1 shows a model of the communication system considered in this chapter, see [1], [41].

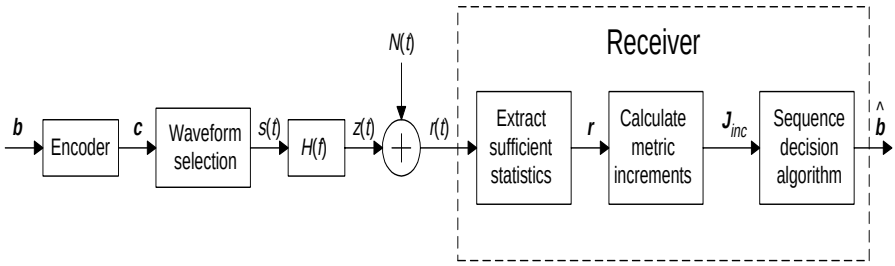

FIGURE 5-1 A model of the communication system considered in this chapter.

In this figure, ***b*** denotes the sequence of information bits having bit rate R_b bit/s. ***c*** denotes the sequence of coded binary symbols, and it is assumed that the encoder outputs an n-tuple of coded binary symbols as a response to an input k-tuple of information bits. Hence, the rate of the encoder is k/n. As a result of the n-tuple of coded bits (or blocks of n-tuples), a waveform is selected and transmitted through the communication channel. If there is memory in the waveform selection unit (e.g., continuous phase modulated signals), then the selection of transmitted waveforms is also a function of previously coded binary symbols.

There are several issues that have to be considered when designing the set of information carrying waveforms. One important parameter is the bandwidth allowed for communication, here denoted by W. Other important parameters are the channel characteristics, e.g., coherence time (the time-variance of the characteristics) and transfer function. The signaling rate is $R_s=1/T_s$, where T_s denotes the time interval between successive transmissions and it is closely related to the communication bandwidth, the information bit rate, the rate of the encoder, and by the choice of modulation method (set of waveforms).

In Figure 5-1, $H(f)$ models the combined effect of the power-line and the coupling and filtering units (at the transmitter and the receiver). In this chapter we assume that $H(f)$ is frequency selective within the communication bandwidth, but stationary in time over several signaling intervals T_s. Hence, the coherence time of the channel is assumed to be larger than T_s (interleaving/deinterleaving units are not explicitly shown in Figure 5-1). Furthermore, we assume that the transmitter has no knowledge of $H(f)$, i.e., no mechanism for delivering channel estimates from the receiver to the transmitter is assumed. Hence, it is here assumed that the transmitter uses a fixed set of waveforms (no adaptation to current channel characteristics is made in the transmitter). The signal $z(t)$ in Figure 5-1 is the information-carrying part of the input signal $r(t)$ to the receiver.

The additive disturbance $N(t)$ in Figure 5-1 is assumed to be a stationary non-white gaussian random process (at least within the coherence time of the channel) with (double-

sided) power spectrum $R_N(f) = N_0/2 + P_{narrow}(f)$ where $P_{narrow}(f)$ represents the narrow-band disturbances within the communication bandwidth W.

To arrive at simple expressions let us here assume that there are J equally strong narrow-band disturbances within the communication bandwidth W, and that the power in each disturbance, denoted by P_{nb}/J, is equally distributed over a frequency interval of length Δ, see Figure 5-2 (where J=5).

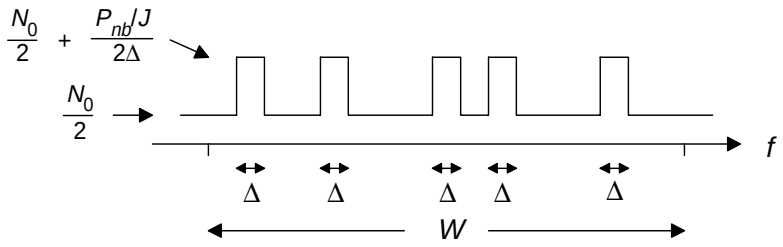

FIGURE 5-2 The power spectrum, $R_N(f)$, of the disturbance.

We define the parameter

$$x = \frac{P_{nb}/J}{2\Delta} \tag{5-1}$$

as a measure of the strength of each of the narrow-band disturbances.

The sequence $\boldsymbol{r}$ in the receiver in Figure 5-1 contains the sufficient statistics extracted from the received signal $r(t)$. Each element in the sequence $\boldsymbol{r}$, $\boldsymbol{r}$=(...,$\boldsymbol{r}[n\text{-}1]$, $\boldsymbol{r}[n]$, $\boldsymbol{r}[n+1]$,...), is in general a vector, and a new element is obtained every T_s seconds. The operations involved to obtain $\boldsymbol{r}$ typically consist of demodulation to baseband, bank of matched filters, and sampling with rate R_s.

For each element in $\boldsymbol{r}$ (or for a block of elements) a set of metric-increments, collected in the vector $J_{inc}[\boldsymbol{n}]$, is calculated. The specific kind of metric used by the decision algorithm depends on several factors such as, coherent or non-coherent demodulation, soft or hard decisions, the amount of channel knowledge, level of complexity etc. In many cases however, it is desired to use a maximum likelihood based sequence detection algorithm, implemented with a state oriented approach like the Viterbi algorithm (i.e., the accumulated metric is recursively updated by metric-increments), see e.g., [41]. After a certain decision delay, the receiver's decision is available.

5.3 Two Receiver Structures

In this section we study the operation and detection performance of ideal coherent maximum likelihood reception when the information-carrying signals are assumed to be dis-

turbed by additive colored gaussian noise. Though the realization of such a receiver can be impractical, it gives valuable insight in how a good suboptimal receiver could be designed. We try to quantify the gain obtained with such an ideal receiver, compared with a receiver which do not whiten the noise. Furthermore, the error performance of the ideal receiver is (by definition) a lower bound on the performance of any practical receiver.

In an ideal situation when the receiver has complete knowledge of the power spectrum $R_N(f)$, and of the (overall) transfer function $H(f)$, the sufficient statistics for detection can be extracted as shown in Figure 5-3, see [1], [41], [51], [54].

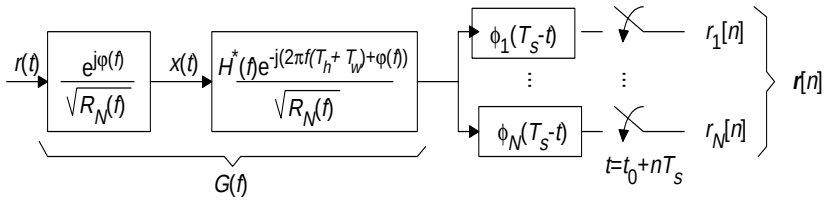

FIGURE 5-3 A model of the first part of the ideal receiver

In Figure 5-3, the received signal is first filtered in a noise-whitening filter. Since the filter is reversible within the communication bandwidth, no information is lost in this process. Hence, the noise in the signal $x(t)$ is white within the communication bandwidth. The next filter in Figure 5-3 is a channel and noise matching filter (T_h and T_w denotes the length of the truncated channel impulse response and whitening filter respectively, and * denotes conjugate). This filter is followed by a bank of filters which are matched to the basis functions required to describe the set of waveforms used in the transmitter. In Figure 5-3 it is assumed that the basis functions are time-limited to T_s s. If they are not, additional delay should be inserted in the filterbank (to make it causal). Note that the filters used in Figure 5-3 are bandpass filters operating within the communication bandwidth. A practical implementation often consists of demodulation to baseband, followed by lowpass filtering of the quadrature components. However, the method of implementation is not critical for the present discussion.

The assumption that the receiver knows the set of basis functions, used in the transmitter, is a mild assumption. However, assuming knowledge of $H(f)$ and $R_N(f)$ imply that mechanisms are implemented for providing the receiver with estimates of these functions within the coherence time of the channel (increased complexity). Furthermore, the noise-whitening filter introduces additional time-dispersion which can give severe intersymbol interference if the signaling rate R_s is too high.

In the next two sections we investigate the ideal receiver (whitening approach, see Figure 5-3), and also a suboptimal receiver which does not whiten the noise. The purpose is to try to evaluate, by simple arguments, the importance of the whitening filter and the channel matching filter.

5.3.1 The Ideal Receiver

For the ideal receiver we know that the Euclidean distance between the noiseless coded signal sequences in $x(t)$ (at the output of the whitening filter), are important. Let $x_i(t)$ and $x_j(t)$ denote two possible noiseless coded signal sequences after the whitening filter. As a measure of detection performance let us study the squared Euclidean distance between these two sequences. The reason that we have chosen the Euclidean distance as a measure of the performance is because it is related to the bit error probability [41]. It is assumed that the signal sequences are equal to zero outside an arbitrary long, but finite, time-interval. In the calculations below, it is also assumed that $H(f)$ and $R_N(f)$ are fixed during the corresponding time-interval.

The squared Euclidean distance between the two noiseless coded signal sequences $x_i(t)$ and $x_j(t)$ is,

$$D^2_{x_i,\,x_j} = \int_{-\infty}^{\infty} (x_i(t) - x_j(t))^2 dt \tag{5-2}$$

According to Parseval's relation the squared Euclidean distance may be expressed as,

$$D^2_{x_i,\,x_j} = \int_{-\infty}^{\infty} (x_i(t) - x_j(t))^2 dt = \int_{-\infty}^{\infty} \left|(X_i(f) - X_j(f))\right|^2 df = \int_{-\infty}^{\infty} \frac{\left|(Z_i(f) - Z_j(f))\right|^2}{R_N(f)} df \tag{5-3}$$

where $Z_i(f)$ and $Z_j(f)$ denote the Fourier transform of the corresponding noiseless coded signal sequences $z_i(t)$ and $z_j(t)$ (see Figure 5-1).

Let W_1 denote the frequency band where no narrow-band disturbances exist and W_2 the corresponding frequency band for the narrow-band disturbances. An expression for $D^2_{x_i,\,x_j}$ is then obtained as,

$$\begin{aligned} D^2_{x_i,\,x_j} &= \int_{W_1} \frac{\left|(Z_i(f) - Z_j(f))\right|^2}{N_0/2} + \int_{W_2} \frac{\left|(Z_i(f) - Z_j(f))\right|^2}{N_0/2 + \dfrac{P_{nb}}{2J\Delta}} \\ &= \int_{W_1} \frac{\left(N_0/2 + \dfrac{P_{nb}}{2J\Delta}\right) \cdot \left|(Z_i(f) - Z_j(f))\right|^2}{N_0/2 \cdot \left(N_0/2 + \dfrac{P_{nb}}{2J\Delta}\right)} + \int_{W_2} \frac{(N_0/2) \cdot \left|(Z_i(f) - Z_j(f))\right|^2}{(N_0/2) \cdot \left(N_0/2 + \dfrac{P_{nb}}{2J\Delta}\right)} \\ &= \frac{(N_0/2) D^2_{z_i,\,z_j} + \dfrac{P_{nb}}{2J\Delta} D^2_{z_i,\,z_j,\,N_0/2}}{(N_0/2) \cdot \left(N_0/2 + \dfrac{P_{nb}}{2J\Delta}\right)} = \frac{D^2_{z_i,\,z_j}}{N_0/2} \cdot \frac{1 + y \cdot \dfrac{P_{nb}}{N_0 J\Delta}}{1 + \dfrac{P_{nb}}{N_0 J\Delta}} \end{aligned} \tag{5-4}$$

where $D^2_{z_i,\,z_j}$ denotes the squared Euclidean distance between the sequences $z_i(t)$ and $z_j(t)$ and $D^2_{z_i,\,z_j,\,N_0/2}$ denotes the contribution to $D^2_{z_i,\,z_j}$ obtained from the frequency interval

within the communication bandwidth, where $R_N(f) = N_0/2$. The parameter y is defined as,

$$y = \frac{D^2_{z_i, z_j, N_0/2}}{D^2_{z_i, z_j}} \tag{5-5}$$

and is a measure of the relative distance contribution (in $z(t)$), due to the AWGN frequency intervals only. y is a parameter of i and j and is determined by the two signal sequences that the receiver compares.

The largest value of y is y=1 which imply that $D^2_{x_i, x_j} = \frac{D^2_{z_i, z_j}}{N_0/2}$ in this ideal case. Hence, no loss in Euclidean distance is then obtained since the narrow-band disturbances and the difference signal $z_i(t)$-$z_j(t)$ are located in disjoint frequency bands. Similarly, the smallest value of y is $y=0$, which represents the worst case for a given $R_N(f)$. Furthermore, from (5-4) it is seen that if the total power P_{nb} in the narrow-band disturbances is increased, then $D^2_{x_i, x_j}$ will approach the value $y\frac{D^2_{z_i, z_j}}{N_0/2}$. For small values of P_{nb}, the value of $D^2_{x_i, x_j}$ is not so sensitive to the precise value of y.

As a measure of the performance loss due to the narrow-band disturbances we calculate the squared Euclidean distance reduction, in dB. When no narrow-band disturbances exist the squared Euclidean distance is $\frac{D^2_{z_i, z_j}}{N_0/2}$ and if we divide (5-4) with this distance we get the reduction,

$$10\log\left(\frac{1 + y\frac{P_{nb}}{N_0 J\Delta}}{1 + \frac{P_{nb}}{N_0 J\Delta}}\right) \tag{5-6}$$

It is not possible to guarantee that $D^2_{x_i, x_j}$ always is large enough (the error probability low enough) since $H(f)$ and $R_N(f)$ are frequency dependent, random, and not known in advance. If, however, the fixed set of transmitter waveforms is designed to cover a large part of the communication bandwidth (frequency diversity), then signal energy will be delivered in all passbands of the current channel. This strategy will also promote a high value of y, especially if the communication bandwidth is large compared with the bandwidth occupied by the narrow-band disturbances ($=J\Delta$).

5.3.2 The Suboptimal Receiver

In this subsection it is assumed that the filter $g(t)$ in Figure 5-3 is chosen such that

$$G(f) = H^*(f)e^{-j2\pi fT_h} \tag{5-7}$$

Hence, it is matched to the communication channel, $H(f)$, but no whitening of the noise is made. This simplified receiver is shown in Figure 5-4.

This is a common receiver structure which is optimal in an AWGN environment, and the receiver in Figure 5-1 then finds the most probable signal sequence $z(t)$, which is closest to $r(t)$. The ideal receiver in the previous subsection finds the signal sequence which is closest to $x(t)$. To obtain a performance parameter in this suboptimal (but usual) case, we calculate the probability that the received signal $r(t)$ is closer (in signal space) to the coded signal sequence $z_j(t)$ than to $z_i(t)$, if $z_i(t)$ is the true signal sequence. The reason for doing this is that we want to compare with the corresponding probability for the ideal receiver, i.e., the probability that $x(t)$ is closer (in signal space) to $x_j(t)$ than to $x_i(t)$, if $x_i(t)$ is the true signal, which equals,

$$P_{x_i \to x_j} = Q\left(\sqrt{D^2_{x_i, x_j}/4}\right) \tag{5-8}$$

where $Q(x)$ is defined as $Q(x) = \frac{1}{\sqrt{2\pi}}\int_x^\infty e^{-y^2/2}dy, \quad y \geq 0$ [41].

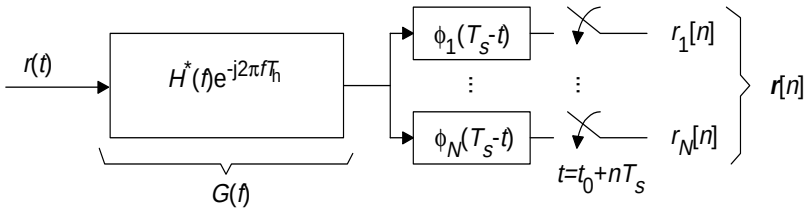

FIGURE 5-4 A model of the first part of the suboptimal receiver

For the suboptimal receiver specified by Figure 5-4, the probability that $r(t)$ is closer (in signal space) to $z_j(t)$ than to $z_i(t)$, if $z_i(t)$ is the true signal sequence, is

$$\begin{aligned}
P_{z_i \to z_j} &= P\left(\int_{-\infty}^{\infty}(r(t)-z_i(t))^2dt > \int_{-\infty}^{\infty}(r(t)-z_j(t))^2dt \,\middle|\, z_i(t)\right) \\
&= P\left(\int_{-\infty}^{\infty}(z_i(t)+N(t)-z_i(t))^2dt > \int_{-\infty}^{\infty}(z_i(t)+N(t)-z_j(t))^2dt \,\middle|\, z_i(t)\right) \\
&= P\left(\int_{-\infty}^{\infty}(N(t))^2dt > \int_{-\infty}^{\infty}(z_i(t)+N(t)-z_j(t))^2dt \,\middle|\, z_i(t)\right) \\
&= P\left(\int_{-\infty}^{\infty}N^2(t)dt > \int_{-\infty}^{\infty}(z_i(t)-z_j(t))^2dt + \int_{-\infty}^{\infty}N^2(t)dt + 2\int_{-\infty}^{\infty}N(t)(z_i(t)-z_j(t))dt \,\middle|\, z_i(t)\right) \\
&= P\left(D^2_{z_i,z_j} > 2\int_{-\infty}^{\infty}(N(t)(z_i(t)-z_j(t)))dt \,\middle|\, z_i(t)\right) = Q(D^2_{z_i,z_j}/(2\sigma))
\end{aligned} \tag{5-9}$$

where

$$\sigma^2 = \int_{-\infty}^{\infty} R_N(f)\left|Z_i(f) - Z_j(f)\right|^2 df \tag{5-10}$$

By using the properties of $R_N(f)$ in Figure 5-2, we obtain σ^2 as

$$\sigma^2 = \int_{W_1} (N_0/2)\left|(Z_i(f) - Z_j(f))\right|^2 + \int_{W_2} \left(N_0/2 + \frac{P_{nb}}{2J\Delta}\right)\left|(Z_i(f) - Z_j(f))\right|^2 = \tag{5-11}$$

$$(N_0/2)D^2_{z_i, z_j} + \frac{P_{nb}}{2J\Delta}(1-y)D^2_{z_i, z_j} = \frac{N_0}{2}D^2_{z_i, z_j} \cdot \left(1 + (1-y) \cdot \frac{P_{nb}}{N_0 J\Delta}\right)$$

and the desired probability as,

$$P_{z_i \to z_j} = Q\left(\sqrt{\frac{D^2_{z_i, z_j}}{2N_0\left(1 + (1-y)\frac{P_{nb}}{N_0 J\Delta}\right)}}\right) \tag{5-12}$$

As in the previous section we consider the Euclidean distance reduction as a measure of the loss in performance. A measure of the distance reduction for this suboptimal receiver, in dB, due to the narrow-band disturbances is given by

$$10\log\left(\frac{1}{1 + (1-y)\frac{P_{nb}}{N_0 J\Delta}}\right) \tag{5-13}$$

5.3.3 Comparisons of the Receiver Structures

Figure 5-5 shows the distance reduction for the ideal receiver, which is given by (5-6). The relation is shown for different values of *x*, which is the strength of the narrow-band disturbances, see (5-1). It is seen that as more narrow-band disturbances are introduced within the communication bandwidth (*y* decreases) the distance reduction increases. The reason is that the total power of the narrow-band disturbances, P_{nb}, increases. Also when *x* increases the reduction increases due to the same reason.

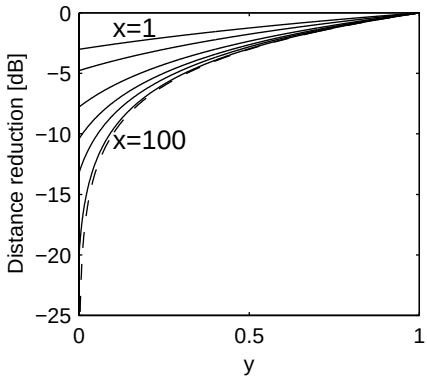

FIGURE 5-5 Distance reduction for the ideal receiver as a function of the parameters x and y defined in (5-1) and (5-5). Examples are shown when x = 1, 2, 5, 10, 20, 100. The dashed line shows an upper limit of the distance reduction.

Figure 5-6 shows the distance reduction (5-13) for the suboptimal receiver. The figure shows that the narrow-band disturbances hurt this receiver significantly harder than the ideal receiver. This is reasonable because no attempt has been made to compensate for the colored noise. We see that when the parameter y decreases (more and/or wider narrow-band disturbances are introduced within the communication bandwidth), the receiver gets a high distance reduction, which also reduces the error probability of the communication system.

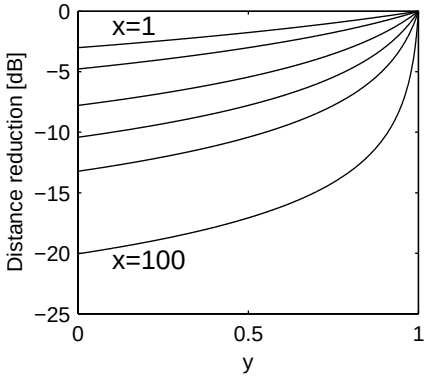

FIGURE 5-6 Distance reduction for the suboptimal receiver as a function of the parameters x and y defined in (5-1) and (5-5). Examples are shown when x = 1, 2, 5, 10, 20, 100.

By comparing the arguments in (5-8) and in (5-12) we get an indication of the difference in performance between the two studied receivers. The ratio between these arguments (expressed in dB) is

$$10\log\left(\frac{1+\frac{P_{nb}}{N_0 J\Delta}}{1+y\frac{P_{nb}}{N_0 J\Delta}}\cdot\frac{1}{1+(1-y)\frac{P_{nb}}{N_0 J\Delta}}\right) \tag{5-14}$$

Figure 5-7 shows the difference in performance between the optimal receiver and the suboptimal receiver.

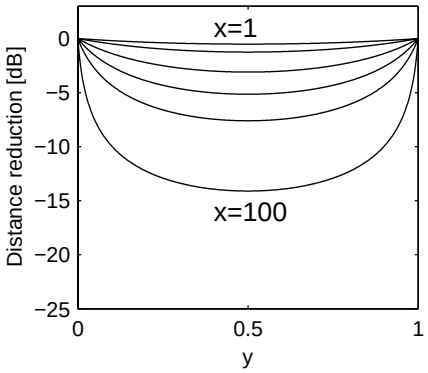

FIGURE 5-7 Difference in performance between the optimal and the suboptimal receivers as a function of the parameters *x* and *y* defined in (5-1) and (5-5). Examples are shown when *x* = 1, 2, 5, 10, 20, 100.

The figure shows that the difference becomes larger as the power P_{nb} of the narrow-band disturbances increases (*x* increases). Note that both receivers are identical if y=0 or if y=1, since both these situations can be considered to be AWGN cases. The figure also shows that if there is a large amount of narrow-band disturbances, even the ideal receiver will have problems.

5.4 Conclusions

Euclidean distance arguments have been applied to coded signal sequences in an attempt to quantify some effects of additive non-white gaussian noise on minimum Euclidean distance receivers. A simple case with AWGN and narrow-band disturbances was considered. The results illustrate the Euclidean distance loss due to the power level and the width of the narrow-band disturbances. Furthermore, the results indicate that a receiver which do not try to counteract the strong narrow-band disturbances can get significantly worse error performance than a receiver which use a whitening approach. Though the realization of an ideal receiver (using a whitening approach) might be impractical, it gives valuable insight in how a robust suboptimal receiver could be designed. If a fixed set of transmitter waveforms are used, and if they are designed to cover a large part of the communication bandwidth (frequency diversity), then signal energy will be delivered in all passbands of the current channel. This strategy can also promote a higher robustness

against narrow-band disturbances, for the two receiver structures studied, especially if the communication bandwidth is large compared with the bandwidth occupied by these disturbances. There are several possible modulation methods that could be considered as possible candidates for power-line communication, e.g., Orthogonal Frequency Division Multiplex (OFDM) [18], Continuous Phase Modulation (CPM), and Code Division Multiple Access (CDMA) [41]. However, many additional technical aspects should also be considered (besides regulatory issues). An example is the technical solution of the equalizer (e.g., channel matching filter) which depends on the choice of modulation method.

CHAPTER 6

A Modulation Method for the Power-Line Communication Channel

As we have seen in previous chapters the power-line channel is a harsh environment. The characteristics of the channel tend to vary in time, location and with different loads. The study in Chapter 2 describes this behavior.

One possible solution to overcome the problems with such a channel, is to use a robust modulation method. Furthermore, if the modulation method is able to handle unknown attenuation and unknown phase shifts, then the receiver can be simplified. The problem is to combine these requirements with the high bit rate needed in today's computer communications and the bandwidth limitation on the power-line channel.

The intention with this chapter is to present a modulation that may be a candidate to be used in a communication system for the power-line channel. Here, the focus is on the error probability properties, for the considered set of uncoded information carrying signals, when these are detected non-coherently. In a practical system (coded) these signals might be combined with a chosen encoder and interleaver structure. This is also discussed in the end of this chapter, using known properties of the power-line channel.

The disposition of the chapter is as follows:

Section 6.1 gives a general description of the modulation method. Section 6.2 shows computer-simulated results of the performance of the method and Section 6.3 theoretically validates the simulations. In Section 6.4 we combine the method with coding, diversity and the use of sub-bands. Finally Section 6.5 concludes the results.

6.1 The Modulation Method

Figure 6-1 shows a model of the communication system considered in this chapter, [1], [41], [54]. The transmitter transmits a signal, $s(t)$, on the channel, which is modeled as a

time-variant linear filter *H(f,t)*. The noise at the receiver, *N*(*t*), is modeled as AWGN (Additive White Gaussian Noise).

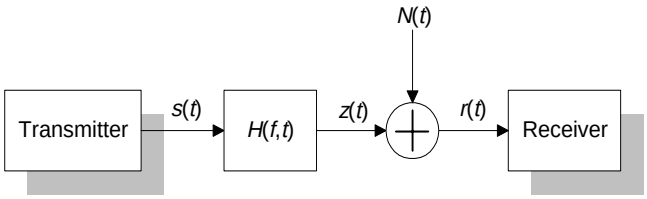

FIGURE 6-1 A model of the communication system.

The sequence of information bits have bit rate R_b b/s and the number of signal alternatives (also symbols), are denoted *M*, thus the symbol rate is $R_b/\log_2 M$ b/s. The bandwidth of the system is denoted *W* and it is assumed that the attenuation in this region is constant. *W* can here be interpreted as, e.g., a single sub-channel in an OFDM-type of arrangement. It is also assumed that the attenuation and the phase shift of the channel are unknown. Other important parameters are the symbol time $T_s=1/R_s$ and the bit time $T_b=1/R_b$, which defines the time needed for transmitting a symbol and a bit respectively.

Two modulation methods often used are orthogonal FSK (Frequency Shift Keying) and PSK (Phase Shift Keying) [41]. FSK (when non-coherently detected) is a robust method that works even when the phase and the attenuation are unknown. However, the attenuation must be constant within the communication bandwidth, which is assumed in this chapter. A disadvantage with FSK is that the bandwidth efficiency is low. Figure 6-2 shows the estimated bandwidth, *W*, of a FSK modulated signal with *M* signal alternatives. It is here assumed that the hcs (Half Cycle Sinusoidal) [41] pulse is used. The double sided mainlobe bandwidth (about 99.5% of the power) of this pulse is $3R_s$ and the frequency separation needed in this case to obtain orthogonality is $2R_s$ (other pulse-shapes are possible). Because each symbol is associated with a certain frequency the bandwidth will be large for large *M*.

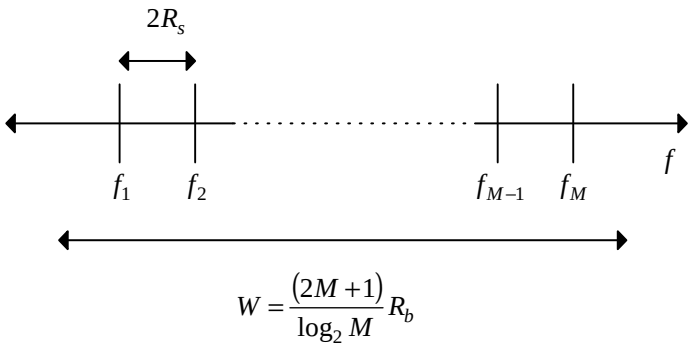

FIGURE 6-2 The estimated bandwidth of a FSK signal.

For pure PSK, the information is modulated in the phase (only one carrier is used) and thus it fails if the unknown phase, which is introduced by the channel, is not compensated for in the receiver. Figure 6-3 shows the estimated bandwidth of a PSK signal. Also here it is assumed that the hcs pulse is used. The bandwidth decreases when M increases (for a fixed R_b), thus the bandwidth efficiency increases with increasing number of symbols.

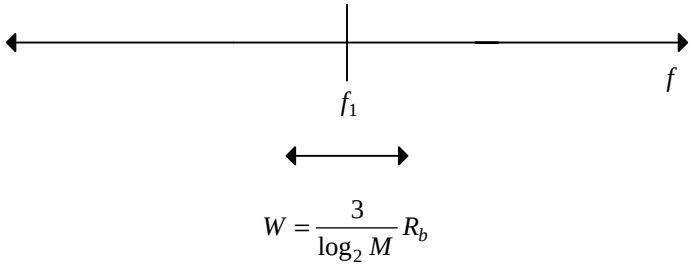

FIGURE 6-3 The estimated bandwidth of a PSK signal.

An extension of PSK, DPSK (Differential Phase Shift Keying) [41], [51] is sometimes used when the phase is unknown. The bandwidth efficiency of DPSK is high, the same as for PSK, but it requires the phase to be stable (or slowly varying) during at least two symbol intervals.

The modulation method investigated in this chapter is supposed to achieve robustness, a variety of bandwidth efficiencies and ease of implementation. It is designed to handle, to a certain extent, unknown attenuation and phase shifts. The method consists of one FSK modulated signal (with M_0 signal alternatives) and J PSK modulated signals, where each PSK signal is allowed to have an arbitrary number of signal alternatives. The use of the FSK signal is two-fold. It carries information, and it is also used in the receiver to estimate the received phase in the PSK signal. Because the receiver is not dependent on the attenuation and the phase of the channel, within the frequency band W, the system will work on channels where the attenuation and the phase shifts are unknown. Figure 6-4 shows the estimated bandwidth of the modulation method.

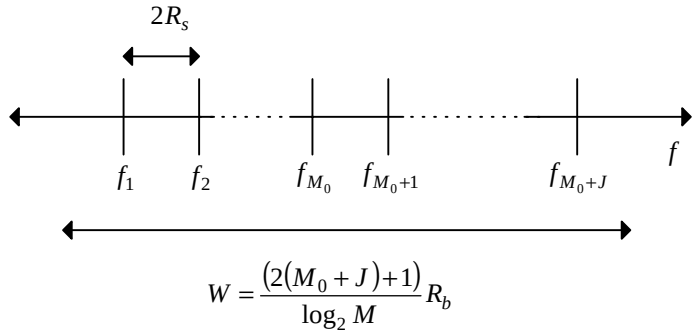

FIGURE 6-4 The estimated bandwidth of the proposed modulation method.

In the following sections each part of the communication system is described.

6.1.1 The Transmitter

The transmitter is shown in Figure 6-5. ***b*** is the sequence of information bits having bit rate $R_b=1/T_b$ bps. The bits are converted into one or more bit streams $\{\boldsymbol{b_0}, \boldsymbol{b_1}, ...\boldsymbol{b_J}\}$ by a serial to parallel converter and each stream is associated with one of the sub-modulation methods.

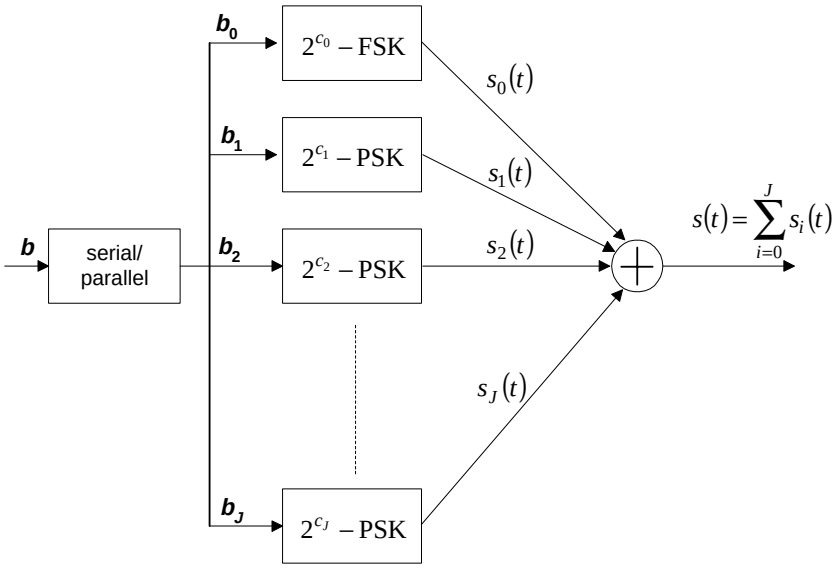

FIGURE 6-5 The transmitter.

A sub-modulation scheme, *i*, transmits c_i number of bits in each symbol interval, T_s, and thus has $M_i = 2^{c_i}$ different symbols or signals. In a symbol interval T_s, $c = \sum_{i=0}^{J} c_i$ bits are transmitted, hence the symbol rate equals $R_s=R_b/c$. The bit rate in each sub-sequence $\boldsymbol{b_i}$ equals c_iR_s and the total number of symbols is $M=2^c$.

In each symbol interval the signal $s(t)$ is the sum of the signals $\{s_0(t),.....,s_J(t)\}$ where

$$s_0(t) = \sum_{i=1}^{M_0} A_i g(t)\sqrt{2}\cos(2\pi f_i t + \varphi_{ref}),\ 0 \le t \le T_s \qquad (6\text{-}1)$$

where A_i is A or zero depending on the c_0-tuple of bits. Because $s_0(t)$ is a FSK signal only one of the M_0 frequencies is sent, so only one A_i may be non-zero.

The PSK-signals, $s_i(t)$, are described as,

$$s_i(t) = Bg(t)\sqrt{2}\cos(2\pi f_{M_0+i}t + \varphi_{ref} + \nu_i),\ 0 \le t \le T_s,\ i = 1, ..., J \qquad (6\text{-}2)$$

Depending on the c_i-tuple of bits, ν_i takes one of the phase values $\{\nu_{i,j}\}_{j=1}^{M_i}$. Hence, for i=1,2,....,J, $s_i(t)$ is an M_i-ary PSK signal with amplitude B and frequency f_{M_0+i}.

The reference phase, φ_{ref}, must be the same for all the (M_0+J) frequencies in the interval $0<t<T_s$. However, φ_{ref} is allowed to be different in different symbol intervals. The pulse-shape $g(t)$ is not specified but typically the half cycle sinusoidal (hcs) pulse may be used. The energy of $g(t)$, E_g, is assumed to be one and the frequency spacing is chosen such that an 2(M_0+J)-dimensional signal space is achieved, based on the M_0+J frequencies in (6-1) and (6-2).

As Figure 6-5 shows, a large number of different modulation systems may be described with this model. We will study three of the possible combinations:

- 2-FSK and 2-PSK. Denoted BB.
- 2-FSK and 4-PSK. Denoted BQ.
- 2-FSK, 2-PSK and 2-PSK. Denoted BBB.

The reason for choosing these specific schemes is their simple construction. We are trying to find alternative signal constellations, which eventually can be used combined with coding. Table 6-1 shows the bandwidth efficiency for the considered modulation systems compared to PSK and FSK (assuming the hcs pulseshape in all cases). As the table shows the bandwidth efficiency is better than FSK but smaller than PSK. This means that a larger amount of data can be transmitted with this system than with FSK, but to make a fair comparison it is needed to also consider the symbol/bit error probability.

M	**FSK**	**PSK**	**BB**	**BQ**	**BBB**
2	1/5	1/3	-	-	-
4	2/9	2/3	2/7	-	-
8	3/17	3/3	-	3/7	3/9

TABLE 6-1 The bandwidth efficiency for FSK, PSK and the investigated modulation methods.

6.1.2 Communication Channel

The model used for the communication channel is described in Section 1.3.6. It is here assumed that within the information signal bandwidth, W, the transfer function of the channel can be approximated as (see [23], [51])

$$H(f) = |H(f)|e^{j\beta(f)} \approx \alpha e^{j(\beta(f_c) - 2\pi(f - f_c)\tau_g)}, f_c - \frac{W}{2} \le f \le f_c + \frac{W}{2} \quad (6\text{-}3)$$

where $\alpha = |H(f_c)|$, τ_g is the group delay defined as $\tau_g = -\frac{1}{2\pi}\frac{\partial\beta(f)}{\partial f}\Big|_{f=f_c}$, $\beta(f_c)$ is the phase delay at the point $f=f_c$, and the center (or carrier) frequency $f_c = \frac{f_1 + f_{M_0+J}}{2}$. The attenuation is assumed constant within the communication bandwidth W and τ_g is assumed to be implicitly estimated by the receiver. It is assumed that W is small enough (T_s large enough) such that this model is valid. As a consequence, R_b must be low.

The noise is assumed to be AWGN [41] with double-sided power spectrum $N_0/2$.

6.1.3 The Receiver

The received signal, $r(t)$, (see Figure 6-1) in the first symbol interval, $\tau_g \le t \le \tau_g + T_s$, is

$$\begin{aligned} r(t) = {} & \alpha \sum_{i=1}^{M_0} A_i g(t - \tau_g)\sqrt{2}\cos(\omega_c t + \Delta\omega_i(t - \tau_g) + \varphi_{ref} + \beta(f_c)) + \\ & \alpha \sum_{i=1}^{J} Bg(t - \tau_g)\sqrt{2}\cos(\omega_c t + \Delta\omega_{M_0+i}(t - \tau_g) + \varphi_{ref} + \nu_i + \beta(f_c)) + N(t) \end{aligned} \quad (6\text{-}4)$$

where $\Delta\omega_i = 2\pi(f_i - f_c)$ and $\omega_c = 2\pi f_c$ [41]. Compare with (6-1) and (6-2).

To obtain a ML (Maximum Likelihood) receiver we first find the basis vectors. The receiver is then built of a parallel bank of crosscorrelators, which compute the projection of the received signal on each of the basis functions.

As basis functions for the signals we have (assuming the energy of the pulse $g(t)$ is one)

$$\begin{aligned} \phi_1(t) &= g(t - \tau_g)\sqrt{2}\cos(\omega_c t + \Delta\omega_i(t - \tau_g)), \tau_g \le t \le \tau_g + T_s \\ \phi_1(t) &= -g(t - \tau_g)\sqrt{2}\sin(\omega_c t + \Delta\omega_i(t - \tau_g)), \tau_g \le t \le \tau_g + T_s \end{aligned} \quad (6\text{-}5)$$

With trigonometric identities it can be shown that the correlation demodulator can be divided in two parts, first demodulation to baseband and then a set of filter banks.

The signal is demodulated to baseband by the block shown in Figure 6-6 and the responses to the signal $r(t)$ are

$$
\begin{aligned}
r_1(t) &= \alpha \sum_{i=1}^{M_0} A_i g(t-\tau_g)\cos(\Delta\omega_i(t-\tau_g) + \varphi_{ref} + \beta(f_c) - \varphi_d) + \\
&\quad \alpha \sum_{i=1}^{J} Bg(t-\tau_g)\cos(\Delta\omega_{M_0+i}(t-\tau_g) + \varphi_{ref} + \nu_i + \beta(f_c) - \varphi_d) + n_1(t) \\
r_2(t) &= \alpha \sum_{i=1}^{M_0} A_i g(t-\tau_g)\sin(\Delta\omega_i(t-\tau_g) + \varphi_{ref} + \beta(f_c) - \varphi_d) + \\
&\quad \alpha \sum_{i=1}^{J} Bg(t-\tau_g)\sin(\Delta\omega_{M_0+i}(t-\tau_g) + \varphi_{ref} + \nu_i + \beta(f_c) - \varphi_d) + n_2(t)
\end{aligned}
\tag{6-6}
$$

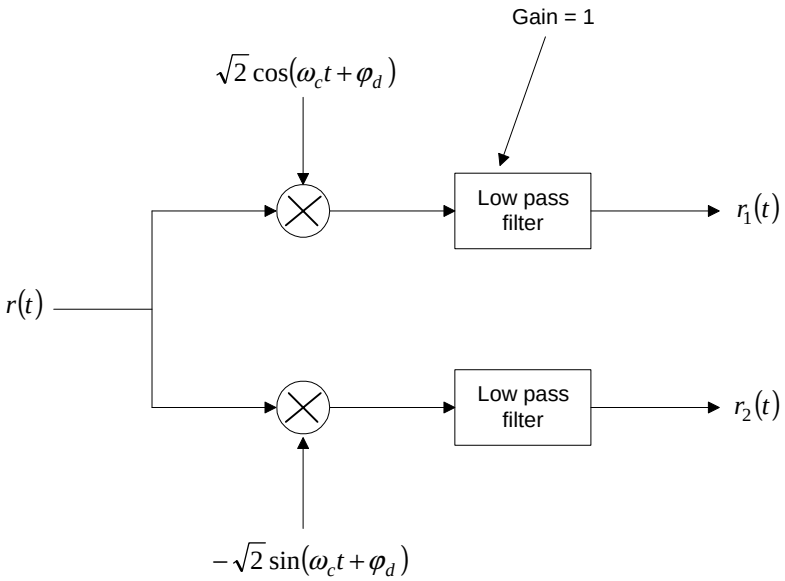

FIGURE 6-6 Demodulation to baseband.

The unknown phase φ_d is the introduced phase in the receiver. This allows an easy implementation of the receiver because no synchronisation is needed. A set of filterbanks is used to extract the decision variables. The filter bank for frequency f_1 is shown in Figure 6-7.

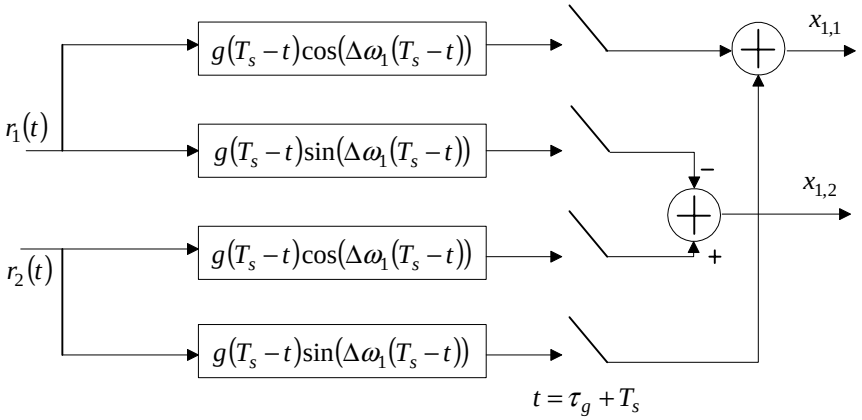

FIGURE 6-7 The filter bank for frequency f_1.

The responses to the filters in Figure 6-7 are:

$$x_{1,1} = \alpha A_1 E_g \frac{\cos(\theta)}{2} + n_{1,1} + \alpha A_1 E_g \frac{\cos(\theta)}{2} + n_{1,2} = \alpha A_1 E_g \cos(\theta) + W_{1,1} \tag{6-7}$$

$$x_{1,2} = \alpha A_1 E_g \frac{\sin(\theta)}{2} + n_{2,1} + \alpha A_1 E_g \frac{\sin(\theta)}{2} + n_{2,2} = \alpha A_1 E_g \sin(\theta) + W_{1,2} \tag{6-8}$$

where

$$\begin{aligned} \theta &= \varphi_{ref} + \beta(f_c) - \varphi_d \\ W_{1,1} &= n_{1,1} + n_{1,2} \\ W_{1,2} &= n_{2,1} + n_{2,2} \end{aligned} \tag{6-9}$$

Assuming that E_g=1 then $W_{1,1}$ and $W_{1,2}$ are independent Gaussian random variables with variance $N_0/2$ and mean zero.

If these calculations are repeated for $\Delta\omega_2 \ldots \Delta\omega_{M_0+J}$ then the set of complex decision variables obtained is:

$$\begin{aligned} X_i &= \alpha A_i e^{j\theta} + W_i,\ i = 1, 2, \ldots, M_0 \\ Y_i &= \alpha B e^{j\nu_i} e^{j\theta} + W_{i+M_0},\ i = 1,2,\ldots,J \end{aligned} \tag{6-10}$$

where

(6-11)

$$\begin{aligned} W_i &= W_{i,1} + jW_{i,2} \\ X_i &= x_{i,1} + jx_{i,2} \\ Y_i &= y_{i,1} + jy_{i,2} \end{aligned} \tag{6-12}$$

These M_0+J complex decision variables contain all information relevant to make a decision of which message was sent. In the equations j^2=-1.

6.1.4 The Maximum Likelihood Decision Rule

Define $\boldsymbol{r}$ as the set $\{x_{1,1}, x_{1,2}, ..., x_{M_0,1}, x_{M_0,2}, y_{1,1}, y_{1,2}, ..., y_{J,1}, y_{J,2}\}$. The ML (Maximum Likelihood) decision rule [41] finds the maximum of the probabilities $p(\boldsymbol{r}|m_l)$ assuming message l was sent. These probability density functions can be obtained by averaging the pdfs $p(\boldsymbol{r}|m_l,\theta)$:

$$p(\boldsymbol{r}|m_l) = \int_0^{2\pi} p(\boldsymbol{r}|m_l, \theta)p(\theta)d\theta \tag{6-13}$$

If we assume that the phase, θ, is uniformly distributed then $p(\theta) = \frac{1}{2\pi}$ in a 2π-interval. The probability $p(\boldsymbol{r}|m_l,\theta)$ can be expressed as a product of the marginal pdfs,

$$p(\boldsymbol{r}|m_l, \theta) = \prod_{i=0}^{M_0} (p(x_{i,1}|m_l, \theta)p(x_{i,2}|m_l, \theta)) \cdot \prod_{i=1}^{J} (p(y_{i,1}|m_l, \theta)p(y_{i,2}|m_l, \theta)) \tag{6-14}$$

Define A_k^l as the value of A_k for message number l and ν_k^l as the value of ν_k for message number l. Because the outputs from the filter banks are independent Gaussian random variables with variance $\sigma^2=N_0/2$ the pdfs may be written as

$$
\begin{aligned}
p(\mathbf{r}|m_l,\theta) &= \prod_{i=1}^{M_0} \frac{1}{2\pi\sigma^2}\exp\left(-\frac{\left(x_{i,1}-\alpha A_i^l\cos(\theta)\right)^2+\left(x_{i,2}-\alpha A_i^l\sin(\theta)\right)^2}{2\sigma^2}\right) \\
&\quad \prod_{i=1}^{J} \frac{1}{2\pi\sigma^2}\exp\left(-\frac{\left(y_{i,1}-\alpha B\cos\left(\nu_i^l+\theta\right)\right)^2+\left(y_{i,2}-\alpha B\sin\left(\nu_i^l+\theta\right)\right)^2}{2\sigma^2}\right) \\
&= \left(\frac{1}{2\pi\sigma^2}\right)^{M_0+J}\prod_{i=1}^{M_0}\exp\left(-\frac{x_{i,1}^2+x_{i,2}^2+\left(\alpha A_i^l\right)^2}{2\sigma^2}\right)\prod_{i=1}^{J}\exp\left(-\frac{y_{i,1}^2+y_{i,2}^2+(\alpha B)^2}{2\sigma^2}\right) \\
&\quad \prod_{i=1}^{M_0}\exp\frac{x_{i,1}\alpha A_i^l\cos(\theta)+x_{i,2}\alpha A_i^l\sin(\theta)}{\sigma^2}\prod_{i=1}^{J}\exp\left(\frac{y_{i,1}\alpha B\cos\left(\nu_i^l+\theta\right)+y_{i,2}\alpha B\sin\left(\nu_i^l+\theta\right)}{\sigma^2}\right)
\end{aligned}
\tag{6-15}
$$

The constants may be removed as they appear in all pdfs and integration yields

$$
\begin{aligned}
&\int_0^{2\pi}\prod_{i=1}^{M_0}\exp\frac{x_{i,1}\alpha A_i^l\cos(\theta)+x_{i,2}\alpha A_i^l\sin(\theta)}{\sigma^2} \\
&\prod_{i=1}^{J}\exp\frac{y_{i,1}\alpha B\left(\cos\left(\nu_i^l\right)\cos(\theta)-\sin\left(\nu_i^l\right)\sin(\theta)\right)+y_{i,2}\alpha B\left(\sin\left(\nu_i^l\right)\cos\theta+\cos\left(\nu_i^l\right)\sin\theta\right)}{\sigma^2}d\theta \\
&= I_0\left(\frac{\sqrt{R^2+S^2}}{\sigma^2}\right)
\end{aligned}
\tag{6-16}
$$

where

$$
\begin{aligned}
R &= \left(\sum_{i=1}^{M_0} x_{i,1}\alpha A_i^l+\sum_{i=1}^{J}\left(y_{i,1}\alpha B\cos\left(\nu_i^l\right)+y_{i,2}\alpha B\sin\left(\nu_i^l\right)\right)\right) \\
S &= \left(\sum_{i=1}^{M_0} x_{i,1}\alpha A_i^l-\sum_{i=1}^{J}\left(y_{i,1}\alpha B\sin\left(\nu_i^l\right)+y_{i,2}\alpha B\cos\left(\nu_i^l\right)\right)\right)
\end{aligned}
\tag{6-17}
$$

and $I_0(x)$ is the modified Bessel function of the zeroth order [23], [41]. Because the Bessel function is monotonously increasing the optimum decision rule maximizes

$$
\sqrt{R^2+S^2} \tag{6-18}
$$

α is a constant and can be removed from the expression so, in order to find the most probable transmitted symbol message, the detector calculates the set

$$C^l = \left| \sum_{i=1}^{M_0} X_i A_i^l + \sum_{i=1}^{J} Y_i B e^{-j\nu_i^l} \right|, 1 \le l \le M \qquad (6\text{-}19)$$

and chooses message m if $C^m = \max_i C^i$. In the noiseless case $C_{max} = A^2 + JB^2$.

6.2 Computer Simulations

In this section we evaluate, by computer simulations, the performance of the three modulation methods described in Section 6.1.1. The reason for choosing these specific schemes is their simple construction. The performance is estimated in terms of the symbol error probability and it is compared to non-coherent FSK and DPSK.

The phase is considered a uniformly distributed variable in the interval 0 to 2π and the signal alternatives are assumed to be equally likely. These parameters are randomly chosen by the simulation program.

The performance depends on the relation between the parameters *A* and *B*. Because the minimum euclidean distance is related to the symbol error probability, the relation between *A* and *B* is chosen such that the minimum Euclidean distance is maximized. This has shown to reduce the symbol error probability. The relation between *A* and *B* also affects the error probability of the specific bits, which is indicated by (6-19).

The relations between *A* and *B* that maximizes the minimum euclidean distance are $A = \sqrt{2}B$, for BB and BBB, and $A = B$ for BQ. This can be obtained by using the fact that the signal space is $2(M_0+J)$ dimensional.

Figure 6-8 shows the symbol error probability versus the average received energy per bit, $E_b = \frac{\alpha^2(A^2 + JB^2)}{\log_2(M)}$, for the three cases considered. Among these the lowest symbol error probabilities are achieved for the case BBB. BB is better than BQ but there is a loss in bandwidth efficiency. If we add a BPSK signal to BB (we get BBB), then the bandwidth efficiency increases, but the symbol error probability also increases.

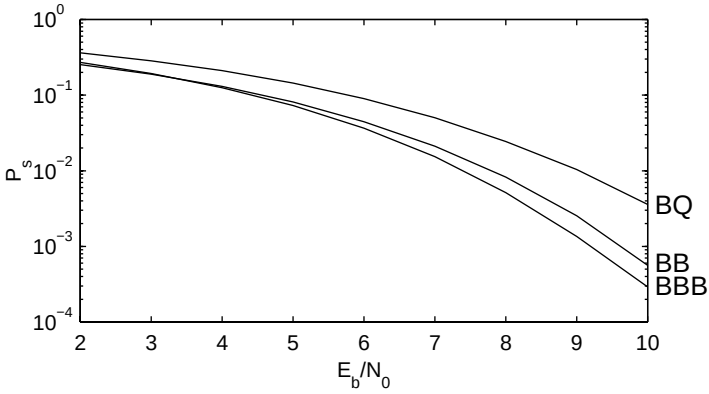

FIGURE 6-8 The symbol error probability for the three systems considered.

Figure 6-9 shows the symbol error probability compared to DPSK and Figure 6-10 shows the symbol error probability compared to non-coherent FSK (NCFSK). The systems are compared with the same number of signal alternatives. The symbol error probabilities for DPSK and FSK are not simulated but calculated, see [41], [51].

Figure 6-9 shows that the symbol error probability for BB is about the same as for 4-DPSK, but at the cost of lower bandwidth efficiency. To increase the bandwidth efficiency BQ can be used. Then there is a loss in energy efficiency but the symbol error probability is better than 8-DPSK. The same is achieved with BBB. The symbol error probability for non-coherent FSK is, in the cases considered, lower than the proposed methods, but the bandwidth efficiency is not as good. We can conclude that the symbol error probability is somewhat between non-coherent FSK and DPSK, and this also holds for the bandwidth efficiency.

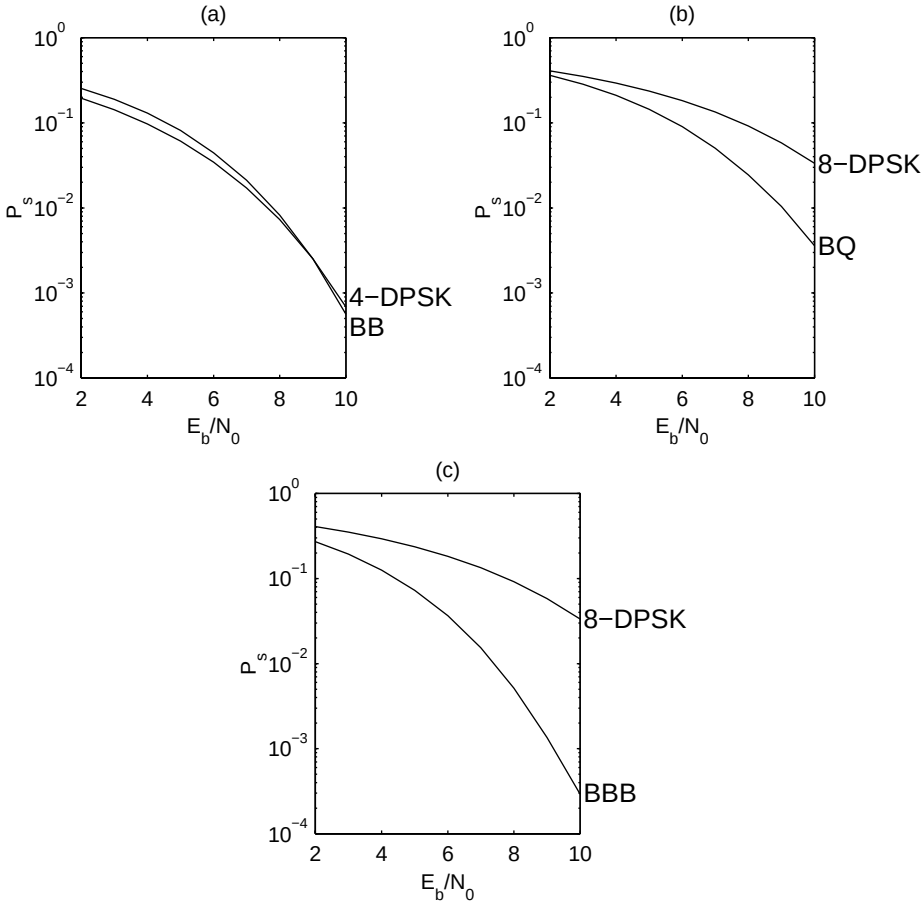

FIGURE 6-9 The symbol error probability compared to DPSK. The methods are compared with the same number of signal alternatives.

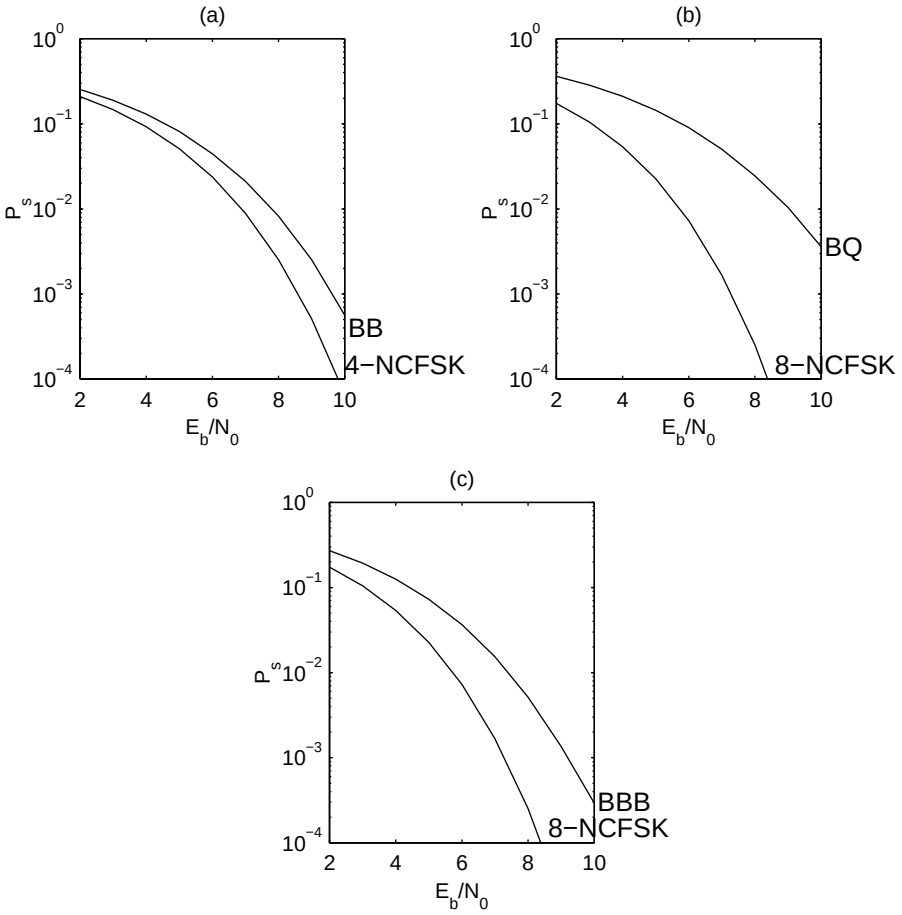

FIGURE 6-10 The symbol error probability compared to non-coherent FSK. The methods are compared with the same number of signal alternatives.

It is clear that it is hard to beat the bandwidth efficiency of DPSK. Additional studies are necessary in order to find competitive alternative signal constellations, when the signals are to be received non-coherently. Furthermore, waveform selection by an appropriate encoder also needs to be investigated.

The relation between *A* and *B* also has to be studied further. Perhaps other constraints than minimizing the euclidean distance could be considered. Also the *J* DPSK signals could have different amplitudes. Here we have considered them as all having amplitude *B*, where *B* is a constant. Because some bits are transmitted as PSK signals and some as FSK signals, different bits can have different error protection.

6.3 Union Bound

The union bound [41] is given by

$$P_s \le \sum_{u=1}^{M} P_u \sum_{\substack{i=1 \\ i \ne u}}^{M} P(C^i > C^u \,|\, m = m_u) \tag{6-20}$$

and is an upper bound on the symbol error probability. P_u is the probability that message u is transmitted and C^u, C^i the metrics for message u and i given in (6-19). In order to calculate the union bound, we have to find the probability $P(C^i > C^u \,|\, m = m_u)$. This probability may also be expressed as

$$P(C^i > C^u \,|\, m = m_u) = P((C^u)^2 < (C^i)^2 \,|\, m = m_u) = P((C^u)^2 - (C^i)^2 < 0 \,|\, m = m_u) \tag{6-21}$$

To arrive at an expression for this probability we first find the distribution of an arbitrary C^l. From (6-19) and (6-10) we obtain

$$\begin{aligned}
C^l &= \left| \sum_{k=1}^{M_0} X_k A_k^l + \sum_{k=1}^{J} Y_k B e^{-j\nu_k^l} \right| \\
&= \left| \sum_{k=1}^{M_0} (\alpha A_k e^{j\theta} + W_k) A_k^l + \sum_{k=1}^{J} \left(\alpha B e^{j\nu_k} e^{j\theta} + W_{k+M_0} \right) B e^{-j\nu_k^l} \right| \\
&= \left| \sum_{k=1}^{M_0} (\alpha A_k^l A_k e^{j\theta} + A_k^l W_k) + \sum_{k=1}^{J} \left(\alpha B e^{-j\nu_k^l} B e^{j\nu_k} e^{j\theta} + B e^{-j\nu_k^l} W_{k+M_0} \right) \right| \\
&= \left| e^{j\theta} \left(\sum_{k=1}^{M_0} (\alpha A_k^l A_k + A_k^l W_k e^{-j\theta}) + \sum_{k=1}^{J} \left(\alpha B^2 e^{j\nu_k - j\nu_k^l} + B e^{-j\nu_k^l} W_{k+M_0} e^{-j\theta} \right) \right) \right| \\
&= \left| \sum_{k=1}^{M_0} (\alpha A_k^l A_k + A_k^l W_k e^{-j\theta}) + \sum_{k=1}^{J} \left(\alpha B^2 e^{j\nu_k - j\nu_k^l} + B W_{k+M_0} e^{-j\nu_k^l} e^{-j\theta} \right) \right| \\
&= \left| \sum_{k=1}^{M_0} \alpha A_k^l A_k + \sum_{k=1}^{M_0} A_k^l W_k e^{-j\theta} + \sum_{k=1}^{J} \alpha B^2 e^{j\nu_k - j\nu_k^l} + \sum_{k=1}^{J} B W_{k+M_0} e^{-j\nu_k^l - j\theta} \right|
\end{aligned} \tag{6-22}$$

Thus there are two constant terms (assuming a given message is sent) and two terms with random variables. The constant part is

$$\sum_{k=1}^{M_0} \alpha A_k^l A_k + \sum_{k=1}^{J} \alpha B^2 e^{jv_k - j\nu_k^l} = \left(\sum_{k=1}^{M_0} \alpha A_k^l A_k + \sum_{k=1}^{J} \alpha B^2 \cos(v_k - \nu_k^l) \right) + j \left(\sum_{k=1}^{J} \alpha B^2 \sin(v_k - \nu_k^l) \right) \tag{6-23}$$

and the random part

$$\begin{aligned}
&\sum_{k=1}^{M_0} A_k^l W_k e^{-j\theta} + \sum_{k=1}^{J} B W_{k+M_0} e^{-j\nu_k^l - j\theta} \\
&= \sum_{k=1}^{M_0} A_k^l W_k \cos(\theta) - j \sum_{k=1}^{M_0} A_k^l W_k \sin(\theta) \\
&+ \sum_{k=1}^{J} B W_{k+M_0} \cos(-\nu_k^l - \theta) + j \sum_{k=1}^{J} B W_{k+M_0} \sin(-\nu_k^l - \theta) \\
&= \sum_{k=1}^{M_0} A_k^l (W_{k,1} + jW_{k,2}) \cos(\theta) - j \sum_{k=1}^{M_0} A_k^l (W_{k,1} + jW_{k,2}) \sin(\theta) \\
&+ \sum_{k=1}^{J} B (W_{k+M_0,1} + jW_{k+M_0,2}) \cos(-\nu_k^l - \theta) \\
&+ j \sum_{k=1}^{J} B (W_{k+M_0,1} + jW_{k+M_0,2}) \sin(-\nu_k^l - \theta)
\end{aligned} \tag{6-24}$$

$$\begin{aligned}
&= \sum_{k=1}^{M_0} A_k^l W_{k,1} \cos(\theta) + \sum_{k=1}^{M_0} A_k^l W_{k,2} \sin(\theta) \\
&+ \sum_{k=1}^{J} B W_{k+M_0,1} \cos(-\nu_k^l - \theta) - \sum_{k=1}^{J} B W_{k+M_0,2} \sin(-\nu_k^l - \theta) \\
&- j \sum_{k=1}^{M_0} A_k^l W_{k,1} \sin(\theta) + j \sum_{k=1}^{M_0} A_k^l W_{k,2} \cos(\theta) \\
&+ j \sum_{k=1}^{J} B W_{k+M_0,2} \cos(-\nu_k^l - \theta) + j \sum_{i=1}^{J} B W_{k+M_0,1} \sin(-\nu_k^l - \theta)
\end{aligned} \tag{6-25}$$

Because $W_{i,j}$ are independent Gaussian random variables with variance $N_0/2$ and zero-mean the variance of the real part in (6-25) is (given θ)

$$\begin{aligned}
&\sum_{k=1}^{M_0} (A_k^l)^2 \frac{N_0}{2} (\cos(\theta))^2 + \sum_{k=1}^{M_0} (A_k^l)^2 \frac{N_0}{2} (\sin(\theta))^2 \\
&+ \sum_{k=1}^{J} B^2 \frac{N_0}{2} (\cos(-\nu_k^l - \theta))^2 + \sum_{i=k}^{J} B^2 \frac{N_0}{2} (\sin(-\nu_k^l - \theta))^2 \\
&= A^2 \frac{N_0}{2} + JB^2 \frac{N_0}{2}
\end{aligned} \tag{6-26}$$

and in the same way the variance of the complex part in (6-25) is

$$\begin{aligned}
&\sum_{k=1}^{M_0} (A_k^l)^2 \frac{N_0}{2} (\cos(\theta))^2 + \sum_{k=1}^{M_0} (A_k^l)^2 \frac{N_0}{2} (\sin(\theta))^2 \\
&+ \sum_{k=1}^{J} B^2 \frac{N_0}{2} (\cos(-\nu_k^l - \theta))^2 + \sum_{k=1}^{J} B^2 \frac{N_0}{2} (\sin(-\nu_k^l - \theta))^2 \\
&= A^2 \frac{N_0}{2} + JB^2 \frac{N_0}{2}
\end{aligned} \tag{6-27}$$

Define the variables X and Y such that

$$\begin{aligned}
|X|^2 &= (C^u)^2 \\
|Y|^2 &= (C^i)^2
\end{aligned} \tag{6-28}$$

Assume message u is transmitted, then X and Y are complex-valued Gaussian random variables (see [41]) with mean

$$\begin{aligned}
\bar{X} &= \left(\sum_{k=1}^{M_0} \alpha A_k^u A_k^u + \sum_{k=1}^{J} \alpha B^2 \cos(\nu_k^u - \nu_k^u) \right) + j \left(\sum_{k=1}^{J} \alpha B^2 \sin(\nu_k^u - \nu_k^u) \right) \\
\bar{Y} &= \left(\sum_{k=1}^{M_0} \alpha A_k^i A_k^u + \sum_{k=1}^{J} \alpha B^2 \cos(\nu_k^u - \nu_k^i) \right) + j \left(\sum_{k=1}^{J} \alpha B^2 \sin(\nu_k^u - \nu_k^i) \right)
\end{aligned} \tag{6-29}$$

The covariance of the random variables X and Y is

$$
\begin{aligned}
\sigma_{XY}^2 &= \frac{1}{2}E\left((X-\bar{X})(Y-\bar{Y})^*\right) \\
&= \frac{1}{2}E\Bigg[\Bigg(\sum_{k=1}^{M_0} A_k^u W_{k,1}\cos(\theta) + \sum_{k=1}^{M_0} A_k^u W_{k,2}\sin(\theta) \\
&+ \sum_{k=1}^{J} BW_{k+M_0,1}\cos\left(-\nu_k^u-\theta\right) - \sum_{k=1}^{J} BW_{k+M_0,2}\sin\left(-\nu_k^u-\theta\right) \\
&+ j\sum_{k=1}^{M_0} A_k^u W_{k,2}\cos(\theta) - j\sum_{k=1}^{M_0} A_k^u W_{k,1}\sin(\theta) \\
&+ j\sum_{k=1}^{J} BW_{k+M_0,2}\cos\left(-\nu_k^u-\theta\right) + j\sum_{k=1}^{J} BW_{k+M_0,1}\sin\left(-\nu_k^u-\theta\right)\Bigg) \\
&\Bigg(\sum_{k=1}^{M_0} A_k^i W_{k,1}\cos(\theta) + \sum_{k=1}^{M_0} A_k^i W_{k,2}\sin(\theta) \\
&+ \sum_{k=1}^{J} BW_{k+M_0,1}\cos\left(-\nu_k^i-\theta\right) - \sum_{k=1}^{J} BW_{k+M_0,2}\sin\left(-\nu_k^i-\theta\right) \\
&- j\sum_{k=1}^{M_0} A_k^i W_{k,2}\cos(\theta) + j\sum_{k=1}^{M_0} A_k^i W_{k,1}\sin(\theta) \\
&- j\sum_{k=1}^{J} BW_{k+M_0,2}\cos\left(-\nu_k^i-\theta\right) - j\sum_{k=1}^{J} BW_{k+M_0,1}\sin\left(-\nu_k^i-\theta\right)\Bigg)\Bigg]
\end{aligned}
\tag{6-30}
$$

Using the fact that the product of two independent zero-mean random processes has zero mean, and the trigonometric identities

$$
\begin{aligned}
\sin(\alpha-\beta) &= \sin\alpha\cos\beta - \cos\alpha\sin\beta \\
\cos(\alpha-\beta) &= \cos\alpha\cos\beta + \sin\alpha\sin\beta
\end{aligned}
\tag{6-31}
$$

we arrive at

$$\sigma_{XY}^2 = \frac{1}{2}E\Big(\sum_{k=1}^{M_0} A_k^u A_k^i W_{k,1}^2 (\cos(\theta))^2 + \sum_{k=1}^{M_0} A_k^u A_k^i W_{k,1}^2 (\sin(\theta))^2$$
$$+ \sum_{k=1}^{M_0} A_k^u A_k^i W_{k,2}^2 (\sin(\theta))^2 + \sum_{k=1}^{M_0} A_k^u A_k^i W_{k,2}^2 (\cos(\theta))^2$$
$$+ \sum_{k=1}^{J} B^2 W_{k+M_0,2}^2 \cos(-\nu_k^u - \theta - (-\nu_k^i - \theta))$$
$$+ j \sum_{k=1}^{J} B^2 W_{k+M_0,2}^2 \sin(-\nu_k^u - \theta - (-\nu_k^i - \theta)) \qquad (6\text{-}32)$$
$$+ \sum_{k=1}^{J} B^2 W_{k+M_0,1}^2 \cos(-\nu_k^u - \theta - (-\nu_k^i - \theta))$$
$$+ j \sum_{k=1}^{J} B^2 W_{k+M_0,1}^2 \sin(-\nu_k^u - \theta - (-\nu_k^i - \theta)) \Big)$$

If we simplify this we get

$$\sigma_{XY}^2 = \frac{1}{2}E\Big(\sum_{k=1}^{M_0} A_k^u A_k^i W_{k,1}^2 + \sum_{k=1}^{M_0} A_k^u A_k^i W_{k,2}^2$$
$$+ \sum_{k=1}^{J} B^2 W_{k+M_0,2}^2 \cos(-\nu_k^u + \nu_k^i) + j \sum_{k=1}^{J} B^2 W_{k+M_0,2}^2 \sin(-\nu_k^u + \nu_k^i) \qquad (6\text{-}33)$$
$$+ \sum_{k=1}^{J} B^2 W_{k+M_0,1}^2 \cos(-\nu_k^u + \nu_k^i) + j \sum_{k=1}^{J} B^2 W_{k+M_0,1}^2 \sin(-\nu_k^u + \nu_k^i) \Big)$$

$$\sigma_{XY}^2 = (\mu_{W^2}) \frac{1}{2}E\Big(\sum_{k=1}^{M_0} A_k^u A_k^i + \sum_{k=1}^{M_0} A_k^u A_k^i + \sum_{k=1}^{J} B^2 \cos(-\nu_k^u + \nu_k^i)$$
$$+ j \sum_{k=1}^{J} B^2 \sin(-\nu_k^u + \nu_k^i) + \sum_{k=1}^{J} B^2 \cos(-\nu_k^u + \nu_k^i) + j \sum_{k=1}^{J} B^2 \sin(-\nu_k^u + \nu_k^i) \Big) \qquad (6\text{-}34)$$

where μ_{W^2} (the mean of $W_{i,j}^2$) is equal to $N_0/2$. The variance of a complex-valued random variable Z is given by

$$\sigma_Z^2 = \frac{1}{2}E((Z - \bar{Z})(Z - \bar{Z})^*) \qquad (6\text{-}35)$$

Similar calculations as above yields the variance of X and Y

$$\sigma_X^2 = \sigma_Y^2 = \mu_{W^2}(A^2 + JB^2) \tag{6-36}$$

This is also seen by setting $i = u$ in (6-34).

Using X and Y the probability $P((C^u)^2 - (C^i)^2 < 0 \,|\, m = m_u)$ may be written as

$$P(|X|^2 - |Y|^2 < 0 \,|\, m = m_u) \tag{6-37}$$

This probability is a special case of a quadratic form given in [41], where it is shown that

$$P(|X|^2 - |Y|^2 < 0 \,|\, m = m_u) = Q_1(a, b) - \frac{v_2/v_1}{1 + v_2/v_1} I_0(ab) \exp\left(-\frac{1}{2}(a^2 + b^2)\right) \tag{6-38}$$

where

$$\begin{aligned}
Q_1(a, b) &= \int_b^\infty x \exp\left(-\frac{1}{2}(x^2 + a^2)\right) I_0(ax) dx \\
a &= \sqrt{\frac{2v_1^2 v_2(\alpha_1 v_2 - \alpha_2)}{(v_1 + v_2)^2}} \\
b &= \sqrt{\frac{2v_1 v_2^2(\alpha_1 v_1 + \alpha_2)}{(v_1 + v_2)^2}} \\
\alpha_1 &= 2(|\bar{X}|^2 \sigma_{YY}^2 + |\bar{Y}|^2 \sigma_{XX}^2 - \bar{X}^* \bar{Y} \sigma_{XY}^2 - \bar{X}\bar{Y}^* (\sigma_{XY}^2)^*) \\
\alpha_2 &= (|\bar{X}|^2 - |\bar{Y}|^2) \\
v_1 &= \sqrt{w^2 + \frac{1}{4(\sigma_{XX}^2 \sigma_{YY}^2 - |\sigma_{XY}^2|^2)}} - w \\
v_2 &= \sqrt{w^2 + \frac{1}{4(\sigma_{XX}^2 \sigma_{YY}^2 - |\sigma_{XY}^2|^2)}} + w \\
w &= \frac{\sigma_{XX}^2 - \sigma_{YY}^2}{4(\sigma_{XX}^2 \sigma_{YY}^2 - |\sigma_{XY}^2|^2)} = 0
\end{aligned} \tag{6-39}$$

$I_0(x)$ is the zeroth-order modified Bessel function of the first kind and $Q_1(x)$ is the generalized Marcum's Q-function.

If we consider (6-20) we see that it is now possible to calculate the union bound. Figure 6-11 - 6-13 show the union bound for each system assuming equally likely signal alternatives. Each figure also shows the simulated symbol error probability. The figures clearly show that, for high signal to noise ratios, the union bound approaches the simulated results.

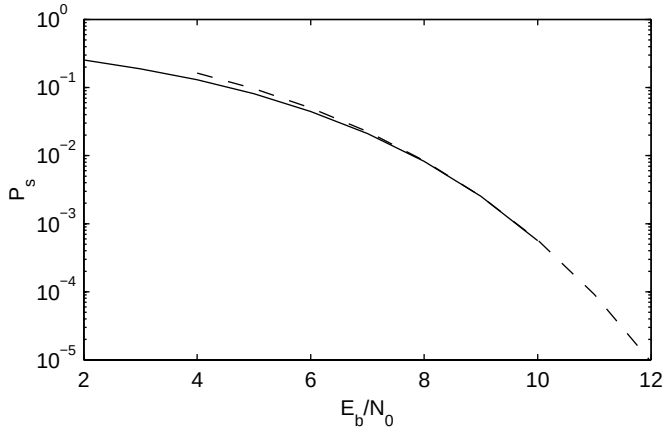

FIGURE 6-11 The union bound of the symbol error probability (the dashed line) and the simulated error probability (the solid line) for BB.

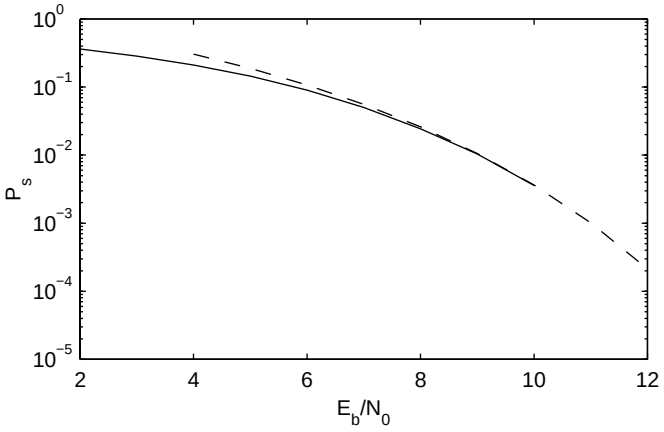

FIGURE 6-12 The union bound of the symbol error probability (the dashed line) and the simulated error probability (the solid line) for BQ.

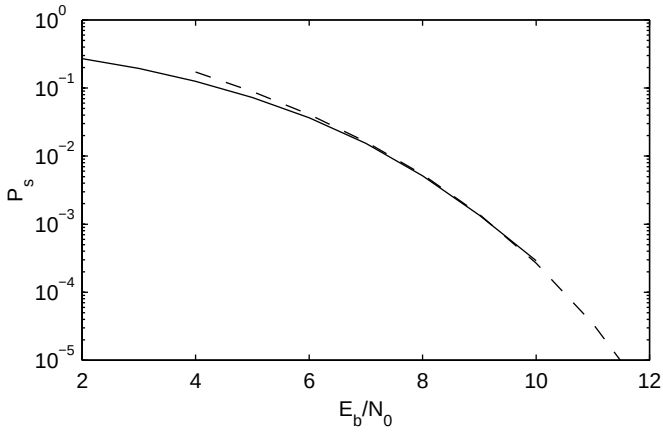

FIGURE 6-13 The union bound of the symbol error probability (the dashed line) and the simulated error probability (the solid line) for BBB.

6.4 Communication Aspects of the Power-Line Communication Channel

In this section we briefly summarize the most important results from this thesis and use them to motivate a structure of a communication system for the power-line channel.

In Chapter 2 and Chapter 3 we study a meter reading system and the results show several parameters that affect the communication in this system. It is shown that the quality of the channels varies in time, physical channel length and with different loads. From these measurements it is already clear that advanced communication methods are needed in order to combat the varying properties of the channel.

Chapter 4 shows measurements of the noise level and the signal attenuation of the power-line channel. The transfer function of the power-line is found to be frequency selective and the magnitude decays with frequency. It is found that the noise is non-white (maybe not even Gaussian), thus it can not be described as AWGN (Additive White Gaussian Noise), which is used to model noise in several communication systems. The power of the noise decays with frequency but there is also a contribution from several narrow-band disturbances.

In Chapter 5 we study the effect of non-white Gaussian noise (narrow-band disturbances) on specific receiver structures and find that if the narrow-band disturbances are not properly dealt with in the receiver, then it can cause a severe degradation in performance. It was also seen that one way to reduce the effects of narrow-band disturbances is to use frequency-diversity.

To communicate on a varying channel like the power-line, a communication method is needed which is able to provide the receiver with large enough signal energy (most of the

time) such that the decision algorithm of the receiver efficiently can combat the disturbances. This can be achieved in several ways. One solution is to let the transmitter and/or the receiver adapt to the channel characteristics. At any time, the characteristics of the channel are estimated and used to change the parameters of the communication system, such that efficient communication is achieved. The complexity of this solution is relatively high and it might be expensive to implement. Another solution is to let the communication system have a robust modulation method that functions well even when the phase and/or the attenuation is unknown. Such a system is less dependent on the channel parameters and, hence, robust communication may be achieved. This is the approach outlined below and is mainly chosen because of the non-complex and less expensive implementation of the receiver.

In this chapter we have studied a modulation method that is a combination of FSK and PSK signals. Because the studied receiver is not dependent on the attenuation of the channel, nor the phase shift, the system is quite robust.

Because the power-line channel is found to be frequency selective it may suggest the use of an OFDM-like (Orthogonal Frequency Division Multiplex) [41], [47] modulation system. In an OFDM system the available bandwidth, *W*, is divided into several small frequency bands, W_1, W_2, ….. W_n, see Figure 6-14. If the bandwidth is divided into small enough sub-bands then the attenuation and the phase shift is approximately constant within each sub-band and, hence, these sub-channels are not frequency-selective. The use of OFDM has also been suggested by other researchers [7], [11], [12], [21], [37].

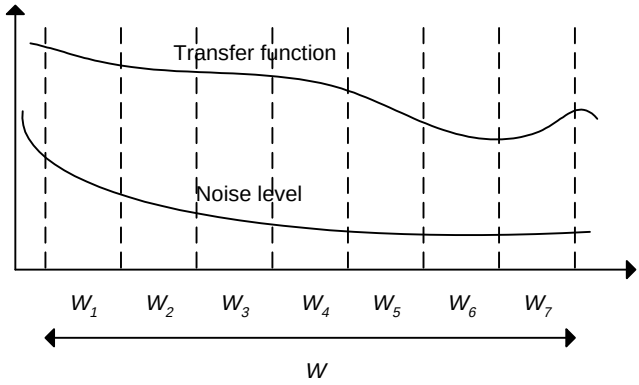

FIGURE 6-14 An example of how the available bandwidth, *W*, is divided into several small sub-bands.

In each sub-band a modulation method is assigned, transmitting bits. Often QAM (Quadrature Amplitude Modulation) signals are used. QAM normally require that the phase and amplitude must be estimated by the receiver. The modulation methods described in this chapter can also be used (combined with proper coding and interleaving). It might be that some sub-bands with known low channel qualities are left unused, e.g., frequency bands containing broadcast radio.

Assume that we assign one BB signal (described in Chapter 6) in each sub-band. This system consists of one BFSK signal and one BPSK signal, thus it transmits two bits each symbol time. If we have n sub-bands then we have n BB systems and the whole communication system transmits $2n$ bits in each symbol interval.

To further increase the performance we could use a convolutional encoder [27] with, e.g., rate 1/2. If bursts of errors exist on the channel then several sequential bits may be lost, and the convolutional encoder might not be able to correct these errors. To try to overcome this impairment an interleaver could be used. An interleaver changes the order of the bits such that they are interleaved in a controlled way. Assume that we have five coded bits $\{a, b, c, d, e\}$ then a simple implementation could be to change the order of the bits such that the new transmitted coded sequence is $\{a, c, e, b, d\}$. Thus, if two sequential bits are lost on the channel then they are not sequential in the original sequence and the decoder might be able to correct the errors.

Figure 6-15 shows a schematic of the whole system. In this example the bandwidth is divided into five sub-bands and in each band a BB signal is used. First the uncoded bit stream is fed to the rate 1/2 convolutional encoder, then the coded sequence is run through the interleaver and the interleaved bit stream is sent to n ($n = 5$) modulators.

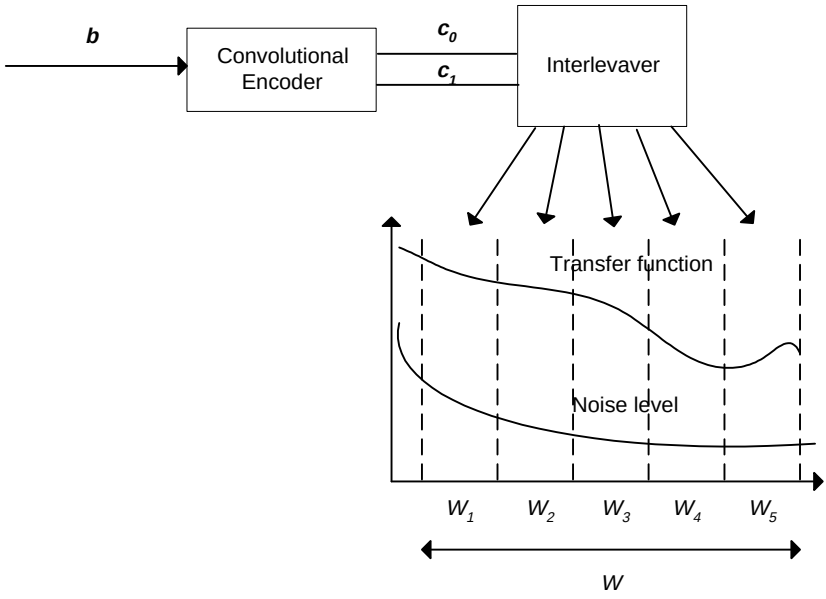

FIGURE 6-15 An example of a communication system for the power-line channel.

Additional research, concerning the system outlined in this section, is needed. Especially important are performance studies, for different choices of encoder, interleaver, modulator and receiver, when communicating over frequency-selective channels.

6.5 Conclusions

In this chapter we have studied a set of modulation methods, which are able to handle unknown phase and attenuation. The reason of doing this is that we want to come up with a communication system with a simple implementation of the receiver. The system consists of one FSK signal and one or more PSK signals, where the FSK signal is used to estimate the received phase for the PSK signals.

It is shown, theoretically and by simulations, that the symbol error probability is higher than for non-coherent FSK and lower than for DPSK, and the same holds for the bandwidth efficiency. This system may be a candidate to be used in power-line communications, but more studies are needed in order to know if the modulation is competitive, especially combined with coding.

This modulation is used combined with coding, frequency diversity and the use of subchannels (similar to Orthogonal Frequency Division Multiplex) to propose a communication system for the power-line channel. The result is a flexible structure which can be upgraded and adapted to future needs.

CHAPTER 7 *Conclusions*

This thesis is about power-line communication, communication over the existing power-lines. The main advantage of this kind of communication system is the existing infrastructure, which simplifies the implementation. We start this thesis, after a general introduction to power-line communication, by doing some measurements of basic properties, to understand the behavior of the power-line as a communication channel. Then we use these results combined with coding, modulation methods, different receiver structures, diversity and coding to present a communication strategy for the power-line channel.

In Chapter 2 we study an existing application, using the low-voltage grid as a communication channel. By observing this system it has been possible to extract information of which properties that affect the communication on the power-line channel. Properties that we have seen affect the communication are: different time-windows, the location in the grid, and the load profile.

To further study the effect of loads we have used a specially designed load consisting of a set of industrial machines, described in Chapter 3. We have used this load in the same grid as observed in Chapter 2 and we have studied how this impairment affects the communication channels. It is shown that channels close to the load are subject to a severe degradation in communication performance.

After these large-scale studies we report measurements (shown in Chapter 4) of the characteristics in the 1-16 MHz frequency band and the 20-450 kHz frequency band. Measurements are shown of the attenuation of the channel and the noise level at the receiver. We see that the noise level is non-white and decays with frequency. The transfer function is found to be frequency-selective and the attenuation increases with frequency. The measured characteristics are also related to the performance of the communication system observed in Chapter 2 and 3. The noise at the receiver is non-white and in Chapter 5 we study the effect of this noise on different receiver structures, one ideal and one suboptimal. We see that a receiver which do not counteract for narrow-band disturbances, experience a severe decrease in performance.

Our approach in designing a communication system for the power-line channel, is a simple implementation of the receiver, which lowers the cost. In Chapter 6 we study a set of modulation methods that may be a candidate to be used in power-line communications. A robust set of methods, which are able to handle unknown phase and attenuation. These methods are then used combined with coding, frequency diversity, and the use of subchannels (similar to Orthogonal Frequency Division Multiplex) to suggest a communication system for the power-line channel, a flexible structure that can be upgraded to future needs.

Bibliography

[1] J.B. Anderson, "Digital Transmission Engineering", IEEE Press, 1998.

[2] M. Arzberger, K. Dostert, T. Waldeck, M. Zimmermann, "Fundamental Properties of the Low Voltage Power Distribution Grid", Proc. 1997 International Symposium on Power-line Communications and its Applications", Essen, Germany, 1997.

[3] J.S. Barnes, "A Physical Multi-path Model for Power Distribution Network Propagation", Proc. 1998 International Symposium on Power-line Communications and its Applications", Tokyo, Japan, 1998.

[4] Paul Brown, "Directional Coupling of High Frequency Signals onto Power Networks", Proc. 1997 International Symposium on Power-line Communications and its Applications", Essen, Germany, 1997.

[5] P. A. Brown, "Some Key Factors Influencing Data Transmission Rates in the Power Line Environment when Utilising Carrier Frequencies above 1 MHz", Proc. 1998 International Symposium on Power-line Communications and its Applications", Tokyo, Japan, 1998.

[6] A.G. Burr, D.M.W. Reed, P.A. Brown, "HF Broadcast Interference on LV Mains Distribution Networks", Proc. 1998 International Symposium on Power-line Communications and its Applications", Tokyo, Japan, 1998.

[7] A.G. Burr, P.A. Brown, "Application of OFDM to Powerline Telecommunications", 3rd International Symposium on Power-line Communications and its Applications, Lancaster, UK, 1999.

[8] CENELEC, "EN50065-1, Signalling on low-voltage electrical installations in the frequency range 3 kHz to 148.5 kHz".

[9] CENELEC, EN 50160, "Voltage Characteristics of Electricity Supplied by Public Distribution Systems", 1995.

[10] A.B. Dalby, "Signal Transmission on Power Lines; (Analysis of power line circuits)" , Proc. 1997 International Symposium on Power-line Communications and its Applications", Essen, Germany, 1997.

[11] M. Darnell, N. Pem, "OFDM Using Complementary Sequences for Data Transmission Over Non-Gaussian Channel", Proc. 3rd International Symposium on Power-line Communications and its Applications, Lancaster, UK, 1999.

[12] M. Deinzer and M. Stoger, "Integrated PLC-Modem based on OFDM", Proc. 3rd International Symposium on Power-line Communications and its Applications, Lancaster, UK, 1999.

[13] J. Dickinson, P. Nicholson, "Calculating the High Frequency Transmission Line Parameters of Power Cables", Proc. 1997 International Symposium on Power-line Communications and its Applications", Essen, Germany, 1997.

[14] K. Dostert, "Telecommunications over the Power Distribution Grid; Possibilities and Limitations", Proc. 1997 International Symposium on Power-line Communications and its Applications", Essen, Germany, 1997.

[15] K. Dostert, "RF-Models of the Electrical Power Distribution Grid", Proc. 1998 International Symposium on Power-line Communications and its Applications", Tokyo, Japan, 1998.

[16] G. Duval, "Low Voltage Network Models to the Analysis of Unexpected Phenomena in PLC Communications", Proc. 1998 International Symposium on Power-line Communications and its Applications", Tokyo, Japan, 1998.

[17] Echelon Corporation, " LonWorks PLT-30 A-Band Power Line Transceiver Module, User's Guide", Version 1.3.

[18] O. Edfors, M. Sandell, J-J van de Beek, D. Landström, F. Sjöberg, "An Introduction to Orthogonal Frequency-Division Multiplexing, 1996.

[19] Fluke Corporation, "http://www.fluke.com".

[20] I. Fröroth, "More than Power Down the Line", Licentiate of Technology Thesis, Department of Teleinformatics, Royal Institute of Technology, Stockholm, Sweden, 1999.

[21] D. Galda, T. Giebel, U. Zölzer, H. Rohling, "An Experimental OFDM-Modem for the CENELEC B Band", Proc. 3rd International Symposium on Power-line Communications and its Applications, Lancaster, UK, 1999.

[22] M. Harris, "Powerline Communications - a Regulatory Perspective", Proc. 3rd International Symposium on Power-line Communications and its Applications, Lancaster, UK, 1999.

[23] S. Haykin, "Communication Systems", Wiley, 1994.

[24] O. Hooijen, "A Channel Model for the Low-Voltage Power-Line Channel", Proc. 1997 International Symposium on Power-line Communications and its Applications", Essen, Germany, 1997.

[25] O.G. Hooijen, A.J. Han Vinck, "On the Channel Capacity of a European-style Residential Power Circuit", Proc. 1998 International Symposium on Power-line Communications and its Applications", Tokyo, Japan, 1998.

[26] O.G. Hooijen, "On the Relation Between Network-topology and Power Line Signal Attenuation", Proc. 1998 International Symposium on Power-line Communications and its Applications", Tokyo, Japan, 1998.

[27] R. Johanneson, K. Sh. Zigangirov, "Fundamentals of Convolutional Coding", IEEE Press, 1999

[28] D. Lauder, Y. Sun, "Modelling and Measurement of Radiated Emission Characteristics of Power Line Communication Systems for Standards Development", Proc. 3rd International Symposium on Power-line Communications and its Applications, Lancaster, UK, 1999.

[29] Lecroy, "http://www.lecroy.com".

[30] G. Lindell, L. Selander, "On Coding-, Diversity- and Receiver Strategies for the Powerline Communication Channel", Proc. 3rd International Symposium on Power-line Communications and its Applications, Lancaster, UK, 1999.

[31] J.A. Malack, J.R. Engström, "RF Impedance of United States and European Power Lines", IEEE Trans. on Electromagnetic Compatibility, 1976.

[32] G. Marubayashi, "Noise Measurements of the Residential Powerline", Proc. 1997 International Symposium on Power-line Communications and its Applications", Essen, Germany, 1997.

[33] M. Mouly, M-B. Pautet, "The GSM System for Mobile Communications", Cell & Sys 1992.

[34] J.R. Nicholson, J.A. Malack, "RF Impedance of Power Lines and Line Impedance Stabilization Networks in Conducted Interference Measurements", IEEE Trans. on Electromagnetic Compatibility, 1973.

[35] J. Newbury, "Technical Developments in Power Line Communications", Proc. 3rd International Symposium on Power-line Communications and its Applications, Lancaster, UK, 1999.

[36] H. Ottosson, H. Akkermans, F. Ygge, "The ISES Project", Enersearch AB, 1998.

[37] F Petre and M Engels, "DMT-Based Power Line Modem for the CENELEC A-Band", Proc. 3rd International Symposium on Power-line Communications and its Applications, Lancaster, UK, 1999.

[38] H. Philipps, "Performance Measurements of Powerline Channels at High Frequencies", Proc. 1998 International Symposium on Power-line Communications and its Applications", Tokyo, Japan, 1998.

[39] H. Philipps, "Modelling of Powerline Communication Channels" , Proc. 3rd International Symposium on Power-line Communications and its Applications, Lancaster, UK, 1999.

[40] Post- och Telestyrelsen, http://www.pts.se.

[41] J.G. Proakis, "Digital Communications", McGraw-Hill, 1995.

[42] J.G. Proakis, D.G. Manolakis, "Digital Signal Processing Principles, Algorithms, and Applications", Macmillan Publishing Company, 1992.

[43] "Proc. 1997 International Symposium on Power-line Communications and its Applications", Essen, Germany, 1997.

[44] "Proc. 1998 International Symposium on Power-line Communications and its Applications", Tokyo, Japan, 1998.

[45] Proc. 3rd International Symposium on Power-line Communications and its Applications, Lancaster, UK, 1999.

[46] R. Richard, J. James, "A Pragmatic Approach to Setting Limits to Radiation from Power Line Communication Systems", 3rd International Symposium on Power-line Communications and its Applications, Lancaster, UK, 1999.

[47] H. Sari, G. Karam, I. Jeanclaude "Transmission Techniques for Digital Terrestrial TV Broadcasting", IEEE Communications Magazine, February 1995, pp. 100-109.

[48] L. Selander, T. I. Mortensen, G. Lindell, "Load Profile and Communication Channel Characteristics of the Low Voltage Grid", Proc. DistribuTECH DA/DSM Europe 98, London, U.K., 1998.

[49] L. Selander, T. I. Mortensen, "Technical and Commercial Evaluation of the IDAM System in Ronneby, Sweden", Proceedings, NORDAC-98, Bålsta, Sweden, 1998.

[50] Siemens AG, "Oscillostore P513 - Operation Instructions", 1996.

[51] M.K. Simon, S.M. Hinedi, W.C. Lindsey, "Digital Communication Techniques", Prentice-Hall, 1995.

[52] The Mathworks, Inc., "Matlab Signal Processing Toolbox User's Guide", 1996.

[53] R.M. Vines, H.J. Trussel, K.C. Shuey, J.B. O'Neal, JR., "Impedance of the Residential Power-Distribution Circuit", IEEE Trans. on Electromagnetic Compatibility, 1985.

[54] M. Wozencraft, I.M. Jacobs, "Principles of Communication Engineering", Wiley, 1965.

[55] J. Yazdani, P. Brown, B. Honary, "Power Line In-House Near & Far-field Propagation Measurements and Simulation", Proc. 3rd International Symposium on Power-line Communications and its Applications, Lancaster, UK, 1999.

[56] M. Zimmermann and K. Dostert, "A Multi-Path Signal Propagation Model for the Power Line Channel in the High Frequency Range", Proc. 3rd International Symposium on Power-line Communications and its Applications, Lancaster, UK, 1999.